SHEAR CAPACITY
IN ADHESIVE GLASS-JOINTS

OSKAR LARSSON

Master's Dissertation

SHEAR CAPACITY
IN ADHESIVE GLASS-JOINTS

Master's Dissertation by
OSKAR LARSSON

Supervisors:

Kent Persson, PhD,
Div. of Structural Mechanics

Peter Möller,
Bostik AB, Helsingborg

Examiner:

Göran Sandberg, Professor,
Div. of Structural Mechanics

Acknowledgement

Abstract

In this report the shear-capacity of adhesive glass-joints was investigated. A number of various adhesives were tested; glues and silicones. Tests were conducted with small specimens to evaluate the characteristics of the adhesives. With the results of the tests material models were evaluated in the finite element program Abaqus. Linear-elastic and hyper-elastic models were used.

Large-scale tests were conducted to verify the material models from the test of the small specimens.

Keywords: Glass, Structural Glass, Adhesive, Glue, Silicone, Adhesive Joint, FEM, Finite Element, Linear-Elastic, Hyper-Elastic, Shear Capacity.

ii

Summary

Objective

The objective of this investigation was to develop a test method for testing the shear capacity of adhesive glass joints. The shear capacity was investigated in a short-term load-case. The tests were conducted on small specimens. With the results of the tests material models was evaluated in the finite element analysis program Abaqus. Eventually the material models were to be verified in large scale-tests.

Tests and Analysis

Test of small specimens were conducted with specimens consisting of two glass plates measuring 20×20×4.8 mm. The glass plates were joined with adhesive joints of thickness 6–0.2 mm. Different adhesives were used in the tests of the specimens. Silicone sealants were tested with thickness of 6–2 mm. Stiffer adhesives (glues) were tested with joint thickness of 0.2–0.3 mm.

The tests were conducted in a state of pure shear. In order to create this state a special test arrangement was designed. This test arrangement consisted of two steel-bars causing the applied force to act in the centre-line of the adhesive joint. The steel-bars also allowed expansion of the joint in order to avoid stresses caused by constraining the specimens.

The tests of the small specimens showed that the softer adhesives (silcones) had a very good adhesive capacity in the interface between glass and adhesive. In general fractures occured internally in the softer adhesives. The stiffer adhesives generally fractured in the interface between glass and adhesive. The specimens with the stiffer adhesives (glues) generally had a higher ultimate load than the softer adhesives (silicones) in the tests of the small specimens.

The tests were evaluated in a finite element analysis with the software Abaqus. The stiffer adhesives (glues) were evaluated with linear-elastic material models and the softer adhesives (silicones) with hyper-elastic material models.

Large scale tests were done in order to verify the material models. The large-scale tests were arranged as a 4-point bending test with a beam connected at the mid-point with an adhesive joint measuring 250×250 mm. The finite element calculations of the large-scale tests showed a higher ultimate load of the softer adhesives due to less stress concentrations at the edges of the adhesive joint.

Conclusions

The test method of the small specimens is a functioning method. The specimens with a joint geometry of 5×20 mm should be used in order to ensure a state of homogenous stress in the specimens and to avoid forces of to high magnitude.

Due to the high concentration of stress at the edges the stiffer adhesives (glues) showed a lower ultimate load than the softer adhesives (silicones) in the joint of larger geometry.

Further large-scale tests are needed to verify the material models evaluated from the tests of the small specimens.

Sammanfattning

Målsättning

Målet med detta examensarbetet var att utveckla en metod för att prova skjuvkapaciteten i limförband vid fogning av glas. Skjuvkapaciteten utvärderades för ett korttidslastfall och testerna genomfördes på små provkroppar. Utifrån dessa provningar utvärderades materialmodeller i finita element-programmet Abaqus. För att verifiera dessa materialmodeller genomfördes slutligen prov med en större foggeometri.

Provningar och analys

Provningarna genomfördes med små provkroppar, bestående av två glasbitar med dimensionen 20×20×4.8 mm. Glasbitarna sammanfogades med olika typer av limmer med tjocklekar varierande mellan 6–0.2 mm. Till tjocklekarna 6–2 mm användes silikoner och till de tunnare fogarna (0.3–0.2 mm) användes olika typer av lim.

Testerna genomfördes i ren skjuvning. För att skapa ett tillstånd av ren skjuvning användes en speciell uppställning. Uppställningen bestod av två stålkryckor som säkerställde att de pålagda krafterna angrep i centrumlinjen av den testade limfogen. Stålkryckorna säkerställde även att limfogen kunde expandera fritt, vinkelrätt skjuvriktningen vilket innebar att spänningar på grund av tvångskrafter inte uppstod.

Provningarna visade att de mjukare fogarna (silikoner) hade en god vidhäftning till glaset. Brotten i de mjukare fogarna uppkom vanligtvis i fogen och endast undantagsvis uppstod vidhäftningsbrott mellan glas och silikon. De tunnare fogarna (limmer) uppvisade generellt vidhäftningsbrott till glaset. Generellt hade limmerna en högre brottlast än silikonerna.

Testerna modellerades och utvärderades i finita element-programmet Abaqus. Linjärelastiska materialmodeller användes för att beskriva limmerna och hyperelastiska materialmodeller för att beskriva silikonerna.

Prover i större skala genomfördes för att verifiera materialmodellerna. Dessa test genomfördes som 4-punkts böjprov av en balk. Balken sammanfogades i mitten av limfog med dimensionen 250×250 mm. Vid beräkningar visade det sig att de mjukare silikonerna uppvisade en högre brottlast än de styvare limmerna. Detta berodde på att större spänningskoncentrationer uppstod i kanterna i de styvare limfogarna.

Slutsats

Testmetoden för att utvärdera skjuvkapaciteten var en väl fungerande metod. Dock så bör provkroppar med den mindre fogarean 5×20 mm användas. Detta för att säkerställa ett homogent spänningstillstånd i fogen och för att minska storleken på de pålagda krafterna.

I de storskaliga provningarna uppvisar de styva limmerna en lägre brottlast än de mjukare silikonerna. Detta beror på stora spänningskoncentrationer vid kanterna som uppkommer i en större fog. De mjukare limmerna/fogmassorna uppvisar en jämnare spänningsfördelning i den större fogen.

Vidare undersökningar bör göras för att verifirera materialmodellerna för större foggemetrier.

Contents

Chapter 1

Introduction

1.1 Background

Glass is a common material in buildings and probably one of the most common construction materials. As a construction material it has traditionally been used for windows in the facades of buildings. However, an increasing interest for glass as a structural material is showing.

More and more structures can be seen constructed with glass, not only in the facade but with glass in the load-supporting structures such as columns, beams and walls. Various structures, such as roofs, canopies, floors, stair-cases and even bridges have been constructed with glass as load-carrying material.

Glass is a very strong but also brittle material. In compression it is stronger than concrete but at the same time very sensitive to impacts. On impact the glass easily fractures.

Constructing with glass makes it necessary to connect different structural elements. The brittle characteristics of glass makes it vulnerable to concentrated forces which easily can create over-stressing.

The dominating way of joining glass elements today is by bolted joints. The bolted joints inevitably leads to stress-concentrations with the consequence of a fairly large number of bolts in the joints. The bolts disrupt the aesthetically appealing, transparent characteristics of the glass.

Adhesive joints are not used in a very large scale when joining structural elements of glass. However, many adhesive joints have the capability of distributing the stress over the surface of the joint and thus being more appropriate when joining glass elements. Also many adhesives have the ability of keeping the transparency of the glass over the joint which makes adhesive joints an aesthetically appealing alternative.

This masters thesis will investigate how some of the common adhesives act when joining glass.

1.2 Objective

The objective of this masters thesis is to investigate the shear-capacity of adhesive glass-joints in a short-term load-case. Common glues and silicones, available on the market, will be investigated. Different adhesive products will be investigated in order to get as wide span as possible of different adhesive characteristics.
The objectives of this investigation are:

- Development of an experimental method for determining the mechanical characteristics for an adhesive in pure shear.

- From the experimental data determine a corresponding material model for the adhesive. This will be done through a finite element analysis of the experimental tests.

- Verify the finite element model through large-scale tests.

Chapter 2

Properties and Use of Glass

2.1 Glass as a Construction Material

Glass has been used by man for thousands of years. The first glass to be used was naturally created in vulcanic activity. This glass was polished and sharpened and then used for arrow-heads and knives. Glass manufactured by man has been found in finds from the ancient persian empire and dates back to 5000 B.C. The majority of finds of ancient glass has been found in Egypt and glass manufacturing in a fairly large scale took place in Egypt at around 2000 B.C. [5].

Glass in buildings and in architecture has been used since the roman empire. Initially it was mainly used in mosaics for decoration but also for windows in official buildings. The first processes of manufacturing flat glass were complicated and consequently flat glass was expensive. Therefore it was not used in common buildings. However, in churches and monasteries, constructed from the 12:th century and on, glass windows are found. Glass was regarded as a luxury material and was not commonly spread until the end of 19:th century when industrial processes made the flat glass available at a lower cost [5].

During the 20:th century the manufacturing processes for flat glass was refined and new processes were developed. This meant that glass was used for windows in buildings at a larger scale. Since the 1950:s flat glass has been manufactured in the Float-glass process developed by Pilkington. This process meant a far more efficient way of manufacturing flat glass with nearly perfectly plane surfaces [5].

During the 20:th century glass in architecture has mainly been used in facades and roofs with the purpose of letting light into the buildings. The span of utilization of glass is wide, glass is used in everything from small windows of less than a squaremeter to large facades of hundreds of squaremeters.

Traditionally, large glass facades have been supported by a framework constructed of other materials, mostly steel. The framework is supporting the greater part of the loads (mainly from self-weight, wind and snow) and the glass is merely supporting the separate wind and snow loads acting on each single glass pane and transmitting

them to the framework.

For architectural and aesthetical reasons the framework is often sought to be minimized. This is done in order to avoid the restraining effect it has on the light. An example of a minimized framework is the facade of Kempinski Hotel in Munich constructed in 1988. In this building the glass facade is supported by a truss, consisting of a cable net with pre-stressed cables, connected to the glass in the corners of the glass panes with bolt connections [12].

To avoid frameworks that disrupt the glass, constructions have been made with glass forming the load carrying beams and pillars. Examples of this are the pavillon of the Broadfield House Glass Museum and the canopy over the entrance of the subway station at Tokyo International Forum in Tokyo [3]. Both examples show fully transparent structures.

In the pavillon in Broadfield the glass walls are supported by glass pillars/fins and the glass roof is supported by flat glass beams. Judging by the pictures in [3] the beams and fins seems to be connected with adhesive joints wich create perfect transparency and give a very nice appearance. In the canopy in Tokyo the supporting glass-beams are connected with bolted joints.

Another example of a load carrying glass-structure is a canopy, sheltering a stairwell descending to an underground carpark on the main square in Schaffhausen, Switzerland. In this case the canopy consists of flat-glass walls fixed with bolted fixings in a concrete foundation. The roof is supported by glass beams resting on cuts in the glass-walls on an interlayer of a nylon material to avoid stress-concentrations. The canopy in Schaffhausen is shown on the photographs in figure 2.1.

Figure 2.1: *The glass canopy over the stairwell to an underground carpark on the main square in Schaffhausen, Switzerland. The canopy is constructed with glass-beams supporting the roof. The right photograph shows a detail of the support of the beams with a spacer in a plastic material to distribute stresses*

2.1.1 The Material Glass

Pure silica glass is made by melting sand (sillimanite (silicon dioxide) SiO_2). The molted sand forms a liquid with high viscosity. Due to the high viscosity of the melt, the molecules of the glass are unable to form the crystalline pattern which normally is created when a liquid is cooling down and stiffens. Therefore the molecules create a completely random pattern. This amorphous structure gives glass its characteristic transparency.

If the glass would be kept in a liquid state for a very long time it would crystallize. In fact, pure silicon dioxide exists in nature in its crystalline form quartz.

Pure silica glass demands a very high temperature for melting; above 2000°C. To lower the melting point of the glass a series of other ingredients are added. The most common of this ingredients are soda (sodium oxide (Na_2O)), lime (calcium carbonate ($CaCO_3$)) and potash (potassium oxide (K_2O)). Addition of these substances lowers the melting point to around 1400-1600°C. The formula of a typical soda-lime-silica glass is described in table 2.1.

The soda-lime-silica glass with some additional substances in minor amounts is commonly used when manufacturing annealed flat glass.

Table 2.1: *Ingredients in a simple soda-lime-silica glass* [14], [1].

Substance		Amount (%)
Sillimanite	(SiO_2)	70 %
Soda	(Na_2O)	15 %
Lime	(CaO)	10 %
Potash	(K_2O)	5 %

Manufacturing Process

Since the 1950:s flat glass has been manufactured in the so-called float process. This process was developed by Pilkington Glass Co. in England.

In the float process the melted glass runs from the furnace in a continuous strip onto a bath of molten tin. Due to the higher density of the tin the glass floats on the bath of tin and as it floats the glass levels and almost perfectly parallell lower and upper surfaces are obtained. The thickness of the glass is controlled by the speed of which the glass ribbon is drawn off the tin bath.

The glass ribbon is drawn off the tin bath when it has reached a temperature where it is hard enough for the surfaces to withstand further treatment. Today more than 90 % of the flat glass is manufactured through the float glass process [1].

The width of the tin bath determines the different sizes of which the glass can be manufactured. The float glass process is based on the continuous floating of the glass ribbon on the bath of tin. This means that an infinite length of the flat glass can theoretically be obtained. However, for practical reasons, in manufacturing and

for transport, the maximum size available is 3180 x 6080 mm in the thicknesses 3, 4, 5, 6, 8, 10 and 12 mm. Thicker glasses can be manufactured (15, 19 and 25 mm) but are not always available in the full size (3180 x 6080 mm) [4].

Different types of Glass

Annealed Glass
The low heat-conductivity in the glass creates big differences in temperature within the glass, if it is cooled down rapidly. The colder areas of the glass shrink and stiffen faster than the still warmer areas of the glass. The stiffer areas thus restrain the shrinking of the warmer areas as the warmer areas cool down. This situation of cooler areas restraining the shrinkage of the warmer areas, causes stresses to develop within the glass. Compressive stresses arise in the fast cooling areas and tensile stresses in the slower cooling areas. If the cool-down process is not controlled, it may leed to a big variation of stress within the glass. This may lead to a spontanuous fracture after the glass has cooled down.
To avoid stresses to arise, the glass has to be reheated and cooled down carefully and slowly so that the differences in temperature are minimized. This slow cool-down process is called annealing the glass and therefore the final product is called annealed glass [1].
When overloaded annealed glass cracks into big sharp pieces which can cause injury when falling down on a person or if a person falls on the glass and fractures it.

Tempered Glass (Toughened Glass)
Tempered or toughened glass is manufactured by reheating an annealed glass to 650°C and subsequently recooling it rapidly with cool air streams along the surfaces. Thus compressive stresses are created in the surface and tensile stresses are created within the glass (see figure 2.3). The compressive stresses in the surfaces increase the bending and tensile capacity of the glass about 5 times.
Tempered glass fractures into small fragments which are relatively harmless and less likely to cause injury than the big sharp pieces forming when an annealed glass fractures. This crack pattern is caused by the tensile stress within the tempered glass. When a crack is initiated, e.g. by an impact of a sharp object, and it continues into the tensile zone the high tensile stresses cause it to propagate uncontrollably and thus the glass fractures into small fragments. Due to the less probability of injury on these small fragments, tempered glass is regarded as a safety glass [1].
Due to the tensile stresses within the tempered glass, it can not be worked or cut after the toughening process. If worked, e.g. drilling a whole in the glass, it will fracture completely. Thus no treatment can be done at the construction site. All treatment of the tempered glass, such as drilling holes and cutting it to the right dimensions, must be done to the annealed glass in the industrial process before the toughening of the glass.

Tensile Stress | Compressive Stress
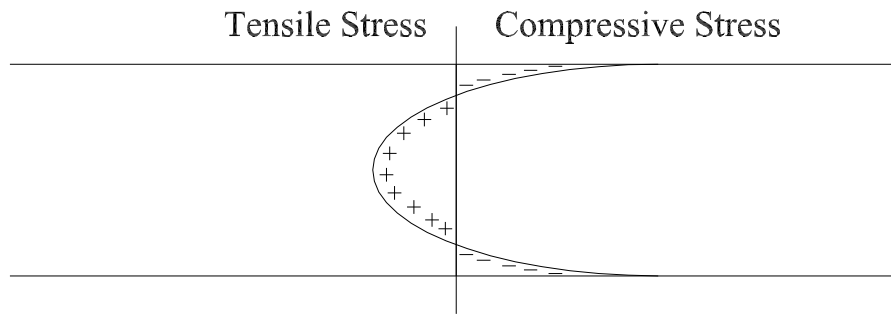
Figure 2.2: *Stress variations in tempered (toughened) glass. The stress distributes as tensile stress within the glass and compressive stress close to the surfaces.*

Heat Treated Glass
Heat treated glass is manufactured in the same way as tempered glass. It is heated to 621°C but the cooling process is slower than the process of tempered glass. In this way the stress distribution within the heat treated glass is similar to the tempered glass but the stresses are not as high as in tempered glass. Due to the lower stresses the heat treated glass does not fracture into small fragments. The crack pattern of heat treated glass resembles the crack pattern of the annealed glass.
Heat treated glass has a bending capacity twice the one of annealed glass [1].
For the heat treated glass, all cutting and working must be done before the heat treatment or else the glass fractures.

Laminated Glass
Laminated glass is formed by several layers of flat glass joined together with interlayers of plastic material. The most common plastic material used is polyvinyl butyral (PVB). The flat glass used may be annealed or tempered and can be of different thicknesses. The laminated glass has the advantage that when breaking the glass stays together as the interlayers keeps the fractured glass together. It also allows one glass layer to break, e.g. by a sudden impact, and the other glass panes can remain unfractured and thus continue to carry the designed loads.

Mechanical Properties

Glass is a strong but brittle material, it can be loaded with great compressive forces but in the same time be completely destroyed by a sudden impact. Glass shows an elastic behaviour and when over-loaded the failure comes suddenly without any plastic deformations. Glass shows a highly different capacity when loaded by a com-
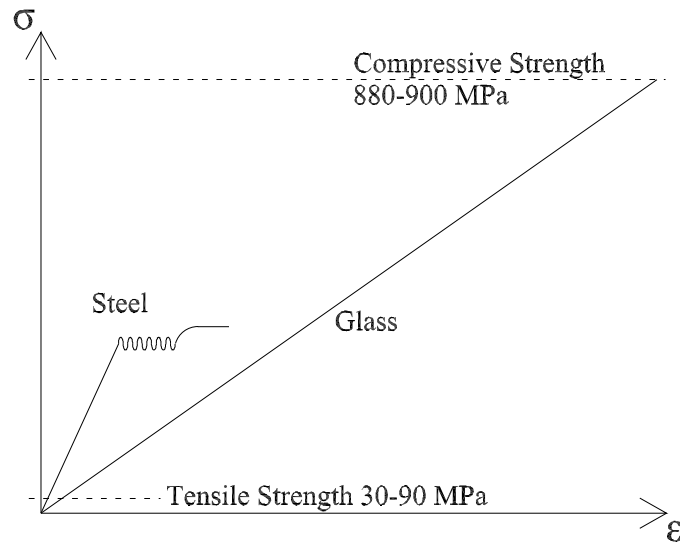
Figure 2.3: *The stress-strain curve of glass compared to the stress-strain curve of steel.*

pressive or a tensile force. Due to the brittle characteristics of glass it is regarded as fragile and not very well suited as a construction material.

Mechanical Behaviour
When loaded, glass shows a perfect linearity in the curve of stress versus strain with a Young's modulus of 70-75 GPa. All the deformations are elastic which means that the glass returns to its original shape when the force or stress is removed.
The absence of plastic deformations means that stresses accumulate in areas where point loads act, such as bolt fixings or at connection points between columns and beams. This means that joints and connections have to be designed carefully to avoid local overstressing.
The glass shows no dynamic fatigue, however it shows a so-called static fatigue when loaded in tension. The static fatigue means that the glass can support a load when it is applied for a short period of time but when it is applied to the same load for a longer period of time it fractures. That is, the glass can for a short period of time support much higher loads than if it is applied to a long-term load. The reasons for this static fatigue are not clearly known but experiments show that glass can support long-term loads of approximately 25-40% of the maximum short-term loads [4].

Tensile Stress
The theoretical tensile stress-capacity of glass is calculated to 21 GPa (based on atomic bond-strength calculations). The highest tensile strength, ever to be measured on glass, has been measured on freshly drawn glass fibres to 5 GPa. However,

flat glass normally fails and fractures at tensile stresses lower than 100 MPa [4].
The explanation to this large difference between the theoretical strength and the
real tensile strength is the presence of defects on the surface of the glass. A crack
leading to failure in the glass is usually initiated on the surface and then propagates
through the glass.

A.A. Griffith put forward a theory in the 1920:s that the cracks leading to failure
of the glass was initiated by small, invisible defects on the surface. These invisible
defects, so-called Griffith flaws, accumulate stress thus causing stress concentrations
which initiate a crack that subsequently propagates and ultimately leads to failure.
The strength of the glass depends on the number, shape and orientation of the Grif-
fith flaws [4].

Larger surface defects, e.g. scratches and vents, also have a significant effect on the
strength of the glass. In this case it is also the accumulation of stresses around the
defects that initiates a crack and leads to failure. A good example of this is the
normal way of cutting annealed glass. The glass is first scribed and then bent in
order to cause tensile stresses at the scribe. Thus the fracture initiates at the scribe
which creates an almost perfect cut.

The tensile capacity of glass used for designing varies from 30–90 MPa [14]. The
lower value is used for design of annealed glass and the higher for tempered glass. In
the tempered glass, it is the initial compressive stress in the surface that increases
the tensile capacity.

Compressive Stress
The theoretical compressive strength of glass is, as in tension, around 21 GPa. In
reality this has never been measured. The compressive capacity used for design
varies from 880–930 MPa [14].

Material Data
Material data for glass is shown in the tables 2.2 and 2.3 below:

Table 2.2: *Mechanical properties for glass* [14].

Compressive strength	880–930	MPa
Tensile strength	30–90	MPa
Bending strength	30–100	MPa
Youngs modulus	70–75	GPa
Shear modulus	20–30	GPa
Poissons ratio	0.23	(-)

Table 2.3: *Properties for glass according to the European norm, EN 572-1:2004* [5].

Density	δ	$2.5 \cdot 10^3$	(kg/m^3)
Youngs modulus	E	$70 \cdot 10^9$	(Pa)
Thermal expansion coeff.	α	$9 \cdot 10^{-6}$	(/K)
Heat conductivity	λ	$1.0 \cdot 10^3$	(W/K)
Spec. heat capacity	c	$0.72 \cdot 10^3$	(J/(kg·K))
Char. bending strength	$f_{g,k}$	$45 \cdot 10^6$	(Pa)

2.2   Joints in Glass-Constructions

2.2.1   General

The manufacturing process and the available possibilities for transport only allows certain sizes of continuous glass elements. Therefore it is necessary to connect glass elements to create glass constructions of larger sizes. The maximum length for flat-glass elements is approximately 6 meters, depending on the thickness of the glass.

Whenever a force is applied to a material, stresses in the material emerge as a response to the applied force. The magnitude of the stress depends on the area of contact; the larger the area of contact the lower the stress will be. If the area of contact is uneven or if the load is applied excentrically, the real area of contact may be less than the designed one thus creating higher stresses (see illustration in fgure 2.4). Most construction materials has the ability to cope with this situation by deforming plastically when over-stressed. This plastic deformation leads to a local yield that increases the area of contact and evens out the stresses. Glass, however, has no capacity of deforming plastically and any overstressing will lead to fracture which subsequently propagates a crack.

Typical areas, where concentrated forces can be found, are at connections and supports. In such areas an often evenly distributed load over one element is to be transmitted to another element over a relatively small area of contact. The mechanical characteristics of glass described above requires a careful design of the joints and connections to avoid overstressed areas. It is often necessary to use finite element calculations in the design process to ensure that over-stressing is avoided. It is also necessary to be careful in the construction process to make sure that critical details are constructed properly.

In many facade glazing systems, bolted connections are used to connect the window panes to the supporting frame. This inevitably leads to stress concentrations around the areas of the bolts. In some glazing systems, foremost in the United States, the window panes are connected to the supporting frame with adhesive sealants, like silicones, without any support of mechanical connectors.
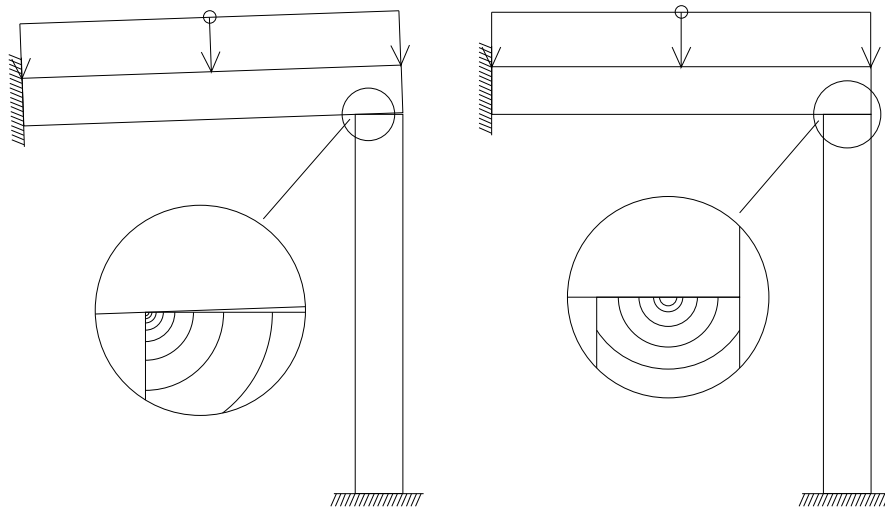
Figure 2.4: *Illustration of how eccentrical loading of a column decreases the area of contact and causes stress concentrations.*

2.2.2 Bolted Joints

The most common way of connecting structural elements of glass is by a bolted joint. If designed carefully it is capable of transmitting the forces from one element to another and avoiding over-stressing at the holes. Bolted connections are used in many facade glazing systems where window panes normally are fixed through bolts in the corners either to a structural frame-work or to each other. Also wind-stabilizing fins in glass facades often can be seen connected with bolts [4].
Bolted connections are also used in connections in structural, load-carrying glass. In the canopy over the entrance of the subway station at Tokyo International Forum in Tokyo the supporting glass-beams are connected with bolts [3].
Liners of neoprene or nylon are often used in bolted connections to even out the stresses and to be able to tighten the bolts without fracturing the glass. There are many examples of different designs of bolted joints in glass constructions both connecting glass to glass and glass to other materials [9].

2.2.3 Adhesive Joints

When constructing structural elements of glass the main method for joining elements of glass is bolted connections. This may seem a bit strange when the bolts disrupt the fantastic aesthetic features of the glass.
Adhesive joints could be a way of connecting glass elements and still keep the visual aspect and transparency intact. Today adhesive joints are used in a minimal scale when connecting glass elements. The only application where adhesive joints can be seen, when constructing with glass, is in facade glazing systems where silicone

sealants are used for attaching window panes to the inner, supporting framework [13]. Structural silicone glazing systems were introduced in the mid 60's. The systems mostly consists of a supporting framework of steel or aluminium with the window panes attached to the frame with silicone sealants. A vast number of different systems exist. In most systems the weight of the glass is supported by a metal beam but in some cases the silicones bear the weight of the glass. The silicone glazing systems are mostly spread in the United States [8].

The silicones have proved an excellent durability and resistance to weather and age. The facade is a very hostile environment exposed to variations in humidity and temperature. To the exposure of ultra-violet light from the sun-light, something that has proven to break down and destroy many materials, the silicone sealants show an excellent resistance [8].

The glass is a brittle material with no capacity of deforming plastically. This makes the glass very sensitive to stress-concentrations. An adhesive joint has the advantage of transmitting the forces from the individual structural element over the surface of the joint. This is a capacity that is highly desirable when designing glass-joints.

Except for the silicone sealants almost no adhesives are used for connecting glass elements. Investigations and research are going on to use adhesive joints, not only in silicone structural glazing systems, but also as adhesive connectores in structural glass elements as beams and stabilizing fins [13].

Chapter 3

Finite Element Modelling of Adhesive Joints

3.1 Modelling of Linear-elastic materials

The following account of the mechanical relationships of the linear-elastic material models is a summary of the derivations in [11]. For more extensive derivations see pages 235-260 in [11].

The stiff adhesives tested in this investigation was modelled with linear-elastic models. The linear-elastic models postulate a linear relationship between the stress and the strain in the material. The relationship describing the behaviour of these materials is Hooke's law. In one dimension, Hooke's law is expressed by

$$\sigma = E\epsilon. \tag{3.1}$$

In equation 3.1, σ is the normal stress defined as $\sigma = \frac{P}{A}$, E the Young's modulus of the material and ϵ the strain of the material defined as $\epsilon = \frac{u}{L}$. The symbols are defined in figure 3.1 on page 15.

In a state of shear the relationship between shear-stress and shear-strain in a linear elastic material is expressed by

$$\tau = G\gamma. \tag{3.2}$$

In equation 3.2, τ is defined as $\tau = \frac{P}{A}$, G is the shear modulus, and γ is the shear-angle defined $\gamma = \frac{\delta}{H}$. The symbols are defined in figure 3.1.

Using the Poisson's ratio (ν), the relationship between the shear modulus and Young's modulus in an isotropic linear-elastic material is expressed

$$G = \frac{E}{2(1+\nu)}. \tag{3.3}$$

In 3 dimensions, the stresses and strains of an isotropic material are described with the generalized Hookes law by

$$\boldsymbol{\sigma} = \boldsymbol{D}\boldsymbol{\epsilon} \tag{3.4}$$

where

$$\boldsymbol{\sigma} = \begin{bmatrix} \sigma_{xx} \\ \sigma_{yy} \\ \sigma_{zz} \\ \tau_{xy} \\ \tau_{xz} \\ \tau_{yz} \end{bmatrix} ; \boldsymbol{\epsilon} = \begin{bmatrix} \epsilon_{xx} \\ \epsilon_{yy} \\ \epsilon_{zz} \\ \epsilon_{xy} \\ \epsilon_{xz} \\ \epsilon_{yz} \end{bmatrix}$$

and

$$\boldsymbol{D} = \frac{E}{(1+\nu)(1-2\nu)} \begin{bmatrix} 1-\nu & \nu & \nu & 0 & 0 & 0 \\ \nu & 1-\nu & \nu & 0 & 0 & 0 \\ \nu & \nu & 1-\nu & 0 & 0 & 0 \\ 0 & 0 & 0 & \frac{1}{2}(1-2\nu) & 0 \\ 0 & 0 & 0 & 0 & \frac{1}{2}(1-2\nu) \\ 0 & 0 & 0 & 0 & 0 \\ \frac{1}{2}(1-2\nu) \end{bmatrix}$$

This constitutional law is used in the finite element programs for describing the stresses and strains in a linear-elastic material.

3.2 Modelling of Hyperelastic Materials
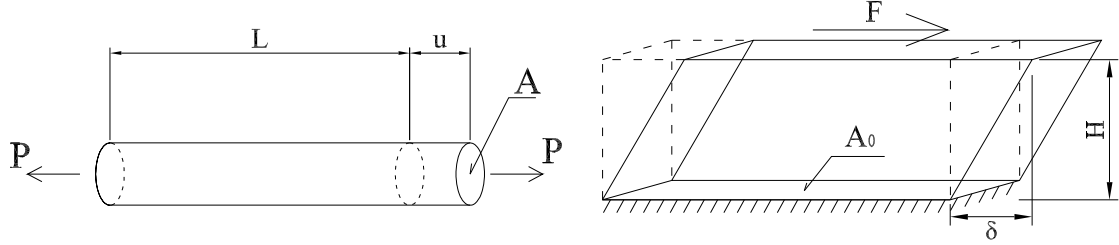
Figure 3.1: *The left drawing show an elastic bar loaded with tensile forces and the right drawing a linear-elastic material loaded with a shear-force.*

The following material constitutions of the hyper-elastic material-models are a summary of the derivations in [2]. A more extensive explanation is given on the pages 17-32 in [2].

The silicones tested in this investigation was modelled in Abaqus with hyperelastic material models. These models are used in order to be able to cope with the high magnitude of deformations that occur when loading this type of materials. This type of models are normally used for modelling rubber materials.

The hyper-elastic material models are derived, using a strain energy function to describe the characteristics of the materials. The concept of the strain energy function is described below by the example of a non-linear elastic bar. The symbols used in the following example are illustrated in figure 3.1.

When analyzing hyper-elastic materials the traditional strain ($\epsilon = \frac{u}{L}$) is replaced by the so called stretch (λ) defined as

$$\lambda = \frac{L+u}{L}(= 1 + \epsilon).$$

The strain energy density is defined as a function $W(\lambda)$, describing the strain energy density per undeformed volume of the bar.

The total strain energy (U), is thus expressed by multiplying $W(\lambda)$ with the undeformed volume

$$U = ALW(\lambda). \tag{3.5}$$

The increments of work done by the external force can be expressed by the energy balance equation

$$dU = Pdu. \tag{3.6}$$

Expressing this same increment of work by using $W(\lambda)$ can be done by the expression

$$dU = ALdW = AL\frac{dW}{d\lambda}d\lambda. \tag{3.7}$$

Rewriting the definition of λ gives

$$\lambda = \frac{L+u}{L} \leftrightarrow u = (\lambda - 1)L.$$

Differentiating u gives

$$du = Ld\lambda. \tag{3.8}$$

Inserting 3.7 and 3.8 into 3.6 gives

$$PLd\lambda = AL\frac{dW}{d\lambda}d\lambda \rightarrow \frac{P}{A} = \frac{dW}{d\lambda}.$$

Thus is an expression of the stress ($\frac{P}{A}$) in the elastic bar derived from the strain energy function.

3.2.1   Strain Energy Function

The strain energy density function can be regarded as a potential function for the stresses. The measure of strains used here is the left Cauchy-Green deformation tensor **B**. Thus W can be written

$$W = W(\boldsymbol{B})$$

The state of deformation is fully determined by the principal stretches $(\lambda_1, \lambda_2, \lambda_3)$ and the principal directions. In an isotropic material the three principal stretches are independent of the principal directions and consequently the strain energy density function can be written

$$W = W(\lambda_1, \lambda_2, \lambda_3).$$

The principal stretches can be obtained from the characteristic polynomial of **B**, however not very easily. Easier to obtain are the strain invariants and thus the strain energy function is expressed in an easier way as a function of the three invariants,

$$W = W(I_1, I_2, I_3).$$

The three invariants can be expressed by the principal stretches

$$\begin{cases} I_1 = \lambda_1^2 + \lambda_2^2 + \lambda_3^2 \\ I_2 = \lambda_1^2\lambda_2^2 + \lambda_1^2\lambda_3^2 + \lambda_2^2\lambda_3^2 \\ I_3 = \lambda_1^2\lambda_2^2\lambda_3^2 \end{cases}$$

The third invariant expresses the change in volume and as rubber materials generally are more or less incompressible, it is assumed that no changes in volume occur, thus $I_3 = 1$. This results in the expression

$$W = W(I_1, I_2),$$

for the strain energy function. Further on, $I_3 = 1$ can be used to for the transcription

$$1 = \lambda_1^2\lambda_2^2\lambda_3^2 \rightarrow \lambda_3 = \frac{1}{\lambda_1\lambda_2},$$

which after insertion into the equations for I_1 and I_2 gives

$$\begin{cases} I_1 = \lambda_1^2 + \lambda_2^2 + \frac{1}{\lambda_1^2 \lambda_2^2} \\ I_2 = \lambda_1^2 \lambda_2^2 + \frac{1}{\lambda_2^2} + \frac{1}{\lambda_3^2} \end{cases}.$$

The constitutive law for a hyperelastic, isotropic and incompressible material is derived from the strain energy density function using the energy principle in an energy balance equation in the same way as in the initial example of the elastic bar. In finite element analysis programs the most common expression used to describe the strain energy density function is the series expansion

$$W = \sum_{i=0,j=0}^{\infty} C_{ij}(I_1 - 3)^i (I_2 - 3)^j. \tag{3.9}$$

Most hyper-elastic material models are based on this sum. They are separated by how many and which of the constants (C_{ij}) that are used.

The following sections will describe the Neo-Hooke and the Mooney-Rivlin material models which were used for the evaluation of the mechanical characteristics of some of the adhesives later in the investigation.

3.2.2 Neo-Hooke Model

The Neo-Hooke material model uses the first term, coefficient C_{10}, of the expression 3.9 to describe the strain energy density function. In Abaqus it is expressed with a second term, coefficient D_1, describing the thermal expansion of the material. In this report the thermal expansion of the material will not be regarded and the coefficient D_1 is therefore not prescribed in the FE-evaluations.

In Abaqus the strain energy density function for the Neo-Hooke model is described by

$$W = C_{10}(I_1 - 3) + \frac{1}{D_1}(\boldsymbol{J^{el}} - 1)^2.$$

The Neo-Hooke model shows a very good correlation with experiments in compression and moderate shear of rubber materials.

For further description of the Neo-Hooke material model see [2] and [15].

3.2.3 Mooney-Rivlin Model

The Mooney-Rivlin model uses the first two terms, coefficients C_{10} and C_{01}, of the expression 3.9 to describe the strain energy density function. In Abaqus it has a third term, coefficient D_1, describing the thermal expansion of the material. In this report the thermal expansion of the material will not be regarded and the coefficient

D_1 is therefore not prescribed in the FE-evaluations.

In Abaqus the strain energy density function for the Mooney-Rivlin model is described by

$$W = C_{10}(I_1 - 3) + C_{01}(I_2 - 3)^2 + \frac{1}{D_1}(\boldsymbol{J^{el}} - 1)^2.$$

The Mooney-Rivlin material model shows very good correlation with experiments on natural rubber and has been widely used in different applications.

For further description of the Mooney-Rivlin material model see [2] and [15].

Chapter 4

Tests of Small Specimens

4.1   Method

In the following section the method for the conduction and evaluation of the shear-capacity tests will be explained. Initially the purpose and objective of the tests will be explained. Subsequently follows an explanation of the testing equipment used to obtain a state as close as possible to pure shear. Eventually the method for evaluating the results from the tests will be explained and illustrated.

4.1.1   Shear-Capacity Tests

The main purpose of the tests in this investigation is to determine the mechanical characteristics of different adhesives connecting glass when applied to a pure shear force. Adhesive joints are normally designed to be loaded in a state of shear rather than in a state of tension. Therefore it is necessary that the test creates a situation close to a state of pure shear.

Small specimens were used in the tests and later the results were evaluated and translated to a FE-model that can be used on a larger joint-geometry. Small specimens were mainly used for two reasons:

- Small specimens ensure a relatively homogenous state of stress. In that sense significant stress concentrations on the edges of the adhesive is avoided, which otherwise may affect the test result.

- It is an advantage if tests can be conducted with small specimens because it is cheaper than testing in full scale. Thus a larger number of specimens can be tested and a statistically valid test result can be obtained to a lower cost than with full-scale testing.

In this investigation large-scale tests were eventually conducted to verify whether the small scale tests can be used for describing the behaviour of a larger joint.
The shear capacity were evaluated in a short-term load case, i.e. a load acting rapidly which eventually leads to failure in the adhesive. The tests were conducted with a constant deformation speed. The speed of the shear strain was intended to be kept constant, at approximately 3 % per second.

Testing Equipment

For evaluating and testing the shear-capacity of a specimen it is of importance to minimize tensile and compressive stresses that may arise from testing equipment that restrains the deformation of the specimen. Furthermore, all loads must be applied centrically to avoid any moment over the specimen caused by eccentricity that may cause tensile and compressive stresses to arise. To obtain a situation of pure shear stresses in the adhesive, the testing equipment has to be designed with the following characteristics:

- No moment must be transmitted from the testing equipment to the specimen in order to avoid stresses in the adhesive caused by the moment.

- Expansion/shrinkage of the adhesive joint perpendicular to the direction of the shear forces must be allowed to avoid stresses caused by constraining the material strains.

The testing equipment must also be able to handle:

- Different thicknesses of the adhesive layer.

- Variations in the magnitude of deformation in the different types of adhesives (stiffer glues, softer silicones).

The testing equipment was designed as shown in figure 4.1 on page 21. It consisted of two steel-parts that transmit the forces from the testing machine to the specimen. Moment in the adhesive joint is avoided by letting the line of action of the forces coincide with the centre-line of the adhesive joint. To avoid deformations in the steel-parts, that could create peel stresses in the joint, the steel-parts have to be infinitely stiff in comparison to the adhesive layer of the specimen. That is, the forces must not reach a level where significant deformation occurs in the steel-parts [6].
To handle the different thickness of the joints, steel-plates can be attached in the notches for the specimens. This allows the line of action of the forces to be kept in the centre line of the joint, independent of the thickness of the joint.
For stiff glues the test equipment was loaded by compressing the steel-parts. In order to avoid eccentricity and moment forces to act on the steel-parts, a steel-ball was placed in a notch where the forces from the machine act on the steel-parts.
To avoid rotation of the steel-parts a linear bearing was placed between the steel-
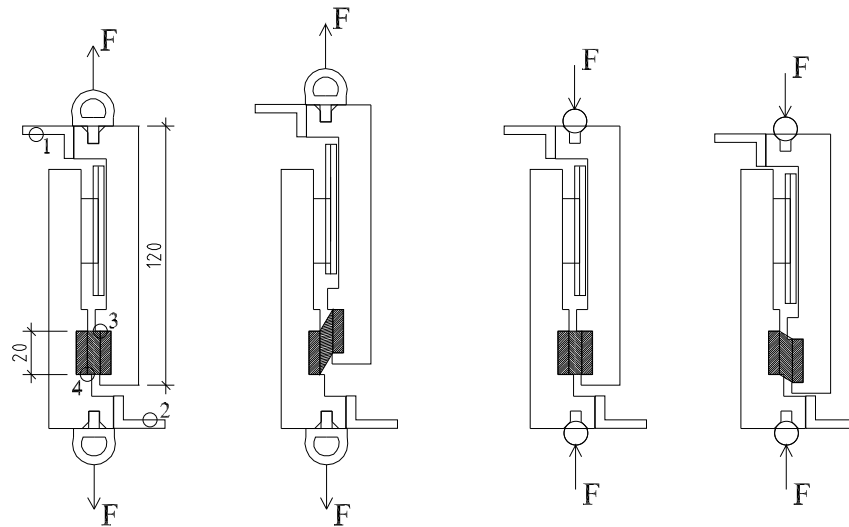
Figure 4.1: *Drawing of the test equipment used in the shear-capacity tests. Tensile forces were used for the softer adhesives and compressive forces for the stiffer adhesives.*

parts and a rubber band made sure that they were held together over the bearing. This kept the steel-parts parallel during the test.

For the softer silicone-based adhesives the test equipment was loaded with tensile forces in order to allow the large deformations in the joints. In this case the bearing was not needed and the test was self-stabilizing.

The test equipment has been used in earlier research, studying adhesive joints in wooden materials, at the Department of Structural Mechanics at the Lund University, Sweden [6].

The specimens in the tests consisted of two pieces of glass measuring 20×20 mm joined together with an adhesive layer. Two different types of specimens were used in the tests, see figure 4.2 on page 22. Specimen 1 had an adhesive layer that fully covered the surface of the glass-parts and it was used for the less stiff adhesives. Specimen 2 had an adhesive layer measuring 5×20 mm. It was used for the stiffer glues to reduce the applied force needed to conduct the test.

Measurements

The applied force and the deformations were collected every 0.5 second. Force was measured with a load-cell in the MTS testing machine, measuring range: ±10 kN. Deformations were measured in two different ways:

- When the deformations exceeded 4 mm they were measured with the length
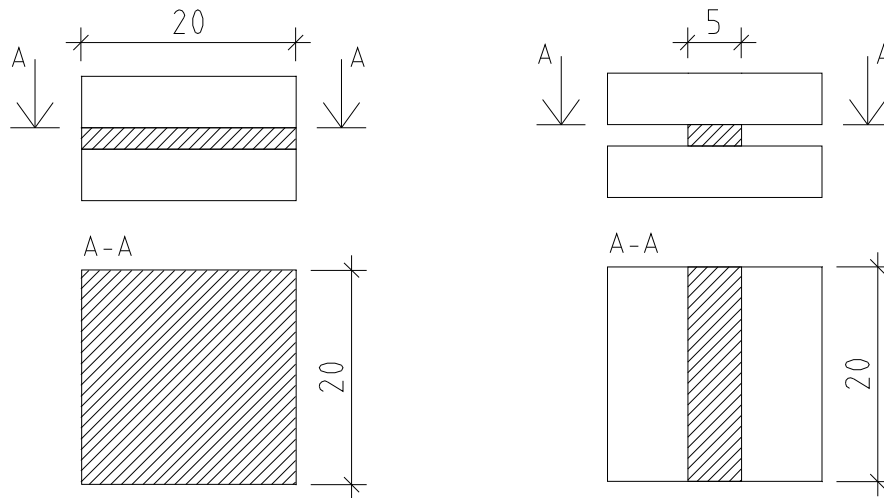
Figure 4.2: *Drawing of the two different types of specimens. The left drawing shows the specimen type 1 with an adhesive layer that fully covers the 20×20 mm surface of the glass. The right drawing shows the specimen type 2 with an adhesive layer measuring 5×20 mm.*

gauge of the MTS-machine which measures the displacement of the hydraulic piston. This measurement includes the deformation of the entire machine including load-cell and the arrangement for attaching the steel-parts of the testing equipment. The deformations in the attaching arrangement and the load-cell was therefore measured without the steel-bars and specimens in order to be able to calibrate the measured data to only get the deformations in the steel-bars and specimens.

• When deformations were less than 4 mm two deformation gauges (± 0.001 mm) were attached to the steel-bars to measure the displacements of the two steel-bars, the deformation value used in the evaluation is a mean-value of these two measurements. By using the mean-value of two deformation gauges, measurement of a possible rotation of the steel-parts is avoided.

4.1.2 Evaluation of Measured Data

In this section the method of evaluating the measured data will be described. This method will later be used for each of the tested adhesives.

Ultimate Shear-Stress.

The ultimate forces were extracted from the measured data. To convert them in to shear-stress a simple division of the initial area (A_0, 400 or 100 mm^2) was made ($\tau_{avg,u} = \frac{F_u}{A_0}$). In the report the minimum, maximum and mean-values from the measured data of each adhesive are given.

Characteristics of the Fracture-Surface.

The fracture surface was studied to observe the characteristics of the fracture. Especially it was searched for signs of fracture initiation and failure in adhesion to the glass.

Relation between the applied force and deformation

The measured data from the tests gives the deformations of the entire test arrangement, i.e. deformations in steel, glass and adhesive. Consequently these measured deformations can not be used as values for the shear-deformation in the adhesive. To evaluate the characteristics of the adhesives an FE-model was created of the entire test arrangement (figure 4.3). From that model strains and stresses of the adhesives was extracted. The model was, in each case, based on the geometry of the tested joints. The steel-parts were modelled with the characteristics E=210 GPa, ν=0.3 and the glass with the characteristics E=70 GPa, ν=0.23.

The evaluation consisted of plotting the measured data of the shear-force versus the deformation of the series of tests. This data was fitted to a polynomial curve in a least-square sense.

Various calculations of the FE-model, each with different mechanical characteristics of the adhesive material, were made and the shear-forces and deformations were extracted from the FE-model. These extracted results were compared with the fitted curve from the measured data. The FE-calculations continued until a match between measured data and the results from the FE-model occured.

For the silicone adhesives the hyperelastic material models Neo-Hooke and Mooney-Rivlin were used and for the stiffer adhesives linear-elastic models with a poissons ratio of ν=0.25 were used.

From the matching models the shear-deformation was extracted and used to establish the relationship of shear-stress versus shear-strain. The results which were compared with the fitted polynomial curve were extracted from points 1 and 2 in
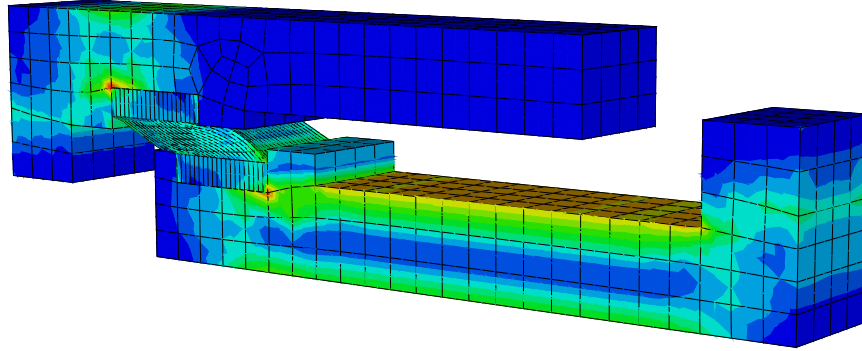
Figure 4.3: *FE-model of the test arrangement.*

figure 4.1 on page 21 and the results extracted from points 3 and 4 were used to determine the shear-strain in the adhesive.

Critical Shear-Stress, τ_{cr}

The distribution of shear stress in the adhesive was analyzed in the FE-model. The analysis was done for the increment closest to the average ultimate load capacity (F_u) of each adhesive. If the stresses were not evenly and homogenously distributed the highest value of shear-stress was extracted from the observed stress concentrations. This maximum value of shear-stress will be called the critical shear-stress (τ_{cr}). Depending on how the shear-stresses are distributed in the adhesive at the point of fracture the critical shear-stress will be equal to or larger than $\tau_{avg,u}$.

Initial Shear-Modulus, $G_{20\%}$

From the curve of shear-stress versus shear-strain an initial shear-modulus of each adhesive was calculated. It was calculated as the inclination of the linear approximation of the stress-strain curve in the interval 0 to 20 % of the mean value of the ultimate shear-stress, $\tau_{avg,u}$. This initial shear-modulus will be called, $G_{20\%}$.

4.1.3 Presentation of Results

In the report the results from the tests and FE-calculations for each adhesive will be presented in the following way:

- Diagram showing the measured data of applied force plotted versus deformation.

- Diagram showing the data of force versus deformation together with the fitted curve.

- Table of ultimate force, stress and deformation.

- Diagram showing fitted curve from the measured data and curve of the force versus deformation extracted from the corresponding FE-model.

- Diagram of shear stress versus shear-strain from the FE-model.

4.2   Symbols and Abbreviations

The following abbreviations will be used in the description of the tests.

Description	Abbreviation
MTS Test-machine	MTS
Displacement gauge of MTS-machine	DSMTS
Displacement gauge ± 0.001 mm	DS$\pm$0.001

To describe the state of shear and the deformations in the tests the following symbols will be used:

Quantity	Symbol	Definition	Unit
Initial area	A_0	Figure 4.4	(m^2)
Height	H	Figure 4.4	(m)
Shear force	F	Figure 4.4	(N)
Ultimate shear force	F_u	Shear force at failure	(N)
Average shear stress	τ_{avg}	$\frac{F}{A_0}$	(Pa)
Ultimate shear stress	$\tau_{avg,u}$	$\frac{F_u}{A_0}$	(Pa)
Critical shear stress	τ_{cr}	Subsection 4.1.2	(Pa)
Shear deformation	δ	Figure 4.4	(m)
Shear strain	γ	$\frac{\delta}{H}$	(-)
Initial shear modulus	$G_{20\%}$	Subsection 4.1.2	(Pa)
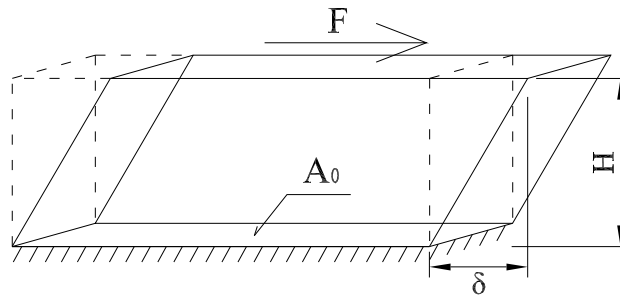
Figure 4.4: *Drawing of the deformations and symbols used for the specimens in pure shear.*

4.3 Tested Adhesives

Various adhesives were tested in this investigation. The following section gives a summary of the most important characteristics of the tested products. For more extensive information the web-sites of the manufacturers offers possibilities to download product-sheets and safety instructions.

The products of the 6 mm tests are not included in this summary, information about these products can be found on the Bostik and Sika web-sites.

Table 4.1: *Adhesives tested in the shear-capacity tests.*

Adhesive	H (mm)
Bostik Silikon Bygg 2685	6
Bostik Marmorsilikon	6
Sika Elastosil SG 20	6
Sika Elastosil 605 S	6
Bostik Multifog 2640	2, 0.3
Bostik Simson ISR 70-03	2, 0.3
Bostik Simson ISR 70-04	2, 0.3
Bostik Simson ISR 70-12	2, 0.3
Casco Polyurethan	0.2
HBM Rapid Adhesive X 60	0.2
Casco Strong Epoxy Professional	0.3
Casco UV-hardening Glass-Glue	0.3

4.3.1 Casco Strong Epoxy Professional 2801, 2803

The Strong Epoxy Professional is a 2-component adhesive. After mixture of the 2 components the adhesive is applicable during a period of time of 100 minutes. The surfaces to be joined shall be clean and free of dust and grease. The time of hardening to full strength is between 10 and 36 hours in the temperature span 10–25°C. The Epoxy Strong is water resistant but shall not be exposed to water for a longer period of time.

The Epoxy has a transparent light-yellow colour, it has a tendency to get more yellow over time. It is durable in temperatures up to 70°C.

When joining glass elements with Epoxy, failures have been observed, over time, in the adhesive interface between glass and adhesive [14].

For product sheets and more extensive information see [16].

4.3.2   Casco Polyurethan Glue 1809

Casco Polyurethan Glue 1809 is a 1-component adhesive that hardens by the presence of moisture. During the hardening process carbon dioxide (CO_2) is released which creates a foam of glue and CO_2-bubbles. Due to this reaction a high pressure is required to keep the joined elements together during the hardening process. The hardening time is 3 hours at 20°C and 65 % RH. Due to the presence of water in the hardening process, lower temperatures than +5°C is not recommended when hardening the adhesive. After hardening, the adhesive is not particularly sensitive to cold temperatures. The polyurethan glue is transparent without colour.
The polyurethan glue is mainly used for joining elements of wood but is also used for joining non-absorbing materials as plastics and steel. When joining non-absorbing materials, it is recommended to spray the applied adhesive with water before pressing the joint together in order to increase the speed of the hardening process.
The joined surfaces shall be clean and free from dust and grease before applying the adhesive.
For product sheets and more extensive information see [16].

4.3.3   Casco UV-hardening Glass-Glue 2987

Casco UV-hardening Glass-Glue 2987 is an adhesive that hardens while exposed to ultra-violet light. When exposed in direct daylight the hardening time varies between 20 seconds and 3 minutes depending on the degree of cloudiness. Full strength is normally gained after 24 hours. It shall be applied at a temperature of 15–25°C and after hardening it can be exposed to a temperature varying between -10–+120°C.
The UV-hardening glass-glue has a good resistance to moisture, water and cleaning detergents. It is transparent and without colour. It can be used for joining glass to glass and glass to metal. The joined surfaces shall be clean and free from dust and grease.
For product sheets and more extensive information see [16].

4.3.4   HBM Rapid Adhesive X 60

The Rapid Adhesive X 60 is a rapidly hardening adhesive consisting of 1 liquid component and 1 powder component. At 20°C the hardening time is approximately 3 minutes.
The X 60 is mainly used when joining measuring equipment to specimens in different types of tests. It has a good capability of joining different materials such as metals, porcelain, glass and concrete. The joined surfaces shall be clean and free from dust and grease before applying the adhesive. The adhesive capacity is increased if the surfaces are roughened.

When hardened, the adhesive capacity remains in a temperature range of -200–+60°C.

For product sheets and more extensive information see [17].

4.3.5   Bostik Multifog 2640

The Bostik Multifog 2640 is a multi-purpose sealant. It is hardening by the humidity in the surrounding air. It adheres to different materials such as metals, glass, plastics and also to porous materials as concrete and brick. The Bostik Multifog 2640 shows very good resistance to UV-light.

The temperature span suitable for application and hardening is +5–+35°C. The depth of hardening is 4 mm after 1 day and 15 mm after 7 days. The hardened sealant shows durability in the temperature span -30–+80°C.

For product sheets and more extensive information see [18].

4.3.6   Bostik Simson ISR

The Bostik Simson ISR (Industrial Special Range) is a series of Bostik products specially developed for industrial use. They are based on the Silyl Modified Polymer (SMP) and hardens as traditional silicones with the moisture of the surrounding air. The Simson ISR products hardens with a depth of 3 mm after 1 day and subsequently with an increasing depth of approximately 1 mm per day.

The thickness recommended for adhesive joints is 2 mm. The products has shown durability in a temperature range of -40-+120°C. For the hardening process a temperature of +5–+35°C i recommended.

The Simson ISR 70-03 is used as adhesive and sealant in various applications. The 70-04 is used as an adhesive when attaching windows in vehicles. The 70-12 is developed for attaching wind-shields in cars and other vehicles.

For product sheets and more extensive information see [18].

4.4   Results

4.4.1   Summary and Analysis, Specimens 6 mm (Silicones)
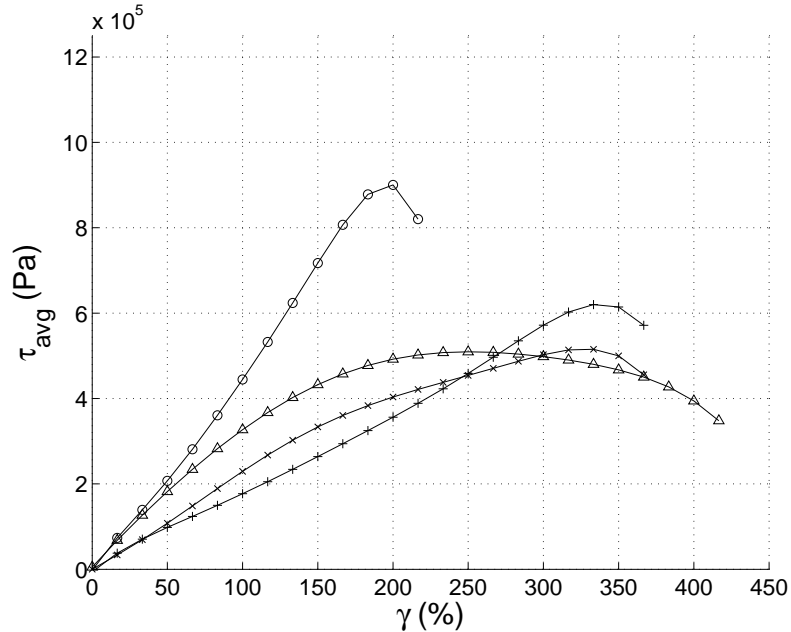
Figure 4.5: *Measured data from the 6 mm specimens. The different mechanical characteristics of the four adhesives can clearly be observed. The curves are marked as follows: Bostik Silikon Bygg 2685 (x), Bostik Marmorsilikon (+), Sika Elastosil SG 20 (o), Sika Elastosil 605 S (triangle).*

Within each product the different specimens showed a very uniform behaviour regarding stiffness, whereas differences were noted in ultimate strength and strain.
When the four different adhesives were compared a very different mechanical behaviour was observed. The diagrams in figure 4.5 show differences regarding stiffness and ultimate load. The adhesives Bostik Marmorsilikon and Sika Elastosil SG 20 show a rising curve that comes to a rapid failure. The other two adhesives, Bostik Silikon Bygg 2685 and especially Sika Elastosil 605 S, show significant deformations without increase in applied load in the ultimate part of the curve before the failure. These deformations may influence positively when a larger geometry of an adhesive joint is studied (because of stress-concentrations on the edges of the adhesive joint). The fracture of the silicones had in general the same characteristics for the four different silicones. The fractures were usually initiated along the edges and at the corners, often at local defects where the silicone were not properly attached to the glass. Though the fracture usually started at local defects in the adhesive interface between silicone and glass, not one single specimen suffered a propagated adhesive failure between the glass and the silicone. All fractures were propagated internally in the silicone which means that the adhesive bonds between the tested silicones and

the glass are good. Photographs of typical fracture surfaces are shown in figure 4.6 on page 32.

The number and size of the defects showed a high degree of variation between the specimens. However, no connection between the defects and the variations in ultimate capacity could be observed. This allows the conclusion to be drawn that the initial defects and imperfections are of minor significance to the load capacity of the specimen.

The FE-simulations revealed concentrations of stress along the edges of the adhesives. From these stress concentrations the critical shear-stress was extracted. Figure 4.7 on page 32 visualizes a typical shear-stress distribution of the 6 mm specimens.

Results

A summary of the results of the tested silicones with joint thickness 6 mm is given in the tables 4.2 and 2.

Table 4.2: *Comparison of the results of the 6 mm specimens. The presented values are the mean values from the measured data.*

	$G_{20\%}$ (MPa)	$\tau_{avg,u}$ (MPa)	τ_{cr} (MPa)	γ_u (%)
Bostik Silikon Bygg 2685	0.24	0.534	1.2	347
Bostik Marmorsilikon	0.18	0.606	1.1	333
Sika Elastosil SG 20	0.46	0.978	2.5	213
Sika Elastosil 605 S	0.37	0.515	0.9	249

Table 4.3: *Corresponding material models used in the FE-simulations for the 6 mm specimens.*

	Material Model	C_{10}	C_{01}	D_1
Bostik Silikon Bygg 2685	Mooney-Rivlin	$51 \cdot 10^3$	$77 \cdot 10^3$	-
Bostik Marmorsilikon	Neo-Hooke	$93 \cdot 10^3$	-	-
Sika Elastosil SG 20	Neo-Hooke	$247 \cdot 10^3$	-	-
Sika Elastosil 605 S	Mooney-Rivlin	$10 \cdot 10^3$	$190 \cdot 10^3$	-
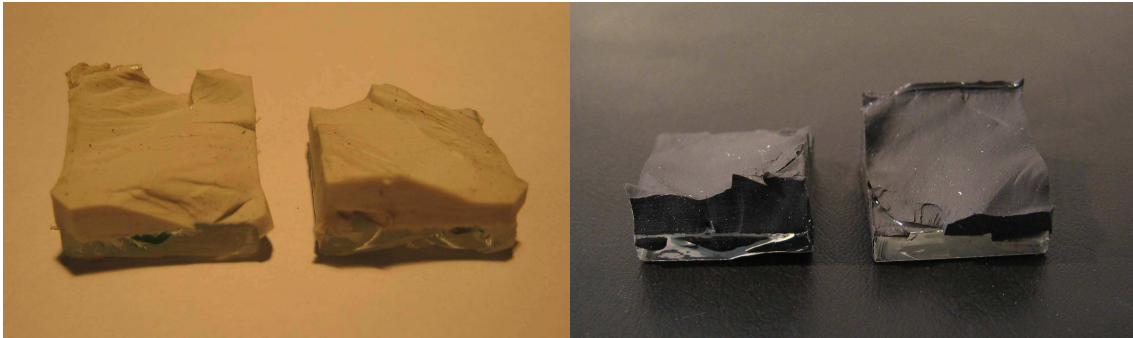
Figure 4.6: *Typical characteristics of the fracture in the 6 mm specimens. On both photographs the small defects where the fracture was initiated can be seen.*
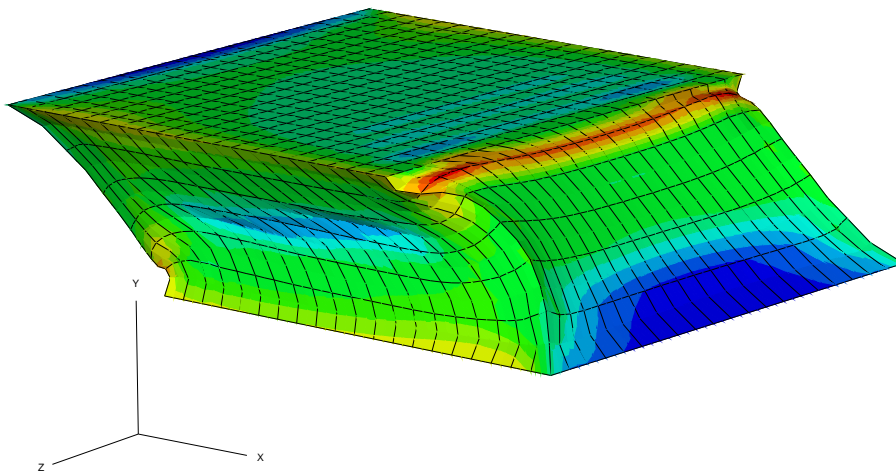
Figure 4.7: *Typical shear stresses (S12) in the 6 mm specimens visualized from the FE-simulation. The critical shear stress was extracted from the darkest coloured area close to the edge, where the highest concentration of shear stress was observed.*

4.4.2 Summary and Analysis, Specimens 2 mm (Silicones)
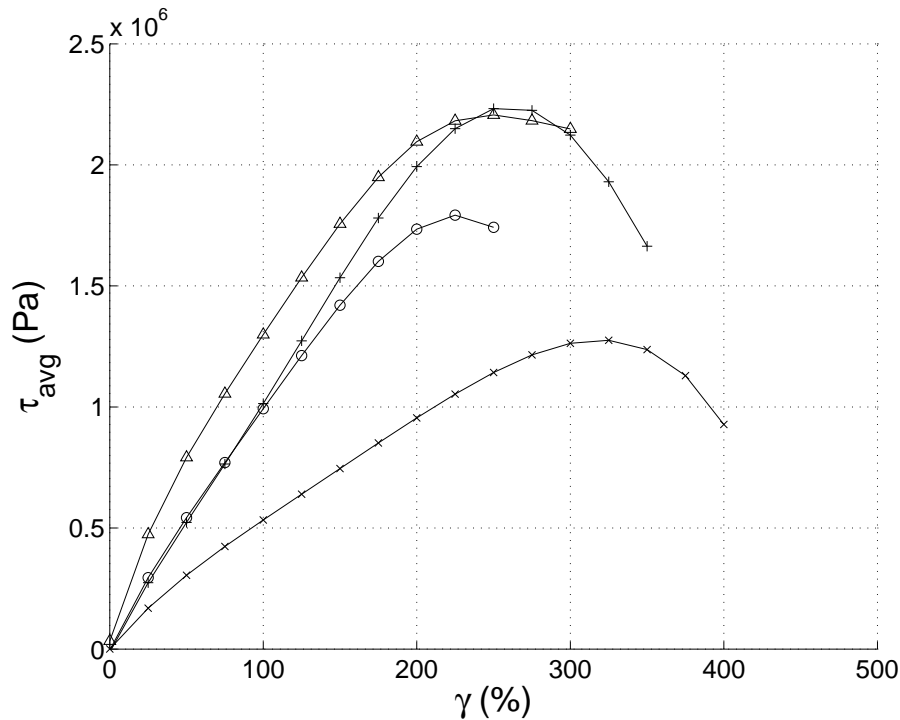
Figure 4.8: *Curves of shear-stress versus shear-strain for the 2 mm specimens of the Bostik adhesives/sealants. The curves are marked as follows: Multifog 2640 (x), Simson ISR 70-03 (+), Simson ISR 70-04 (o), Simson ISR 70-12 (triangle).*

The Bostik adhesives/sealants showed different mechanical behaviour. The softest adhesive was the Multifog 2640, which also had the lowest ultimate strength. Simson ISR 70-03 and 70-04 showed similar initial stiffness but the 70-03 had a higher ultimate strength. Simson ISR 70-12 showed an ultimate strength that was more or less the same as 70-03 but the 70-12 had a higher initial stiffness. A comparison of the curves of average shear-stress versus shear-strain for the four different Bostik silicones is shown in figure 4.8. A summary of the results of the tested silicones with joint thickness 2 mm are given in table 4.4.

The four adhesives/sealants were modelled in Abaqus with the Mooney-Rivlin material model. In table 4.5 the material constants for each adhesive are presented.

The fractures in Multifog 2640 and Simson ISR 70-03 were internal and propagated within the silicone joints. The fractures were, as in the 6 mm joints, initiated at the edges where the highest concentrations of shear stresses were observed in the FE-calculations.

In Simson ISR 70-04 and 70-12 adhesive failure in the interface between glass and adhesive were observed. The adhesive failure was never total and the fracture was propagated within the adhesive. In figure 4.9 on page 35, two photographs of typical fracture surfaces are shown.

The FE-simulations revealed concentrations of stress along the edges of the adhesives. From these stress concentrations, the critical shear-stress was extracted. Figure 4.10 on page 35 visualizes a typical shear-stress distribution of the 2 mm specimens.

Results

A summary of the results of the tested silicones with joint thickness 6 mm is given in the tables 4.4 and 4.5.

Table 4.4: *Comparison of the results from the 2 mm specimens of the Bostik adhesives/sealants. The presented values are the mean values from the measured data.*

	$G_{20\%}$ (MPa)	$\tau_{avg,u}$ (MPa)	τ_{cr} (MPa)	γ_u (%)
Multifog 2640	0.49	1.28	2.1	317
Simson ISR 70-03	1.04	2.28	4.4	263
Simson ISR 70-04	0.98	1.86	3.5	230
Simson ISR 70-12	1.17	2.29	4.0	266

Table 4.5: *Corresponding material models used in the FE-simulations for the 2 mm specimens of the Bostik adhesives.*

	Material Model	C_{10}	C_{01}	D_1
Multifog 2640	Mooney-Rivlin	$100{\cdot}10^3$	$150{\cdot}10^3$	-
Simson ISR 70-03	Mooney-Rivlin	$200{\cdot}10^3$	$330{\cdot}10^3$	-
Simson ISR 70-04	Mooney-Rivlin	$100{\cdot}10^3$	$400{\cdot}10^3$	-
Simson ISR 70-12	Mooney-Rivlin	$100{\cdot}10^3$	$500{\cdot}10^3$	-
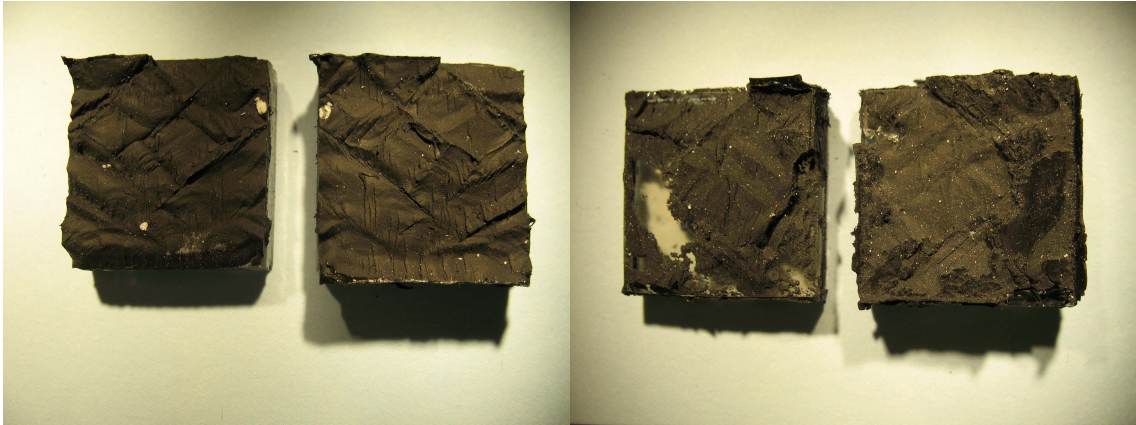
Figure 4.9: *Typical characteristics of the fracture in the 2 mm specimens. The left photograph shows a specimen of Simson ISR 70-03 where the fracture occured internally. The right photograph shows a specimen from Simson ISR 70-12 with an adhesive failure in the interface between glass and adhesive.*
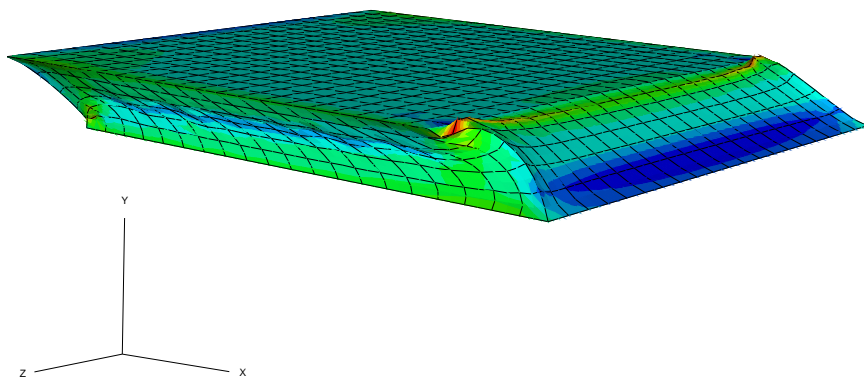
Figure 4.10: *Typical shear stresses (S12) in the 2 mm specimens visualized from the FE-simulation. The critical shear stress was extracted from the darkest coloured area close to the edge, where the highest concentration of shear stress was observed.*

4.4.3   Summary and Analysis, Specimens 0.3 mm (Silicones)
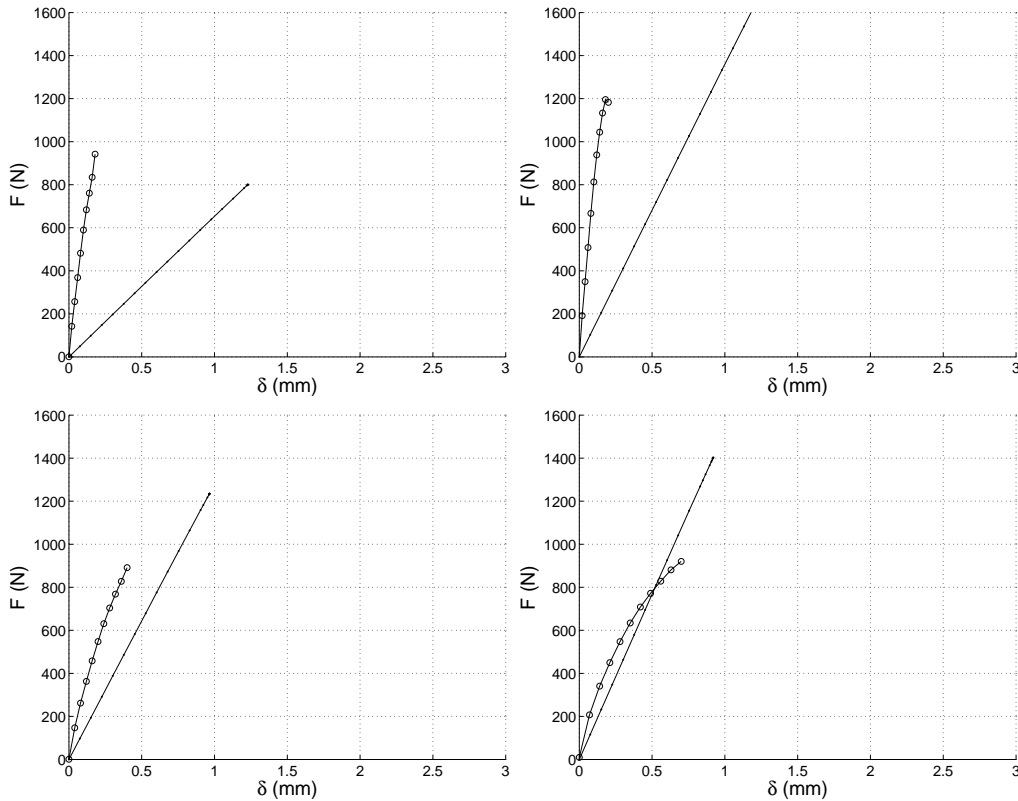
Figure 4.11: *The fitted curve of the measured data (circles and line) compared to FE-calculations (line) with the material models from the 2 mm tests of the same adhesive. Starting from top left and moving clockwise is shown Multifog 2640, Simson ISR 70-03, 70-12, 70-04.*

The Bostik adhesives/sealants tested with the thickness of 2 mm were also tested in a thin joint, squeezed together as much as possible. Three specimens were made for each adhesive. The purpose and objective of these tests was to compare the test results with the material models of the 2 mm specimens in order to evaluate if these models were valid for the thinner joints as well.
The Bostik adhesives showed a different behaviour in the thin joints than in the 2 mm joints. In all tests the silicones showed a stiffer behaviour than the FE-calculations done with the same material models as in the 2 mm tests. The silicone that best corresponds with the 2 mm material model is the Bostik 7012. A comparison of the tests and the FE-calculations is shown in figure 4.11.
The material models evaluated from the test data of the 2 mm specimens of the same adhesives are observed not to be valid for the thinner joints. However it is observed that the stiffer the adhesive is the better the material model corresponds.

4.4.4   Summary and Analysis, Specimens 0.2–0.3 mm (Glues)
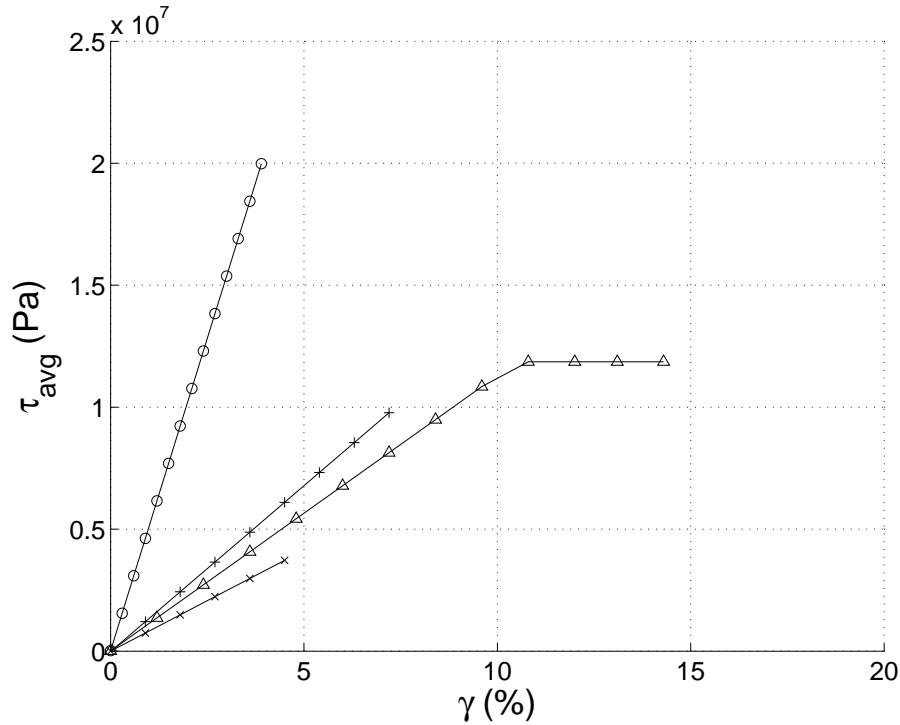
Figure 4.12: *Curves of shear-stress versus shear-strain for the stiff adhesive, 0.2–0.3 mm specimens. The curves are marked as follows: Casco Polyurethan (x), X 60 (+), Casco Strong Epoxy (o), Casco UV-hardening glass-glue (triangle).*

The four tested stiff adhesives showed different mechanical behaviour. A comparison of the curves of average shear-stress versus shear-strain for the four different Bostik silicones is shown in figure 4.12. Table 4.6 shows the mean-values of the different initial shear-modulus and ultimate stresses and strains for the silicones.

The critical shear stress of the stiffer adhesives equaled the mean ultimate shear stress due to the homogenous distribution of the shear stresses.

Epoxy and X60 came to a rapid failure when reaching their ultimate load. The polyurethan glue decreased in stiffness before reaching its ultimate load. The UV-hardening glue reached its ultimate load and was thereafter continuing to deform under constant load until reaching its ultimate strain.

The four stiff adhesives were modelled in Abaqus and described with linear-elastic material models. In table 3 the material constants for each glue are presented.

The fracture in the polyurethan glue seems to be an internal fracture and not due to adhesive failure between glass and glue. However this is hard to evaluate due to the pattern of gas bubbles emerging in the hardening process.

The X-60 glue suffered adhesive failure in the connection between glass and glue. The glue cracked commonly on both glass surfaces and it could be peeled of as a brittle interlayer that fractured when trying to remove it.

The Epoxy and UV-hardening glue also suffered adhesive failure in the interface between glass and adhesive but the adhesive layer stayed together and could be peeled of as one piece, as a non-fractured, soft, thin film. Typical fracture surfaces can be observed in figure 4.13 on page 39.

Results

A summary of the results of the tested adhesives with joint thickness 0.2–0.3 mm is given in the tables 4.6 and 3.

Table 4.6: *Values of initial shear-modulus and mean-values for ultimate strength and strain for the tested stiff adhesives (glues).*

	$G_{20\%}$ (MPa)	$\tau_{avg,u}$ (MPa)	τ_{cr} (MPa)	γ_u (%)
Casco Polyurethan	82.5	3.8	3.8	4.5-10
HBM Rapid Adhesive X 60	139	10.9	10.9	7.8
Casco Strong Epoxy Professional	514	20.5	20.5	3.9
Casco UV-hardening Glass-Glue	113	11.9	11.9	10-15

Table 4.7: *Corresponding material models for the four tested stiff adhesives (glues).*

	Material Model Linear-elastic	*E* (MPa)	*ν* (-)
Casco Polyurethan 1809	Linear-elastic	200	0.25
HBM Rapid Adhesive X 60	Linear-elastic	320	0.25
Casco Strong Epoxy Professional	Linear-elastic	1500	0.25
Casco UV-hardening Glass-Glue	Linear-elastic	300	0.25
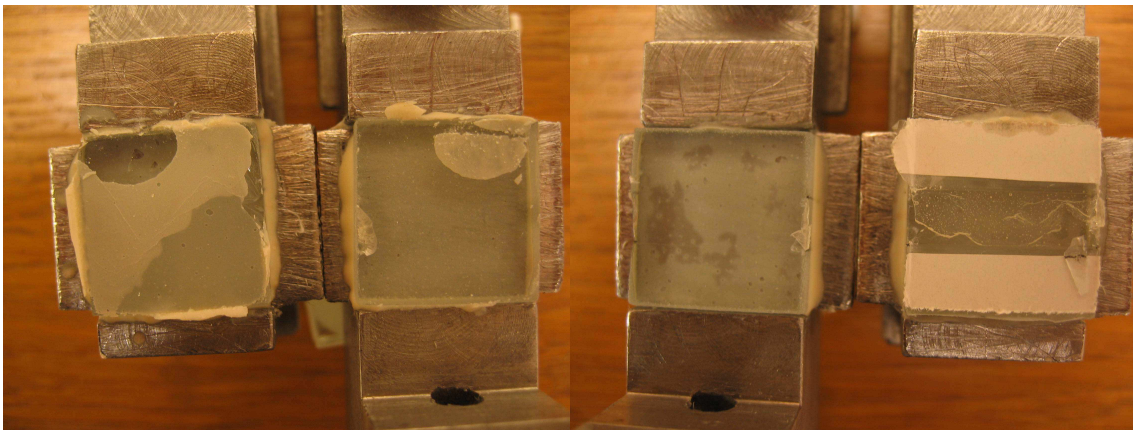
Figure 4.13: *Typical characteristics of the fracture in the specimens of the stiffer adhesives. On the left photograph is the X 60 adhesive. The X 60 fractured in the interface with both glass-surfaces. The thin layer of adhesive could subsequently be peeled of in small brittle flakes. The right picture shows the Casco Strong Epoxy Professional which has failed entirely on one side. At the lower left corner of the adhesive ribbon can be observed a failure in the interface on the other side, under the adhesive layer.*

4.5   Specimens 6 mm (Silicones)

4.5.1   Test Set-Up

Table 4.8: *Test set-up for 6 mm specimens*

Number of specimens	5
Joint thickness	6 mm
Load application	Tension
Deformation speed	10 mm/min
Deformation sensor	DSMTS
Load cell	0-10 kN

Four different silicone adhesives/sealants were tested with the joint thickness 6 mm. Five specimens were tested for each product. These silicones had been prepared 1 year before the tests were conducted. They had been stored in a paper box, in a tempered room without being exposed to direct sun-light.

Tensile forces were used for the application of load in order to admit the large deformations of the thick silicone joints. All application of forces were controlled by deformation with a constant deformation speed of 10 mm per minute.

The tested adhesives/sealants were:

- Bostik Silikon Bygg 2685, Light Grey

- Bostik Marmorsilikon, Marble Grey

- Sika Elastosil SG 20, Black

- Sika Elastosil 605 S, Dull-Black

4.5.2 Bostik Silikon Bygg 2685, Light Grey
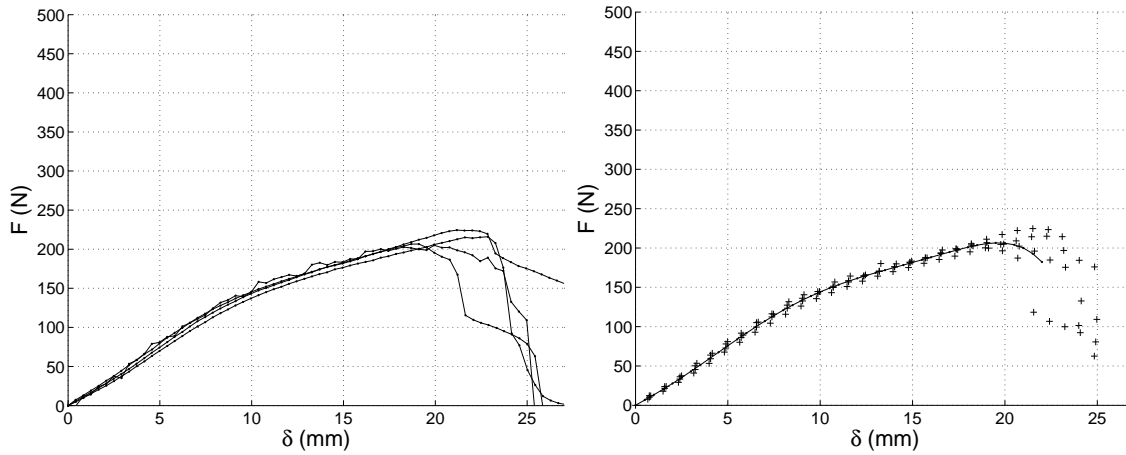
Figure 4.14: *Plots of the measured data of Bostik Silikon Bygg 2685. The diagram to the left shows the applied force versus the deformation. The diagram to the right shows force versus deformation (+) and the curve fitted to the measured data in a least square sense (line).*

The first specimen was used to test the testing equipment and was therefore neglected in the evaluation of the data. The curves of the four remaining specimens showed a uniform behaviour of the silicones, though with variations in ultimate load-capacity and ultimate deformation. The diagrams in figure 4.14 show the results from the four tested specimens.

The stiffnes of the tested specimens show a similar behaviour in the initial part of the tests. The ultimate load capacity and deformations vary between the tested specimens. The maximum, minimum and mean measured values of the four tested specimens are shown in table 4.9.

The test was modelled in Abaqus with the Mooney-Rivlin material model. The best corresponding material constants are shown in table 4.10. A comparison of the test-results and the FE-calculations is shown in the diagrams in figure 4.15.

The initial shear modulus for Bostik Silikon Bygg 2685 was calculated to:

- $G_{20\%} = 0.24$ MPa

Table 4.9: *Maximum, minimum and mean values for the measured data of Bostik Silikon Bygg 2685.*

		Maximum	*Minimum*	*Mean*
Ultimate load	(N)	225	206	213
Ultimate shear stress	(MPa)	0.562	0.515	0.534
Ultimate deformation	(mm)	22.9	19.0	20.8

Table 4.10: *Corresponding material model in the FE-calculations for Bostik Silikon Bygg 2685*

Material Model	C_{10}	C_{01}	D_1
Mooney-Rivlin	$51 \cdot 10^3$	$77 \cdot 10^3$	-

Concentration of shear stress was observed on the edges of the adhesive. Figure 4.7 on page 32 is visualizing the typical stress distribution of the 6 mm specimens. The stress concentrations occured where the fracture was observed to be initiated during the tests. The critical shear stress was extracted from this area of stress concentrations:

- Critical shear stress: $\tau_{cr} = 1.2$ MPa
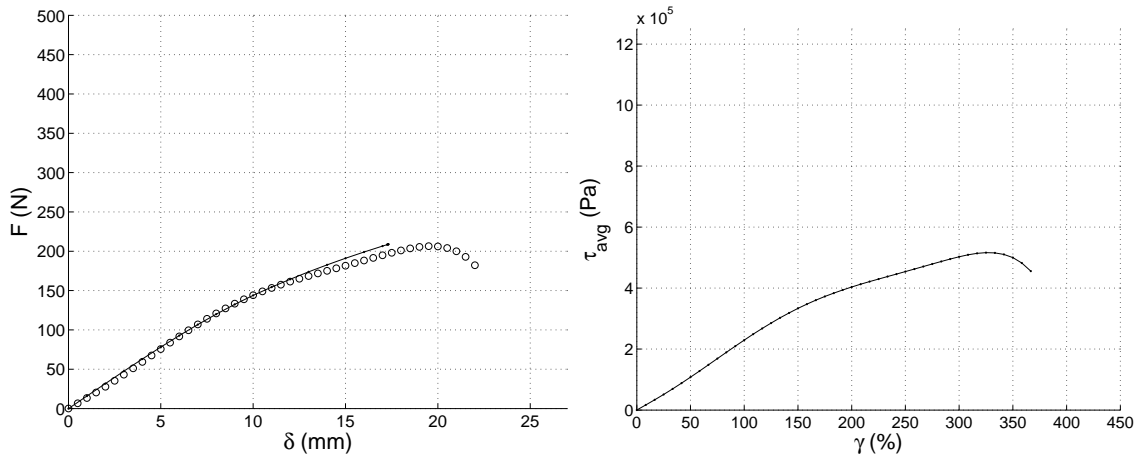
Figure 4.15: *Results from the FE-evaluation of Bostik Silikon Bygg 2685. The diagram to the left is showing the fitted curve from the tests (circles) compared with the calculated results from the FE-evaluation (line). The diagram to the right shows the average shear-stress (τ_{avg}) versus the shear-strain extracted from the FE-model.*

4.5.3   Bostik Marmorsilikon, Marble Grey
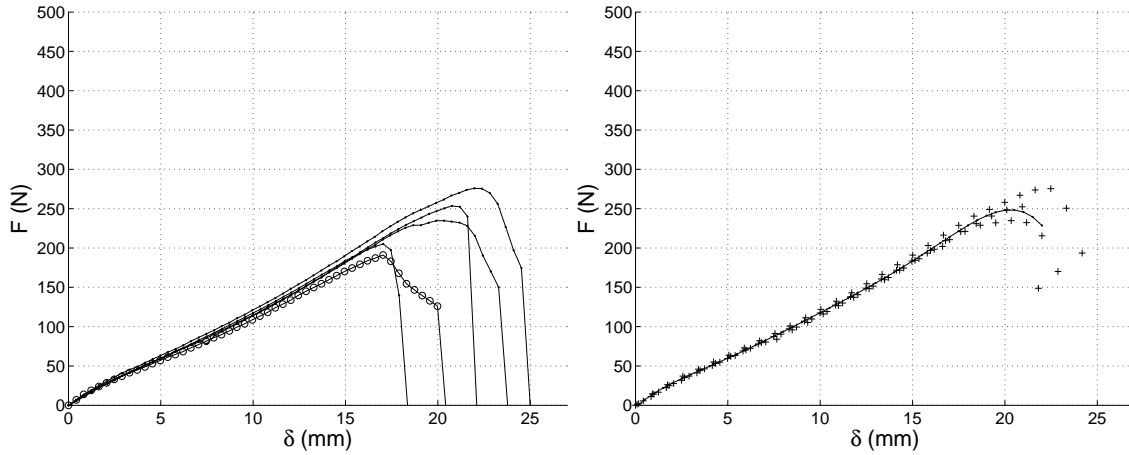
Figure 4.16: *Plots of the measured data of Bostik Marmorsilkon. The diagram to the left shows applied force versus deformation. The diagram to the right shows force versus deformation (+) and the curve fitted to the measured data in a least square sense (line).*

One of the specimens suffered failure in the glass while mounting the specimen in the testing equipment. Therefore only four specimens will be regarded in the evaluation. The specimens showed a uniform behaviour, though with variations in ultimate load and ultimate strain. The diagrams in figur 4.16 show the measured data.

The ultimate load and deformations vary between the tested specimens. The maximum, minimum and mean measured values of the tested specimens are shown in table 4.11.

The test was modelled in Abaqus with the Neo-Hooke material model. The best corresponding material constants are shown in table 4.12. A comparison of the test-results and the FE-calculations is shown in the diagrams in figure 4.17. Due to the large deformations the FE-calculations were unable to follow the measured data to the ultimate load. Therefore the calculated results in this model were lower than the real results.

The initial shear modulus for Bostik Marmorsilikon was calculated to:

- $G_{20\%} = 0.18$ MPa

Table 4.11: *Maximum, minimum and mean values for the measured data of Bostik Marmorsilikon.*

		Maximum	Minimum	Mean
Ultimate load	(N)	276	205	242
Ultimate shear stress	(MPa)	0.690	0.513	0.606
Ultimate deformation	(mm)	22.0	17.0	20.0

Table 4.12: *Corresponding material model in the FE-calculations for Bostik Marmorsilikon*

Material Model	C_{10}	D_1
Neo-Hooke	$93 \cdot 10^3$	-

Concentration of shear stress was observed on the edges of the adhesive. Figure 4.7 on page 32 is visualizing the typical stress distribution of the 6 mm specimens. The stress concentrations occured where the fracture was observed to be initiated during the tests. The critical shear stress was extracted from this area of stress concentrations:

- Critical shear stress: $\tau_{cr} = 1.1$ MPa
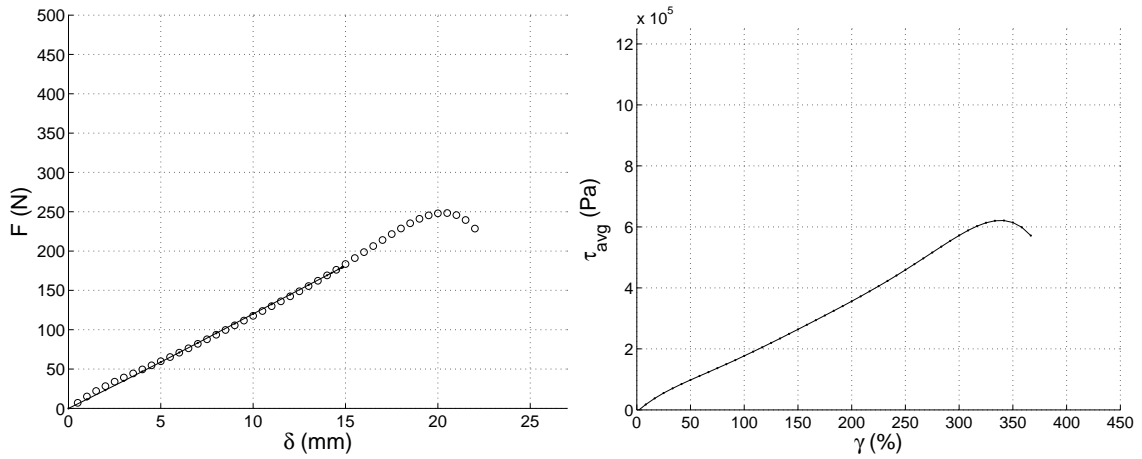
Figure 4.17: *Results from the FE-evaluation of Bostik Marmorsilikon. The diagram to the left shows the fitted curve from the tests (circles) compared with the calculated results from the FE-evaluation (line). The diagram to the right shows the average shear-stress (τ_{avg}) versus the shear-strain extracted from the FE-model.*

4.5.4 Sika Elastosil SG 20, Black
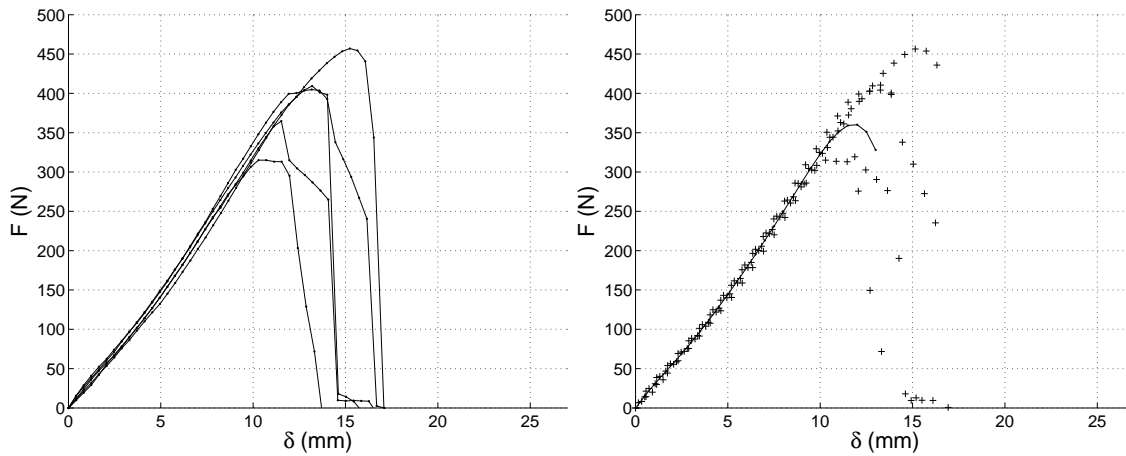
Figure 4.18: *Plots of the measured data of Sika Elastosil SG 20. The diagram to the left shows the applied force versus the deformation. The diagram to the right shows force versus deformation (+) and the idealized curve fitted to the measured data in a least square sense (line).*

As the adhesives in the previous tests the Sika Elastosil SG 20 also showed a very uniform behaviour between the specimens in the initial part of the tests. However, as in the Bostik silicones, there could be seen quite large variations in the ultimate load and ultimate deformation. The diagrams in figure 4.18 show the results from the tested specimens.

The ultimate load and deformations varied between the tested specimens. The maximum, minimum and mean measured values of the tested specimens are shown in table 4.13.

The test was modelled in Abaqus with the Neo-Hooke material model. The best corresponding material constants are shown in table 4.14. A comparison of the test-results and the FE-calculations is shown in the diagrams in figure 4.19. The FE-calculations followed the measured data above the ultimate capacity. The data, extracted from this model, is taken from the step closest to the mean values given in table 4.13.

For Elastosil SG 20 the initial shear modulus was calculated to:

- $G_{20\%} = 0.46$ MPa

Table 4.13: *Maximum, minimum and mean values for the measured data of Sika Elastosil SG 20.*

		Maximum	Minimum	Mean
Ultimate load	(N)	458	317	391
Ultimate shear stress	(MPa)	1.15	0.792	0.978
Ultimate deformation	(mm)	15.5	10.5	12.8

Table 4.14: *Corresponding material model in the FE-simulations for Sika Elastosil SG 20*

Material Model	C_{10}	D_1
Neo-Hooke	$247 \cdot 10^3$	-

Concentration of shear stresses was observed on the edges of the adhesive. Figure 4.7 on page 32 is visualizing the typical stress distribution of the 6 mm specimens. The stress concentrations occured where the fracture was observed to be initiated during the tests. The critical shear stress was extracted from this area of stress concentrations:

- Critical shear stress: $\tau_{Cr} = 2.5$ MPa
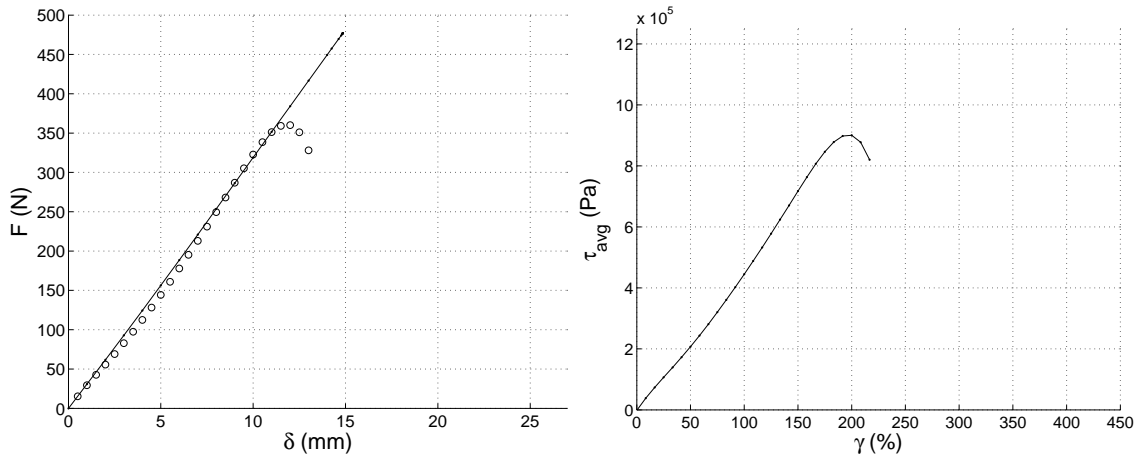
Figure 4.19: *Results from the FE-evaluation of Sika Elastosil SG 20. The diagram to the left is showing the fitted curve from the tests (circles) compared with the calculated results from the FE-evaluation (line). The diagram to the right shows the average shear-stress (τ_{avg}) versus the shear-strain extracted from the FE-model.*

4.5.5 Sika Elastosil 605 S, Dull-Black
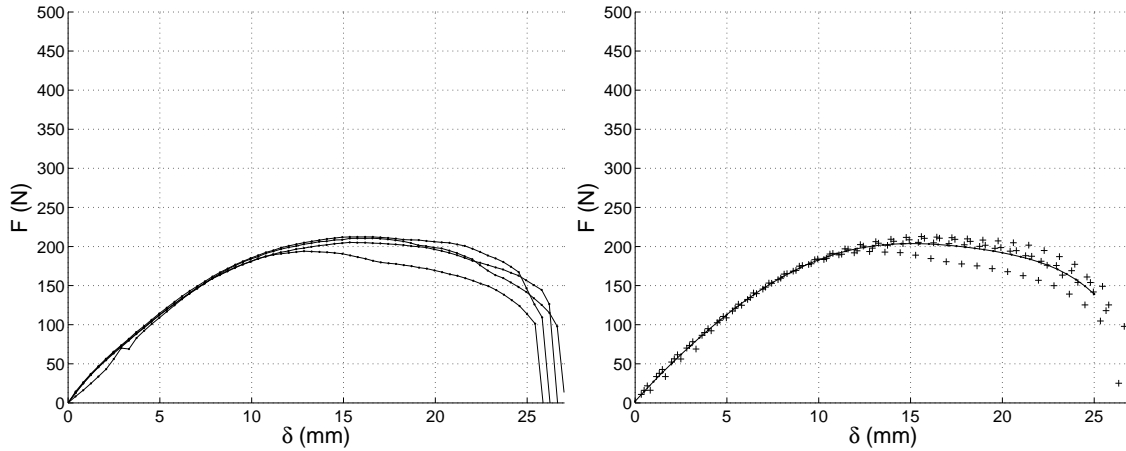
Figure 4.20: *Plots of the measured data of Sika Elastosil 605 S. The diagram to the left shows the applied force versus the deformation. The diagram to the right shows force versus deformation (+) and the curve fitted to the measured data in a least square sense (line).*

The Sika Elastosil 605 S showed a different behaviour than the previously tested silicones (though regarding ultimate load similar to Bostik Silikon Bygg 2685). One could clearly see a behaviour where continuing deformation occured without significant changes in the applied load. This had not been seen in the previously tested silicones.

One of the specimens was fractured while mounted in the testing equipment and therefore only four tests were used in the evaluation. The diagrams in figure 4.20 show the results from the four tested specimens.

The specimens showed a very similar behaviour in stiffness, ultimate load and ultimate deformation. The maximum, minimum and mean measured values of the four tested specimens are shown in table 4.15.

The test was modelled in Abaqus with the Mooney-Rivlin material model. The best corresponding material constants are shown in table 4.16. A comparison of the test-results and the FE-calculations is shown in the diagrams in figure 4.21. The FE-calculations were unable to follow the measured data to the ultimate capacity. Therefore the calculated results in this model was lower than the real results.

Table 4.15: *Maximum, minimum and mean values for the measured data of Sika Elastosil 605 S.*

		Maximum	*Minimum*	*Mean*
Ultimate load	(N)	213	194	206
Ultimate shear stress	(MPa)	0.532	0.486	0.515
Ultimate deformation	(mm)	16.1	13.0	14.9

Table 4.16: *Corresponding material model in the FE-simulations for Sika Elastosil 605 S*

Material Model	C_{10}	C_{01}	D_1
Mooney-Rivlin	$10 \cdot 10^3$	$190 \cdot 10^3$	-

For Elastosil 605 S the initial shear modulus was calculated to:

- $G_{20\%} = 0.37$ MPa

Concentration of shear stresses was observed on the edges of the adhesive. Figure 4.7 on page 32 is visualizing the typical stress distribution of the 6 mm specimens. The stress concentrations occured where the fracture was observed to be initiated during the tests. The critical shear stress was extracted from this area of stress concentrations:

- Critical shear stress: $\tau_{cr} = 0.9$ MPa
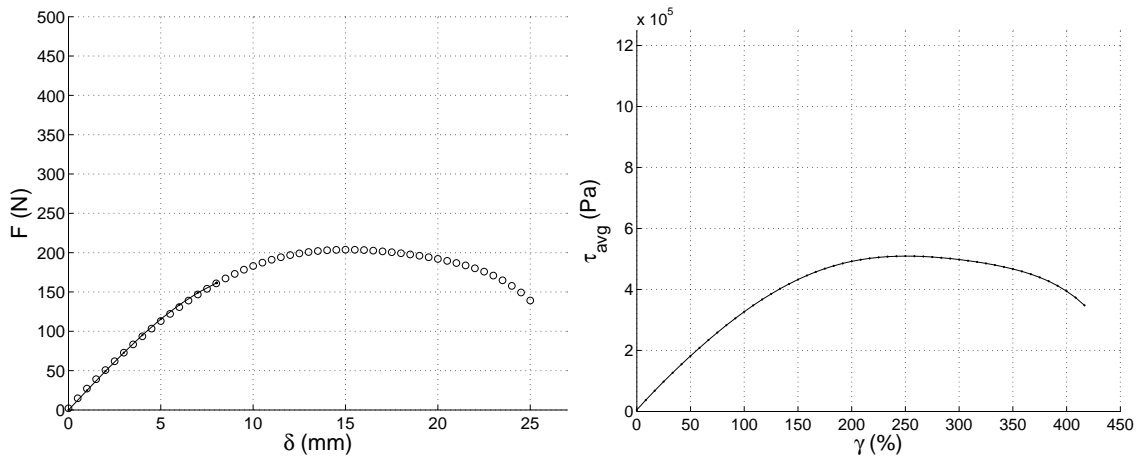
Figure 4.21: *Results from the FE-evaluation of Sika Elastosil 605 S. The diagram to the left is showing the fitted curve from the tests (circles) compared with the calculated results from the FE-simulation (line). The diagram to the right shows the average shear-stress (τ_{avg}) versus the shear-strain extracted from the FE-model.*

4.6 Specimens 2 mm (Silicones)

4.6.1 Test Set-Up

Table 4.17: *Test set-up for 2 mm specimens*

Number of specimens	5
Joint thickness	2 mm
Load application	Tension
Deformation speed	3.5 mm/min
Deformation sensor	DSMTS
Load cell	± 10 kN

Four adhesives/sealants were tested with the joint thickness 2 mm. Each product were tested with five specimens. The products are Bostik silicones and the silicone-like Simson ISR-products based on the Silyl Modidied Polymer (SMP).

Tensile forces were used for the application of force in order to admit the large deformations of the thick silicone joints. All application of force were controlled by deformation with a constant deformation speed of 3.5 mm per minute.

The tested adhesives/sealants were:

- Bostik Multifog 2640, Black

- Bostik Simson ISR 70-03, Black

- Bostik Simson ISR 70-04, Black

- Bostik Simson ISR 70-12, Black

4.6.2   Bostik Multifog 2640, Black
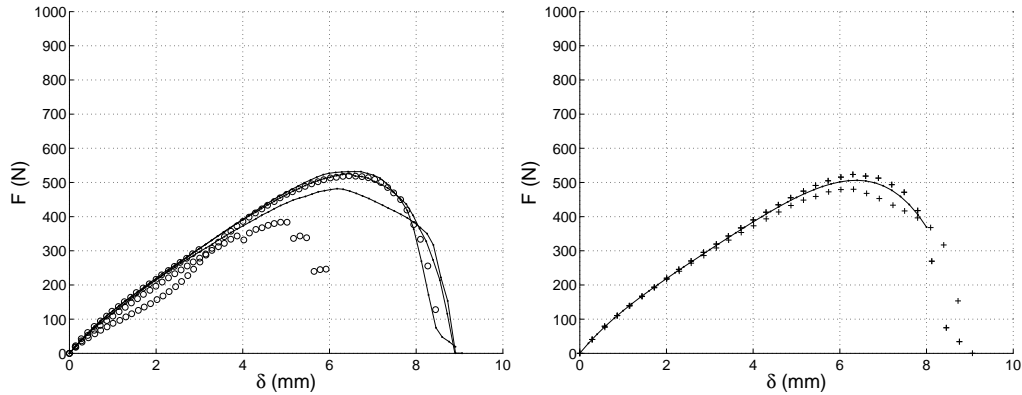
Figure 4.22: *Plots of the measured data of Bostik Multifog 2640. The diagram to the left shows the applied force versus the deformation. The diagram to the right shows force versus deformation (+) and the curve fitted to the measured data in a least square sense (line).*

The specimens showed a uniform behaviour with similar stiffness and ultimate load. Some minor defects were observed in the adhesive joints (bubbles and cuts).

Two specimens (the deviating curves shown with circles in the left diagram in figure 4.22) suffered an adhesive failure between the testing equipment and the specimen. One of them was remounted and tested again. In the second test it showed a less stiff behaviour up until the point of failure where it more or less again followed the previous tests. Due to the adhesive failure in these specimens only the three successful tests was regarded in the evaluation.

The stiffnes of the tested specimens were very similar in the initial part of the tests. However, the ultimate load and deformation varied between the tested specimens. The maximum, minimum and mean measured values of the three tested specimens are shown in table 4.18.

The test was modelled in Abaqus with the Mooney-Rivlin material model. The best corresponding material constants are shown in table 4.19. A comparison of the test-results and the FE-calculations is shown in the diagram in figure 4.23. The FE-calculations were unable to follow the measured data to the ultimate capacity. Therefore the calculated results in this model were lower than the real results.

Table 4.18: *Maximum, minimum and mean values for the measured data of Bostik Multifog 2640.*

		Maximum	*Minimum*	*Mean*
Ultimate load	(N)	533	482	514
Ultimate shear stress	(MPa)	1.33	1.20	1.28
Ultimate deformation	(mm)	6.5	6.2	6.3

Table 4.19: *Corresponding material model in the FE-simulations for Bostik Multifog 2640*

Material Model	C_{10}	C_{01}	D_1
Mooney-Rivlin	$100 \cdot 10^3$	$150 \cdot 10^3$	0

For Bostik Multifog the initial shear modulus was calculated to:

- $G_{20\%} = 0.49$ MPa

Concentration of shear stresses was observed on the edges of the adhesive. Figure 4.10 on page 35 is visualizing the typical stress distribution of the 2 mm specimens. The stress concentrations occured where the fracture was observed to be initiated during the tests. The critical shear stress was extracted from this area of stress concentrations:

- Critical shear stress: $\tau_{cr} = 2.1$ MPa
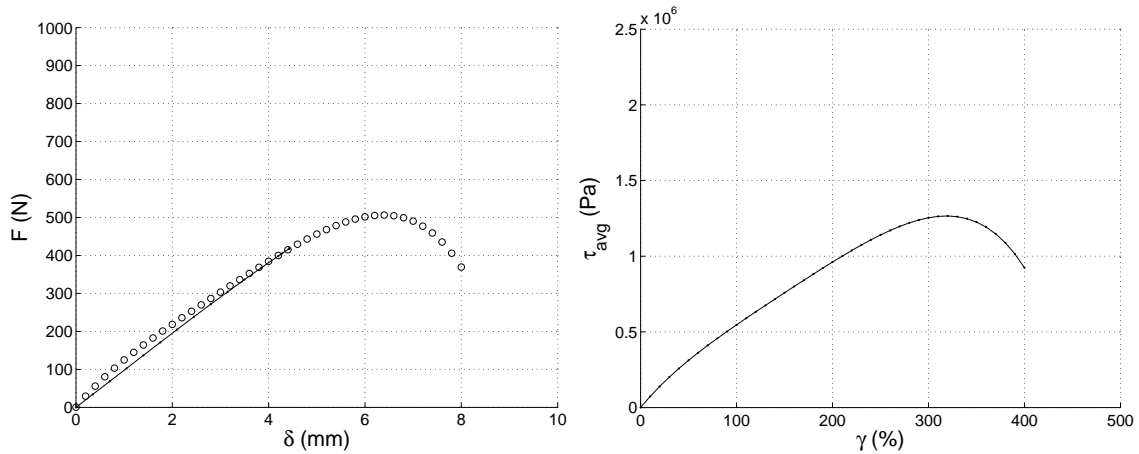
Figure 4.23: *Results from the FE-evaluation of Bostik Multifog 2640. The diagram to the left shows the fitted curve from the tests (circles) compared with the calculated results from the FE-evaluation (line). The diagram to the right shows the average shear-stress (τ_{avg}) versus the shear-strain extracted from the FE-model.*

Fracture Characteristics

The fracture ocurred internally, within the silicone, for all specimens. No failure in
the adhesive interface between the silicone and the glass was observed. Some minor
defects (air-bubbles and cuts) were observed when examining the fracture surface.
However these seem, judged by the uniform behaviour of the specimens, to have
no or minor influence on the ultimate load. Typical fracture surfaces are shown in
figure 4.24.
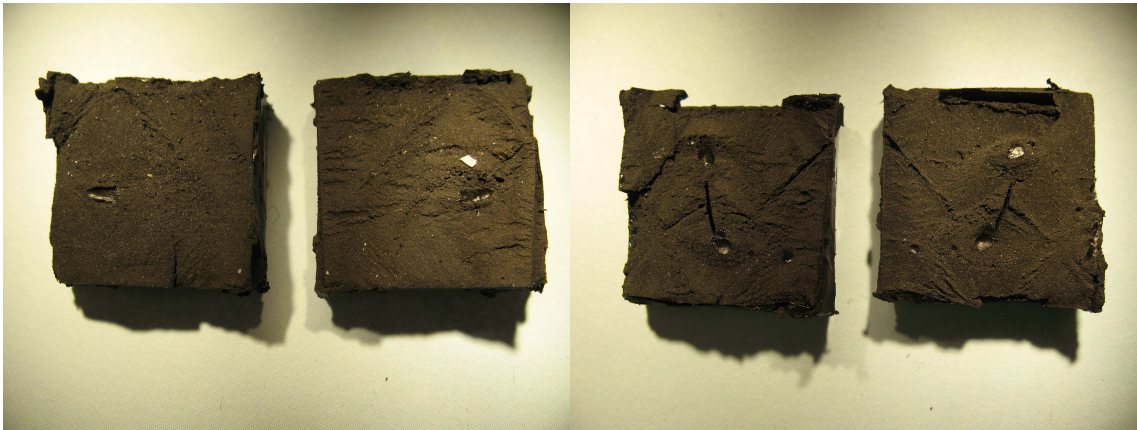
Figure 4.24: *Typical characteristics of the fracture in the specimens of Bostik Mul-
tifog 2640. On both photographs can be seen small defects like air-bubbles and cuts.*

4.6.3 Bostik Simson ISR 70-03, Black
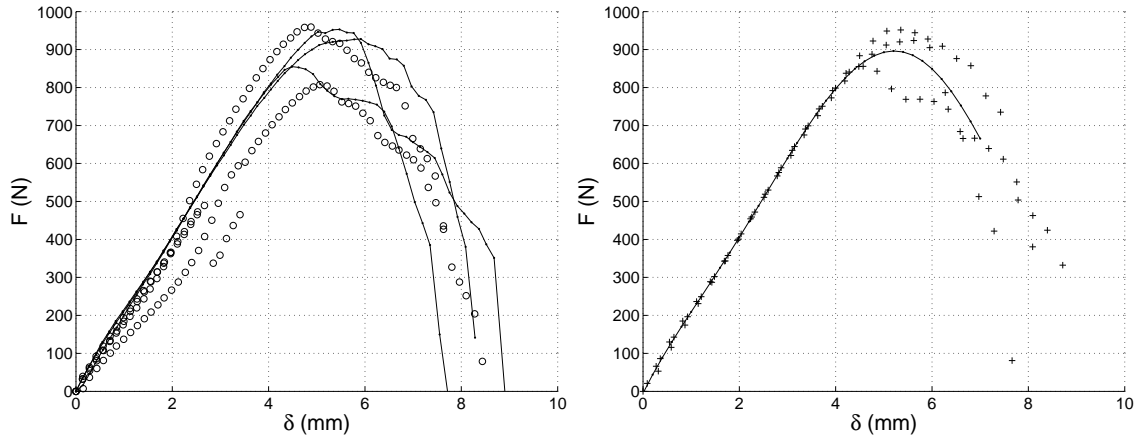
Figure 4.25: *Plots of the measured data of Bostik Simson ISR 70-03. The diagram to the left shows the applied force versus the deformation. The diagram to the right shows force versus deformation (+) and the curve fitted to the measured data in a least square sense (line).*

The specimens showed a uniform behaviour in the initial parts of the curve. In the ultimate load capacity variations was observed between the specimens.

Two specimens, specimens 3 and 4 (the deviating curves shown with circles in the left diagram in figure 4.25), suffered adhesive failure between the testing equipment and the specimen. They were remounted and tested again. In the second test specimen 3 showed a less stiff behaviour up until the breaking point and from the breaking point it followed the initial curve (slightly deviating from the other specimens, with a lower ultimate strength). Specimen 4 showed a decrease in stiffness in the second test up to the breaking point and thereafter an increase in stiffness.

Due to the adhesive failure in specimen 3 and 4, they were disregarded in the evaluation. Thus only three successful tests were regarded in the evaluation.

The stiffnes of the tested specimens showed a similar behaviour in the initial part of the tests. However, the ultimate load capacity and deformations varied slightly between the tested specimens. The maximum, minimum and mean measured values of the three evaluated specimens are shown in table 4.20.

Table 4.20: *Maximum, minimum and mean values for the measured data of Bostik Simson ISR 70-03.*

		Maximum	*Minimum*	*Mean*
Ultimate load	(N)	954	856	913
Ultimate shear stress	(MPa)	2.39	2.14	2.28
Ultimate deformation	(mm)	5.8	4.6	5.3

Table 4.21: *Corresponding material model in the FE-simulations for Bostik Simson ISR 70-03*

Material Model	C_{10}	C_{01}	D_1
Mooney-Rivlin	$200 \cdot 10^3$	$330 \cdot 10^3$	0

The test was modelled in Abaqus with the Mooney-Rivlin material model. The best corresponding material constants are shown in table 4.21. A comparison of the test-results and the FE-calculations is shown in the diagram in figure 4.26. The FE-calculations followed the measured data to the ultimate capacity.

For Simson ISR 70-03 the initial shear modulus was calculated to:

- $G_{20\%}$ = 1.04 MPa.

Concentration of shear stresses was observed on the edges of the adhesive. Figure 4.10 on page 35 is visualizing the typical stress distribution of the 2 mm specimens. The stress concentration occured where the fracture was observed to be initiated during the tests. The critical shear stress was extracted from this area of stress concentrations:

- Critical shear stress: τ_{cr} = 4.4 MPa
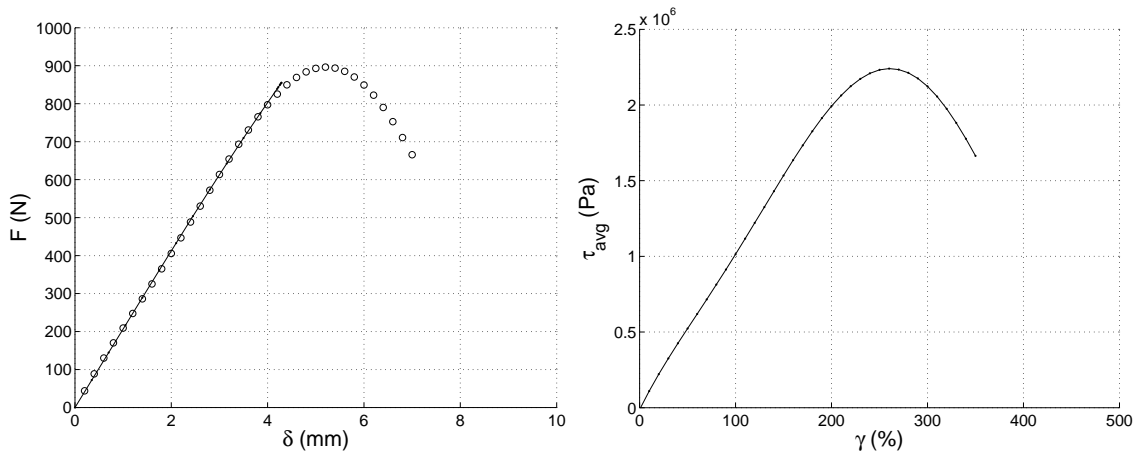
Figure 4.26: *Results from the FE-evaluation of Bostik Simson ISR 70-03. The diagram to the left shows the fitted curve from the tests (circles) compared to the calculated results from the FE-evaluation (line). The diagram to the right shows the average shear-stress (τ_{avg}) versus the shear-strain extracted from the FE-model.*

Fracture Characteristics

The fractures occured internally, within the adhesive, in all specimens. No failure in the interface between the adhesive and the glass was observed. Typical fracture surfaces are shown in figure 4.27.

Figure 4.27: *Typical characteristics of the fracture in the specimens of Bostik Simson ISR 70-03.*

4.6.4   Bostik Simson ISR 70-04, Black
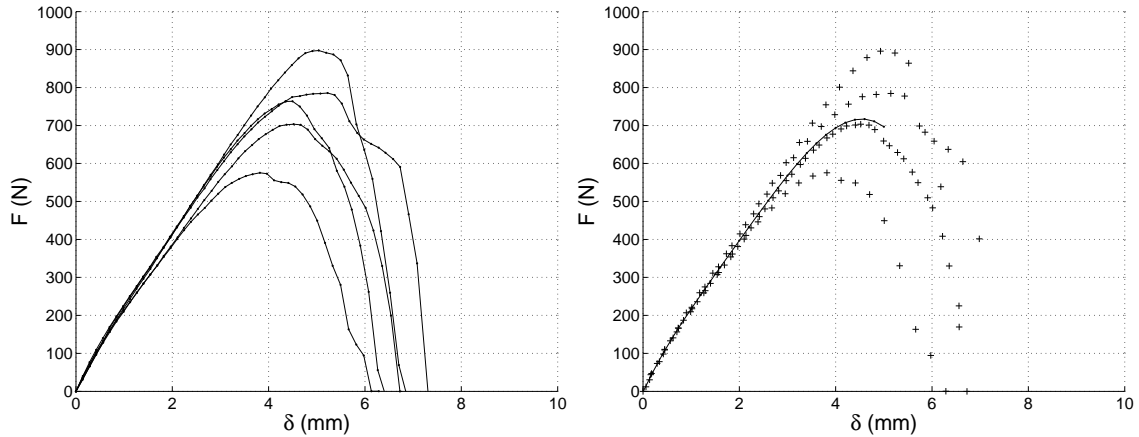
Figure 4.28: *Plots of the measured data of Bostik Simson ISR 70-04. The diagram to the left shows the applied force versus the deformation. The diagram to the right shows force versus deformation (+) and the curve fitted to the measured data in a least square sense (line).*

The specimens initially showed a uniform behaviour with variations in ultimate load and deformation. The ultimate load varied between 900 and 600 N. The two specimens with the lowest ultimate load suffered fracture in the interface between glass and adhesive. A visualization of the measured data is shown in the diagrams in figure 4.28.

The maximum, minimum and mean measured values of the tested specimens are shown in table 4.18.

The test was modelled in Abaqus with the Mooney-Rivlin material model. The best corresponding material constants are shown in table 4.23. A comparison of the test-results and the FE-calculations is shown in the diagram in figure 4.29. The FE-calculations were unable to follow the measured data to the ultimate capacity. Therefore, the calculated results in this model was lower than the real results.

For ISR 70-04 the initial shear modulus was calculated to:

- $G_{20\%} = 0.98$ MPa.

Table 4.22: *Maximum, minimum and mean values for the measured data on Bostik Simson ISR 70-04.*

		Maximum	Minimum	Mean
Ultimate load	(N)	898	576	746
Ultimate shear stress	(MPa)	2.25	1.44	1.86
Ultimate deformation	(mm)	5.2	3.8	4.6

Table 4.23: *Corresponding material model in the FE-simulations for Bostik Simson ISR 70-04*

Material Model	C_{10}	C_{01}	D_1
Mooney-Rivlin	$100 \cdot 10^3$	$400 \cdot 10^3$	0

Concentration of shear stresses was observed on the edges of the adhesive. Figure 4.10 on page 35 is visualizing the typical stress distribution in the 2 mm specimens. The stress concentration occured where the fracture was observed to be initiated during the tests. The critical shear stress was extracted from this area of stress concentrations:

- Critical shear stress: $\tau_{cr} = 3.5$ MPa
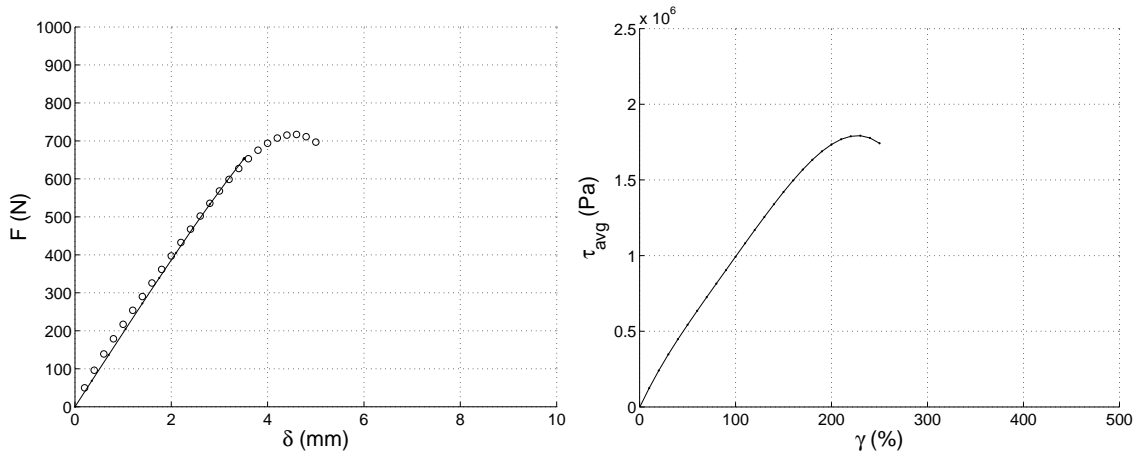
Figure 4.29: *Results from the FE-evaluation of Bostik Simson ISR 70-04. The diagram to the left shows the fitted curve from the tests (circles) compared to the calculated results from the FE-evaluation (line). The diagram to the right shows the average shear-stress (τ_{avg}) versus the shear-strain extracted from the FE-model.*

Fracture Characteristics

The fractures were observed with different characteristics. In three of the five specimens internal fractures occured (as the ones previously seen in Multifog 2640 and Simson ISR 70-03). In these three specimens fractures were initiated on the edges and propagated through the adhesive.
In two of the specimens the fracture was initiated in the interface between glass and adhesive. The fracture leads to a significant failure in the interface for then propagating internally, within the adhesive. These two specimens are the ones with the lowest observed ultimate load in the series of five specimens.
Typical fracture surfaces are shown in figure 4.30.
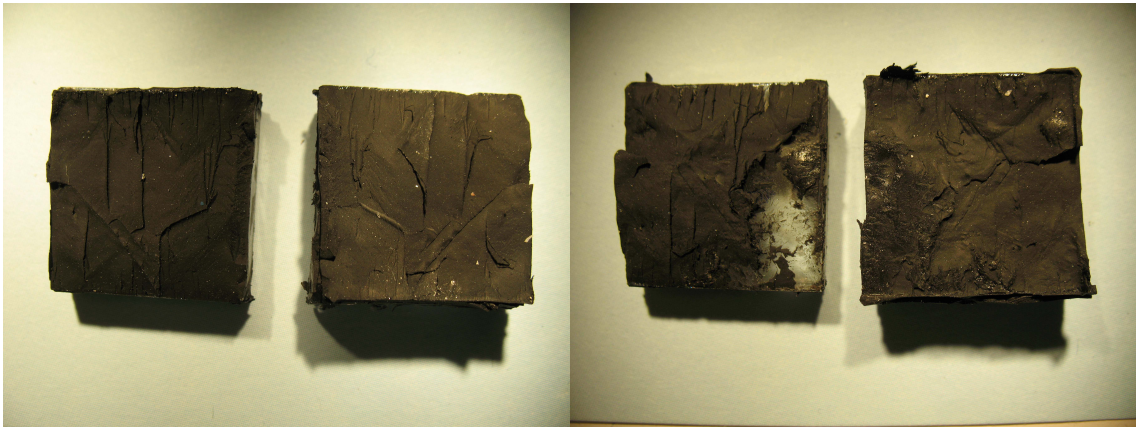
Figure 4.30: *Typical characteristics of the fracture in the specimens of Bostik Simson ISR 70-04. The left photograph shows a specimen with the fracture initiated on the edge and then propagated internally within the adhesive. The right photograph shows a fracture due to adhesive failure in the interface between adhesive and glass.*

4.6.5   Bostik Simson ISR 70-12, Black
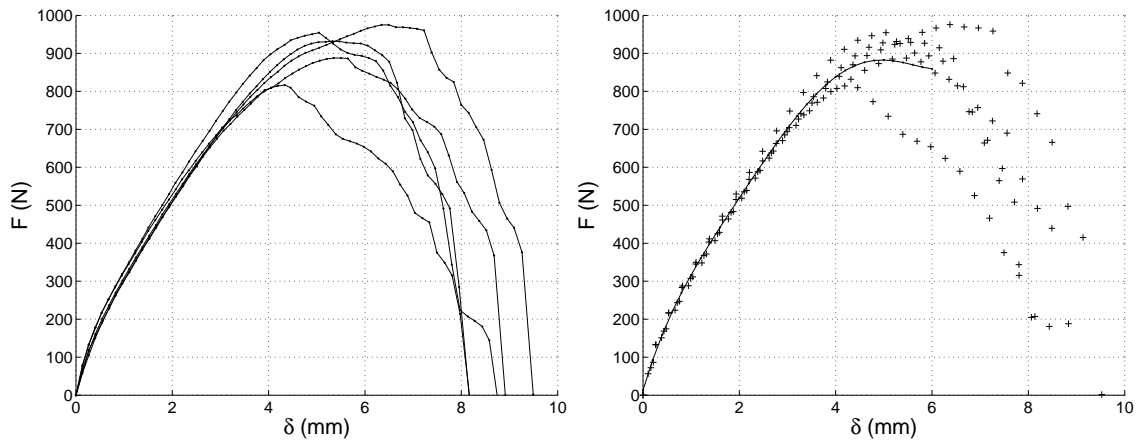
Figure 4.31: *Plots of the measured data of Bostik Simson ISR 70-12. The diagram to the left shows the applied force versus the deformation. The diagram to the right shows force versus deformation (+) and the curve fitted to the measured data in a least square sense (line).*

The curves of the measured data initially showed an almost perfectly uniform behaviour and deviate when reaching the ultimate load. The ultimate load varied between 800 and 1000 N.

The fractures were rather significant adhesive failures in the interface between glass and adhesive which subsequently propagated within the adhesive. The specimens with the largest interface failures were the ones with the lowest ultimate load. The results from the tests are shown in the diagrams of figure 4.31.

The maximum, minimum and mean measured values of tested specimens are shown in table 4.24.

The test was modelled in Abaqus with the Mooney-Rivlin material model. The best corresponding material constants are shown in table 4.25. A comparison of the test-results and the FE-calculations is shown in the diagram in figure 4.32. The FE-calculations were unable to follow the measured data to the ultimate capacity. Therefore the calculated results in this model was lower than the real results.

For Simson ISR 70-12 the initial shear modulus was calculated to:

- $G_{20\%}$ = 1.17 MPa.

Table 4.24: *Maximum, minimum and mean values for the measured data on Bostik Simson ISR 70-12.*

		Maximum	*Minimum*	*Mean*
Ultimate load	(N)	976	818	914
Ultimate shear stress	(MPa)	2.44	2.05	2.29
Ultimate deformation	(mm)	6.4	4.3	5.3

Table 4.25: *Corresponding material model in the FE-simulations for Bostik Simson ISR 70-12*

Material Model	C_{10}	C_{01}	D_1
Mooney-Rivlin	$100 \cdot 10^3$	$500 \cdot 10^3$	0

Concentration of shear stresses was observed on the edges of the adhesive. Figure 4.10 on page 35 is visualizing the typical stress distribution in the 2 mm specimens. The stress concentrations occured where the fracture was observed to be initiated during the tests. The critical shear stress was extracted from this area of stress concentrations:

- Critical shear stress: $\tau_{cr} = 4.0$ MPa
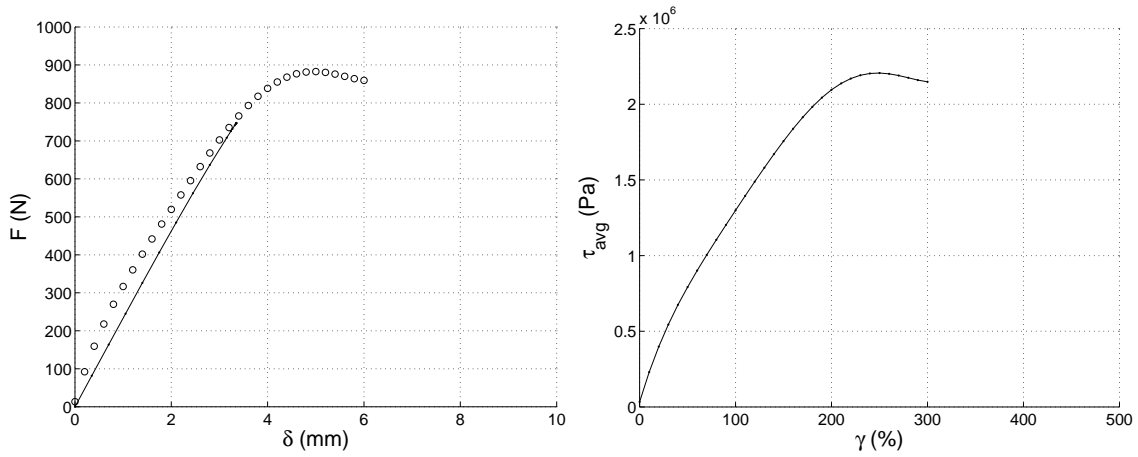
Figure 4.32: *Results from the FE-evaluation of Bostik Simson ISR 70-12. The diagram to the left shows the fitted curve from the tests (circles) compared to the calculated results from the FE-simulation (line). The diagram to the right shows the average shear-stress (τ_{avg}) versus the shear-strain extracted from the FE-model.*

Fracture Characteristics

The fractures occured as adhesive failures in the interface between glass and adhesive which subsequently propagated internally, within the adhesive. The magnitude of the interface failures varied between the specimens. The specimens with the largest interface failure were the ones with the lowest ultimate load. Typical fracture surfaces are shown in figure 4.33.
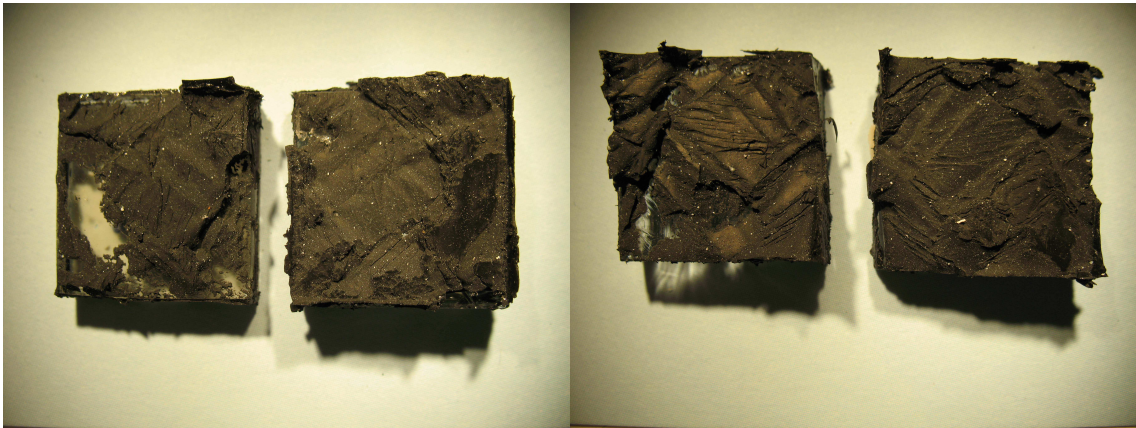
Figure 4.33: *Typical characteristics of the fracture in the specimens of Bostik Simson ISR 70-12. The left photograph shows a specimen with significant interface failure between glass and adhesive. The right photograph shows a fracture with less interface failure.*

4.7   Specimens 0.3 mm (Silicones)

4.7.1   Test Set-Up

Table 4.26: *Test set-up for 0.3 mm silicone specimens*

Number of specimens	3
Joint thickness	0.3 mm
Load application	Compression
Deformation speed	0.33 mm/min
Deformation sensor	DS ±0.001 mm
Load cell	±10 kN

The Bostik adhesives/sealants, tested with the joint thickness of 2 mm, were also tested as a thin joint. They were squeezed together as much as possible to a thickness of about 0.3 mm. Three specimens were tested for each adhesive.

Due to the smaller deformations of these thinner joints the tests were conducted in compression. A constant deformation speed of 0.33 mm per minute were applied. The thin joints of the Bostik adhesives/sealants were compared with the material models from the 2 mm tests. This was done in order to see whether these material models were valid for a thinner thickness of the adhesive layer as well.

As in the tests of the 2 mm specimens, the tested adhesives/sealants were:

- Bostik Multifog 2640, Black

- Bostik Simson ISR 70-03, Black

- Bostik Simson ISR 70-04, Black

- Bostik Simson ISR 70-12, Black

4.7.2 Bostik Multifog 2640, Black
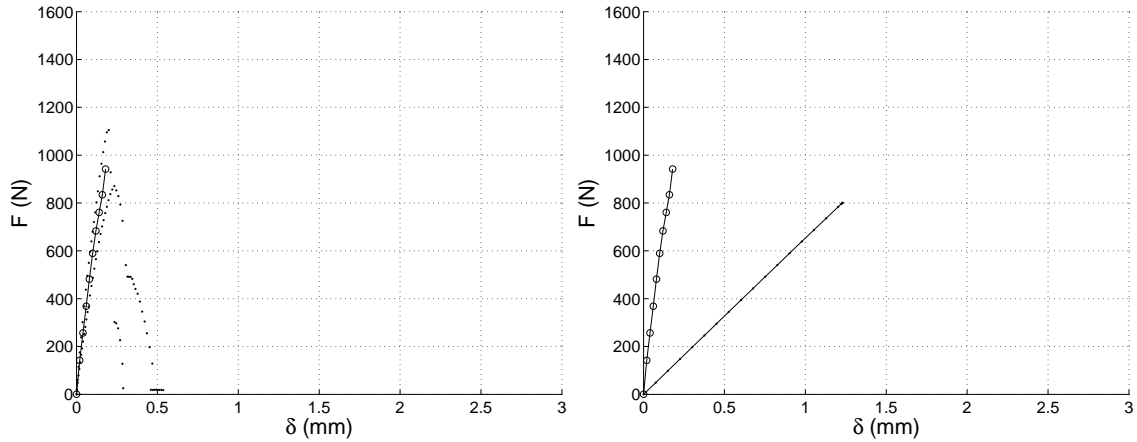
Figure 4.34: *Plots of the measured data of Bostik Multifog 2640 and results from FE-calculations with the material model of the 2 mm tests. The diagram to the left shows force versus deformation (dots) and the curve fitted to the measured data in a least square sense (circles and line). The diagram to the right shows the fitted curve (circles and line) compared to FE-calculations (line) with the material model from the 2 mm tests of the same adhesive*

The specimens showed a slightly different behaviour, regarding both stiffness and ultimate load. The test of the second specimen failed due to a failure in the adhesive bond between steel and glass.

As can be seen in the right diagram of figure 4.34, the measured data deviated significantly from the material model corresponding to the 2 mm tests. The silicone showed a stiffer behaviour in the thinner joints than in the thicker 2 mm joints.

The ultimate load and deformation varied between the tested specimens. The maximum, minimum and mean measured values of the three tested specimens are shown in table 4.27.

Table 4.27: *Maximum, minimum and mean values for the measured data of Multifog 2640.*

		Maximum	*Minimum*	*Mean*
Ultimate load	(N)	1108	870	989
Ultimate shear stress	(MPa)	2.77	2.18	2.47
Ultimate deformation	(mm)	0.23	0.19	0.21

4.7.3   Bostik Simson ISR 70-03, Black
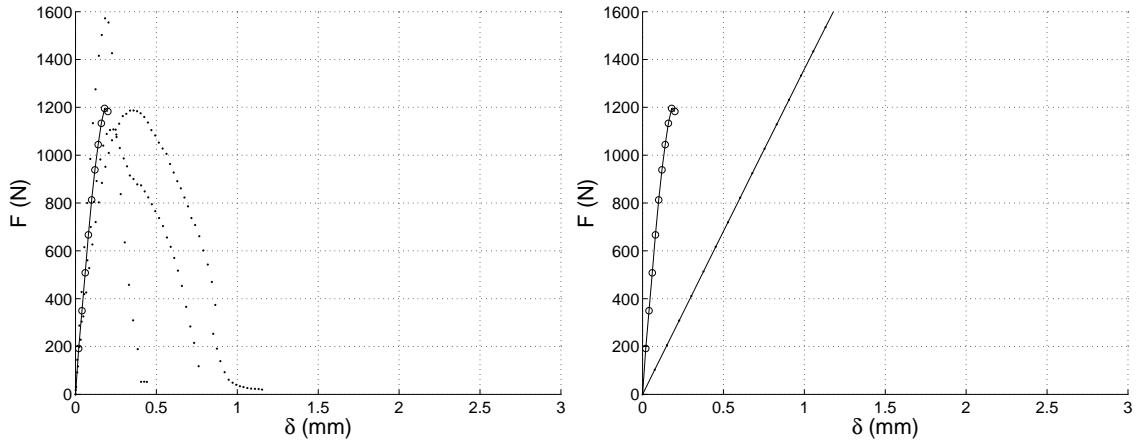
Figure 4.35: *Plots of the measured data of Simson ISR 70-03 and results from FE-calculations with the material model of the 2 mm tests. The diagram to the left shows force versus deformation (dots) and the curve fitted to the measured data in a least square sense (circles and line). The diagram to the right shows the fitted curve (circles and line) compared to the FE-calculations (line) with the material model from the 2 mm tests of the same adhesive*

The specimens showed a slightly different behaviour regarding both stiffness and ultimate load. The measured data of applied force and deformation is shown in figure 4.35.

As can be seen in the right diagram of figure 4.35, the measured data deviated significantly from the material model corresponding to the 2 mm tests. The silicone showed a stiffer behaviour in the thinner joints than in the thicker 2 mm joints.

The ultimate load and deformation varied between the tested specimens. The maximum, minimum and mean measured values of the three tested specimens are shown in table 4.28.

Table 4.28: *Maximum, minimum and mean values for the measured data of Simson ISR 70-03.*

		Maximum	Minimum	Mean
Ultimate load	(N)	1573	1117	1295
Ultimate shear stress	(MPa)	3.93	2.79	3.24
Ultimate deformation	(mm)	0.34	0.19	0.25

4.7.4   Bostik Simson ISR 70-04, Black
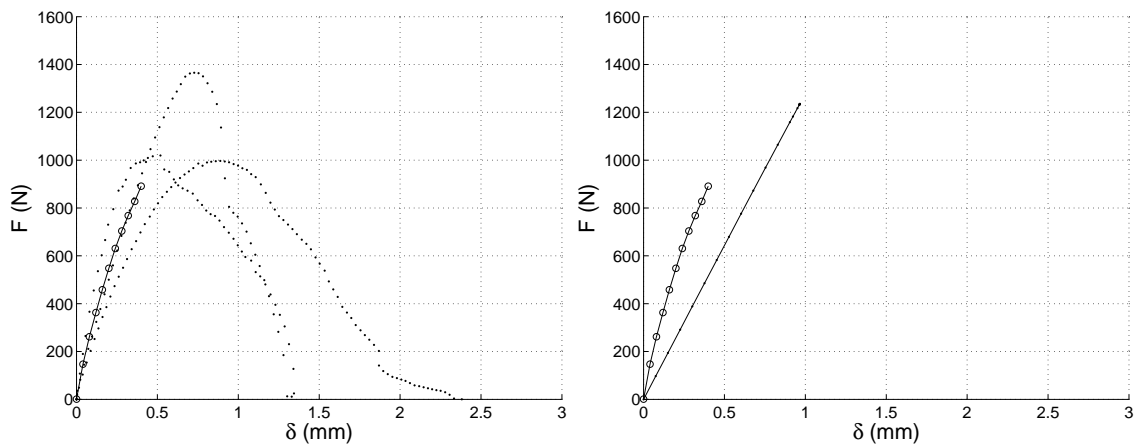
Figure 4.36: *Plots of the measured data of Simson ISR 70-04 and results from FE-calculations with the material model of the 2 mm tests. The diagram to the left shows force versus deformation (dots) and the curve fitted to the measured data in a least square sense (circles and line). The diagram to the right shows the fitted curve (circles and line) compared to the FE-calculations (line) with the material model from the 2 mm tests of the same adhesive*

The specimens showed a slightly different regarding both stiffness and ultimate load. As can be seen in the right diagram of figure 4.36, the measured data deviated from the material model corresponding to the 2 mm tests. The adhesive showed a stiffer behaviour in the thinner joints than in the thicker 2 mm joints. The measured data of applied force and deformation together with the fitted curve compared to the material model from the FE-calculations in the 2 mm tests are shown in figure 4.36. The ultimate load and deformation varied between the tested specimens. The maximum, minimum and mean measured values of the 2 tested specimens are shown in table 4.29.

Table 4.29: *Maximum, minimum and mean values for the measured data on Simson ISR 70-04.*

		Maximum	*Minimum*	*Mean*
Ultimate load	(N)	1373	999	1145
Ultimate shear stress	(MPa)	3.43	2.50	2.86
Ultimate deformation	(mm)	0.84	0.50	0.70

4.7.5   Bostik Simson ISR 70-12, Black
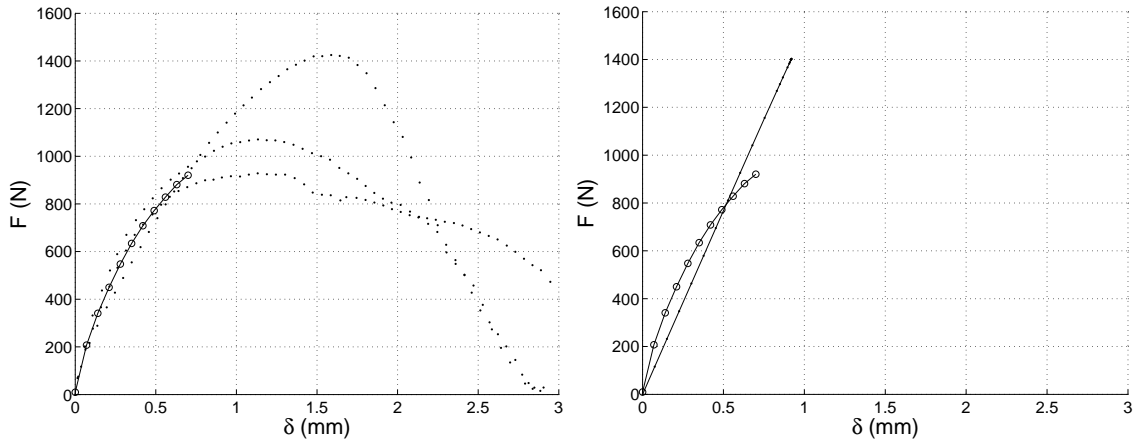
Figure 4.37: *Plots of the measured data of Simson ISR 70-12 and results from FE-calculations with the material model of the 2 mm tests. The diagram to the left shows force versus deformation (dots) and the curve fitted to the measured data in a least square sense (circles and line). The diagram to the right shows the fitted curve (circles and line) compared to the FE-calculations (line) with the material model from the 2 mm tests of the same adhesive*

The specimens showed a slightly different behaviour regarding stiffness and ultimate load.

As can be seen in the right diagram of figure 4.37, the measured data corresponded well to the material model from to the 2 mm tests. The measured data of applied force and deformation together with the fitted curve compared to the material model from the FE-calculations in the 2 mm tests are shown in figure 4.37.

The ultimate load and deformation varied between the tested specimens. The maximum, minimum and mean measured values of the 2 tested specimens are shown in table 4.30.

Table 4.30: *Maximum, minimum and mean values for the measured data on Bostik Simson ISR 70-04.*

		Maximum	Minimum	Mean
Ultimate load	(N)	1427	933	1145
Ultimate shear stress	(MPa)	3.57	2.33	2.86
Ultimate deformation	(mm)	1.54	1.14	1.27

4.8 Specimens 0.2–0.3mm (Glues)

4.8.1 Test Set-Up

Table 4.31: *Test set-up for 0.2-0.3 mm specimens*

Number of specimens	5
Joint thickness	0.2-0.3 mm
Load application	Compression
Deformation speed	0.33 mm/min
Deformation sensor	DS ±0.001 mm
Load cell	±10 kN

Four different adhesives were tested with a joint thickness varying between 0.2 and 0.3 mm. All of the tested adhesives were common glues available on the market. Each adhesive were tested with 5 specimens. These tests were conducted in compression with a constantly applied displacement of 0.33 mm per minute.
The tested adhesives were:

- Casco Polyurethan Glue 1809, Transparent (gas-bubbles)

- HBM Rapid Adhesive X 60, Grey/White

- Casco Strong Epoxy Professional 2801, 2803, Transparent (light-yellow)

- Casco UV-hardening Glass-Glue 2987, Transparent

The difference in thickness is explained by the use of two different types of specimens. The high stiffness and strength of the Strong Epoxy and the Casco UV-hardening 2987 made it impossible to fully join the surfaces of the two glass-parts of the specimens. Therefore specimen type 2 with an adhesive joint of dimensions 5×20 mm (see figure 4.2 on page 22) had to be used for these tests. This meant that the joint became thicker due to the protecting interlayer of paper, partially hindering adhesive contact between the adhesive and the glass-parts.

4.8.2   Casco Polyurethan Glue 1809, Transparent (gas-bubbles)
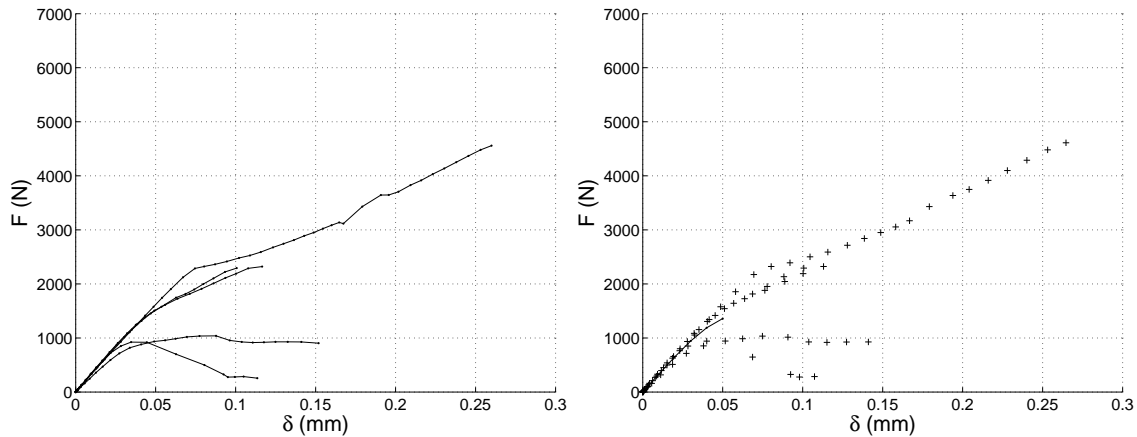
Figure 4.38: *Measured data of Casco Polyurethan Glue 1809. The diagram to the left shows the applied force versus the deformation. The diagram to the right shows force versus deformation (+) and the curve fitted to the measured data in a least square sense (line).*

The specimens showed a linear behaviour with varying ultimate load. A decrease in stiffness with continuing deformation was observed before the specimens reached the ultimate deformation.

While hardening, the polyurethan adhesive reacts with water in a reaction where carbon dioxide is created. The carbon dioxide emerges as gas bubbles which create a white foam. This leads to a fine pattern of gas bubbles within the joint that can clearly be observed through the glass (see figure 4.40, page 70).

Two specimens had a significantly lower ultimate load. On the specimens no visible defects have been observed that could explain this behaviour.

The ultimate load was regarded having been reached when the stiffness started decreasing, even though the load carrying capacity continued in some specimens. The maximum, minimum and mean measured values of the tested specimens are shown in table 4.32.

Table 4.32: *Maximum, minimum and mean values for the measured data of Casco Polyurethan Glue 1809.*

		Maximum	Minimum	Mean
Ultimate load	(N)	2240	669	1531
Ultimate shear stress	(MPa)	5.6	1.7	3.8
Ultimate deformation	(mm)	0.084	0.024	0.057

Table 4.33: *Corresponding material model in the FE-simulations for Casco Polyurethan Glue 1809*

Material Model	E (MPa)	ν
Linear-Elastic	200	0.25

The test was modelled in Abaqus with a linear-elastic material model. The best corresponding material constants are shown in table 4.33. A comparison of the test-results and the FE-calculations is shown in the diagram in figure 4.39. The FE-calculations followed the measured data to the ultimate load.

For Casco Polyurethan Glue the initial shear modulus was calculated to:

- $G_{20\%} = 82.5$ MPa

The FE-calculations showed a homogenous state of shear-stresses. Therefore the critical shear-stress equals the mean average shear-stress from table 4.32.

- Critical shear stress: $\tau_{cr} = 5.6$ MPa
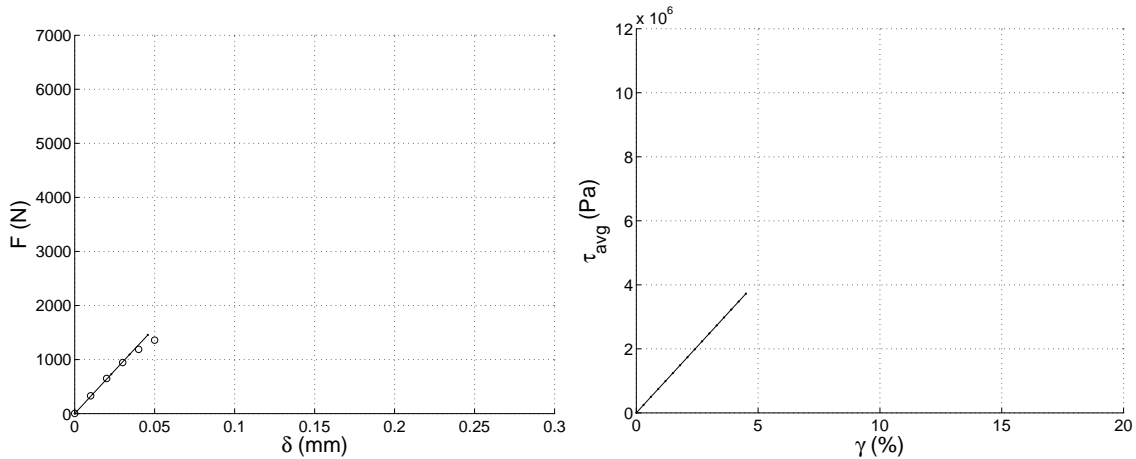
Figure 4.39: *Results from the FE-evaluation of Casco Polyurethan Glue 1809. The diagram to the left is showing the fitted curve from the tests (circles) compared to the calculated results from the FE-evaluation (line). The diagram to the right shows the average shear-stress (τ_{avg}) plotted versus the shear-strain extracted from the FE-model.*

Fracture Characteristics

The fractures occured internally within the adhesive. No failure in the interface between the adhesive and the glass was observed. However it is very difficult to observe the fracture surfaces due to the pattern of gas-bubbles in the adhesive. Typical fracture surfaces are shown in figure 4.40.
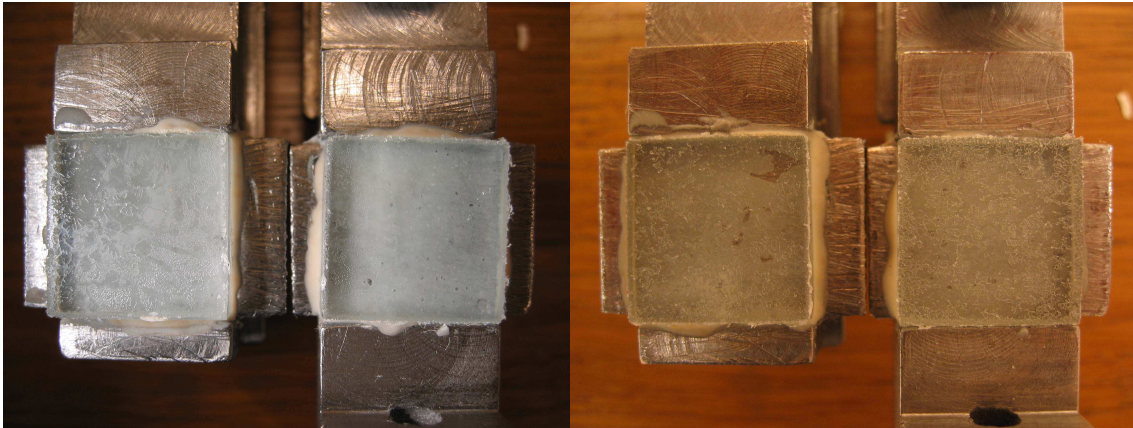
Figure 4.40:   *Typical characteristics of the fracture in the specimens of Casco Polyurethan Glue 1809. The typical pattern of gas bubbles can be seen on the fractured specimens.*

4.8.3 HBM Rapid Adhesive X 60, Grey/White
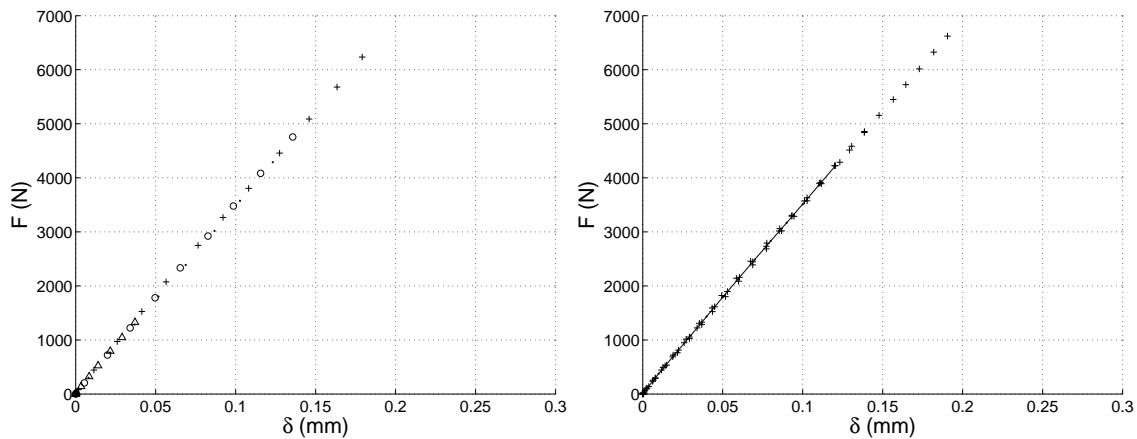
Figure 4.41: *Measured data of HBM Rapid Adhesive X 60. The diagram to the left shows the applied force versus the deformation. To differentiate the specimens they are marked with different symbols and plotted without the connecting line. The diagram to the right shows force versus deformation (+) and the curve fitted to the measured data in a least square sense (line).*

The specimens showed an almost perfect linear behaviour. They were very uniform regarding stiffness but show significant differences in ultimate load. To differentiate the tests they are marked with different symbols in the diagrams in figure 4.41.

The 5:th specimen failed during the mounting of the test and was therefore disregarded in the evaluation.

The maximum, minimum and mean measured values of the 4 tested specimens are shown in table 4.34.

The test was modelled in Abaqus with a linear-elastic material model. The best corresponding material constants are shown in table 4.35. A comparison of the test-results and the FE-calculations is shown in the diagram in figure 4.42. The FE-calculations followed the measured data to the ultimate load.

For the HBM Rapid Adhesive X 60 the initial shear modulus was calculated to:

- $G_{20\%} = 138.6$ MPa.

Table 4.34: *Maximum, minimum and mean values for the measured data of HBM Rapid Adhesive X 60.*

		Maximum	*Minimum*	*Mean*
Ultimate load	(N)	6667	1327	4352
Ultimate shear stress	(MPa)	16.7	3.3	10.9
Ultimate deformation	(mm)	0.192	0.037	0.125

Table 4.35: *Corresponding material model in the FE-simulations for the HBM Rapid Adhesive X 60*

Material Model	E (MPa)	ν
Linear-Elastic	320	0.25

The FE-calculations revealed a homogenous state of shear-stress. Therefore the critical shear-stress equals the mean average shear-stress from table 4.34.

- Critical shear stress: $\tau_{cr} = 10.9$ MPa
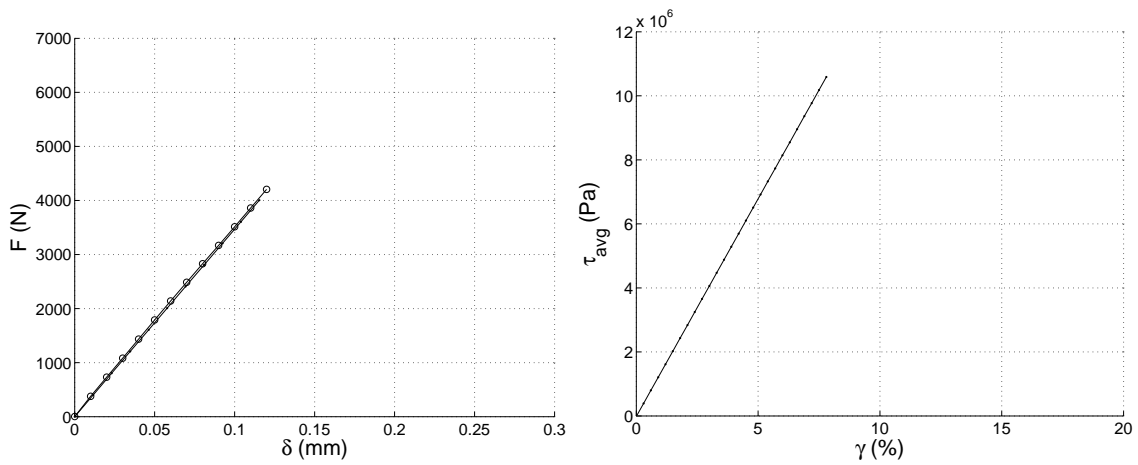
Figure 4.42: *Results from the FE-evaluation of HBM Rapid Adhesive X 60. The diagram to the left is showing the fitted curve from the tests (circles) compared to the calculated results from the FE-evaluation (line). The diagram to the right shows the average shear-stress (τ_{avg}) plotted versus the shear-strain extracted from the FE-model.*

Fracture Characteristics

The fractures occured as adhesive failure in the interface between glass and adhesive. They were normally occurring on both interfaces and the adhesive could be peeled of in small brittle flakes. Typical fracture surfaces are shown in figure 4.43.
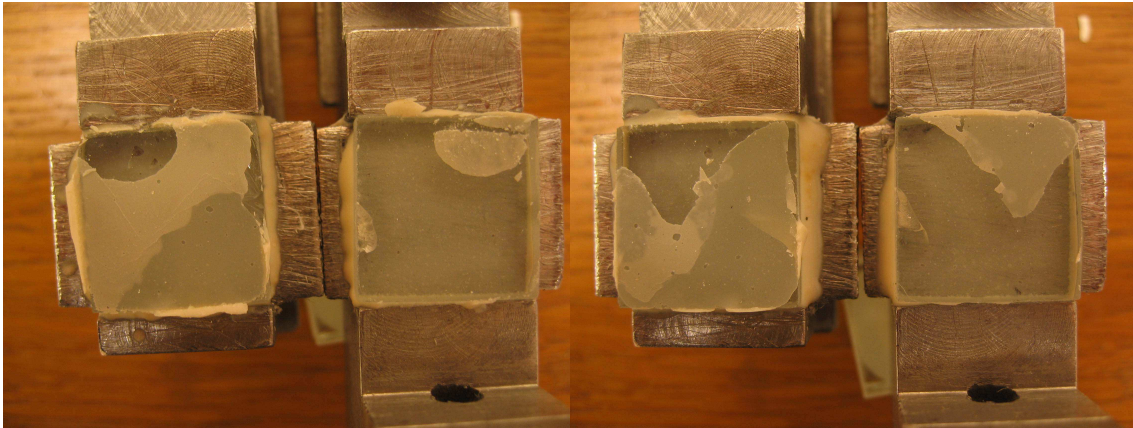
Figure 4.43: *Typical characteristics of the fracture in the specimens of X60 glue. On the left picture can be observed that the adhesive has failed in in the interface with both glass-surfaces. This thin layer of adhesive could subsequently be peeled of in small brittle flakes.*

4.8.4   Casco Strong Epoxy Professional 2801, 2803, Transparent (light-yellow)
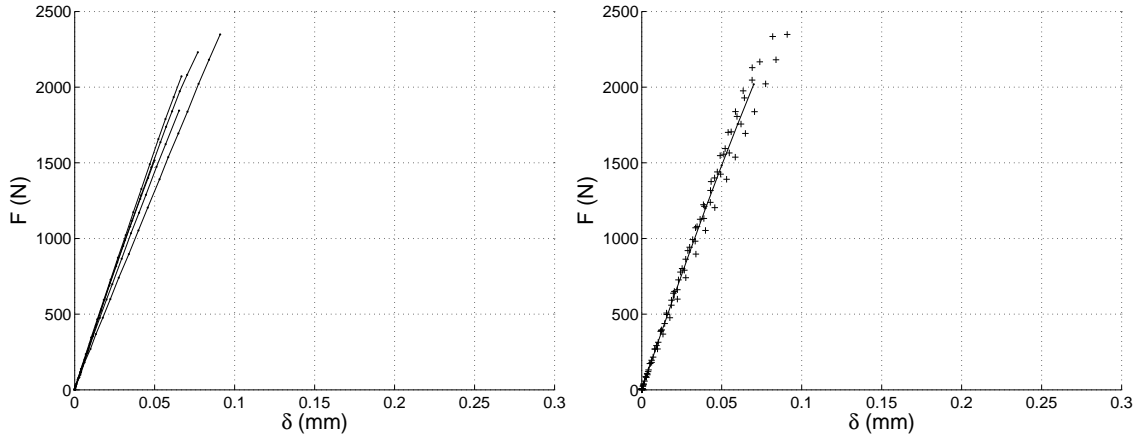
Figure 4.44: *Measured data of Casco Strong Epoxy Professional 2801, 2803. The diagram to the left shows the applied force versus the deformation. The diagram to the right shows force versus deformation (+) and the curve fitted to the measured data in a least square sense (line).*

The stiffness of the Epoxi glue made it impossible to conduct the test with the surfaces of the glass fully joined with the adhesive. Therefore the glass was glued together with a 5 mm wide ribbon of adhesive. The ultimate loads can therefore not be directly compared to the tests of the Polyurethan and the X 60.

The Epoxy specimens showed a linear behaviour with slight differences in stiffness and ultimate load. The maximum, minimum and mean measured values of the four tested specimens are shown in table 4.36.

The test was modelled in Abaqus with a linear-elastic material model. The best corresponding material constants are shown in table 4.37. A comparison of the test-results and the FE-calculations is shown in the diagram in figure 4.45. The FE-calculations followed the measured data to the ultimate load.

For Casco Strong Epoxy Professional the initial shear modulus was calculated to:

- $G_{20\%} = 514.3$ MPa

Table 4.36: *Maximum, minimum and mean values for the measured data on Casco Strong Epoxy Professional 2801, 2803.*

		Maximum	*Minimum*	*Mean*
Ultimate load	(N)	2408	1557	2055
Ultimate shear stress	(MPa)	24.08	15.57	20.55
Ultimate deformation	(mm)	0.093	0.051	0.072

Table 4.37: *Corresponding material model in the FE-simulations for Casco Strong Epoxy Professional*

Material Model	E (MPa)	ν
Linear-Elastic	1500	0.25

The FE-calculations revealed a homogenous state of shear-stresses. Therefore the critical shear-stress equals the mean average shear-stress from table 4.32.

- Critical shear stress: $\tau_{cr} = 20.6$ MPa
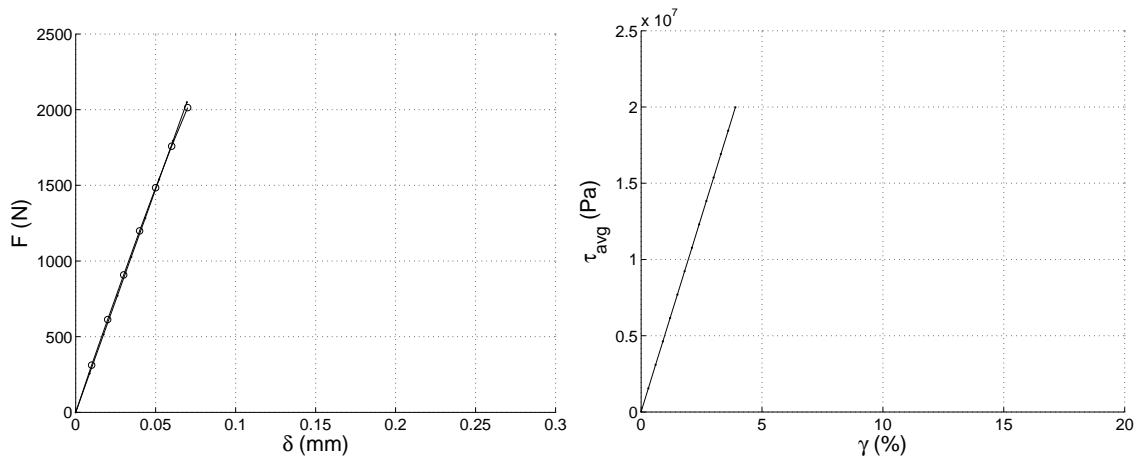
Figure 4.45: *Results from the FE-evaluation of Casco Strong Epoxy Professional 2801, 2803. The diagram to the left is showing the fitted curve from the tests (circles) compared to the calculated results from the FE-evaluation (line). The diagram to the right shows the average shear-stress (τ_{avg}) plotted versus the shear-strain extracted from the FE-model.*

Fracture Characteristics

The fractures occured as adhesive failure in the interface between glass and adhesive. In three of the tests the fracture was entirely on one side with the adhesive still attached to the other glass-part. In two of the specimens the adhesive suffered failure two both glass surfaces, in these cases the adhesive kept together as a rather soft interlayer and did not break into brittle flakes as observed with the X 60. Typical fracture surfaces are shown in figure 4.46.
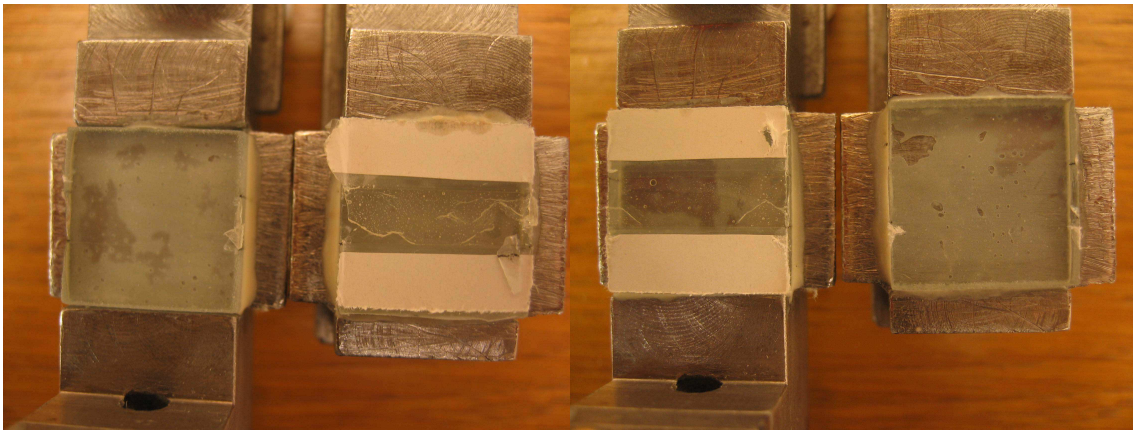
Figure 4.46: *Typical characteristics of the fracture in the specimens of the Casco Strong Epoxy Professional adhesive. On the left photograph, at the lower left corner of the adhesive ribbon can be observed a failure in the interface below the adhesive.*

4.8.5   Casco UV-hardening Glass-Glue 2987, Transparent
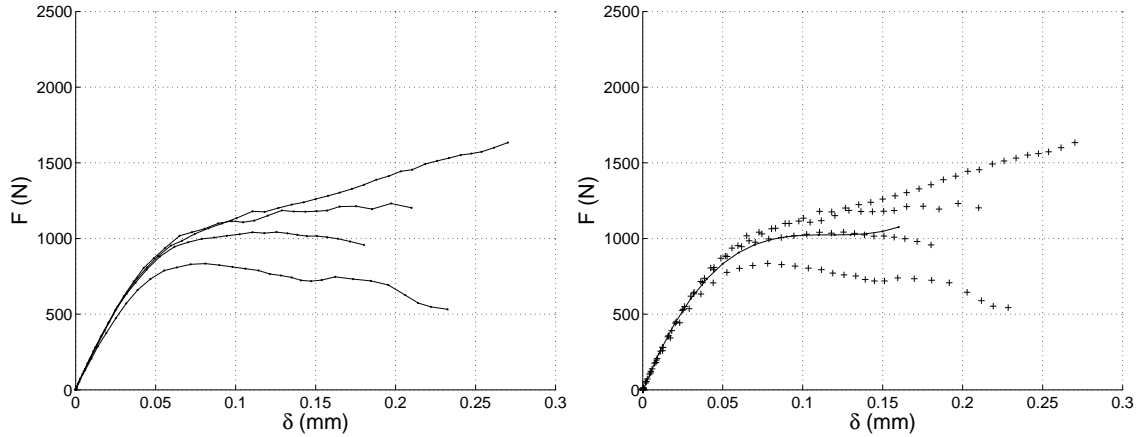
Figure 4.47: *Measured data of Casco UV-hardening Glass-Glue 2987. The diagram to the left shows the applied force versus the deformation. The diagram to the right shows force versus deformation (+) and the curve fitted to the measured data in a least square sense (line).*

The stiffness of the UV-hardening glue made it impossible to conduct the test with the surfaces of the glass fully joined with the adhesive. Therefore the glass was joined with a 5 mm wide ribbon of adhesive. The ultimate loads can therefore not be directly compared to the tests of Polyurethan and X60.

One of the specimens was fractured while mounting the test and was consequently not regarded in the evaluation.

The UV-hardening specimens show an initial uniform and linear curve, subsequently the curve decreases in stiffness to subsequently deform almost without increase in load before the ultimate failure.

The maximum, minimum and mean measured values of the 4 tested specimens are shown in table 4.38.

The test was modelled in Abaqus with a linear-elastic material model. The best corresponding material constants are shown in table 4.39. A comparison of the test-results and the FE-calculations is shown in the diagram in figure 4.48. The FE-calculations followed the measured data to the ultimate load.

Table 4.38: *Maximum, minimum and mean values for the measured data of Casco UV-hardening Glass-Glue 2987.*

		Maximum	*Minimum*	*Mean*
Ultimate load	(N)	1634	835	1187
Ultimate shear stress	(MPa)	16.34	8.35	11.87
Ultimate deformation	(mm)	0.270	0.078	0.166

Table 4.39: *Corresponding material model in the FE-simulations for Casco UV-hardening Glass-Glue 2987*

Material Model	E (MPa)	ν
Linear-Elastic	300	0.25

For Casco UV-hardening Glass-Glue 2987 the initial shear modulus was calculated to:

- $G_{20\%}$ = 113.2 MPa

The FE-calculations revealed a homogenous state of shear-stress in the adhesive. Therefore the critical shear-stress equals the mean average shear-stress from table 4.38:

- Critical shear stress: τ_{cr} = 11.9 MPa
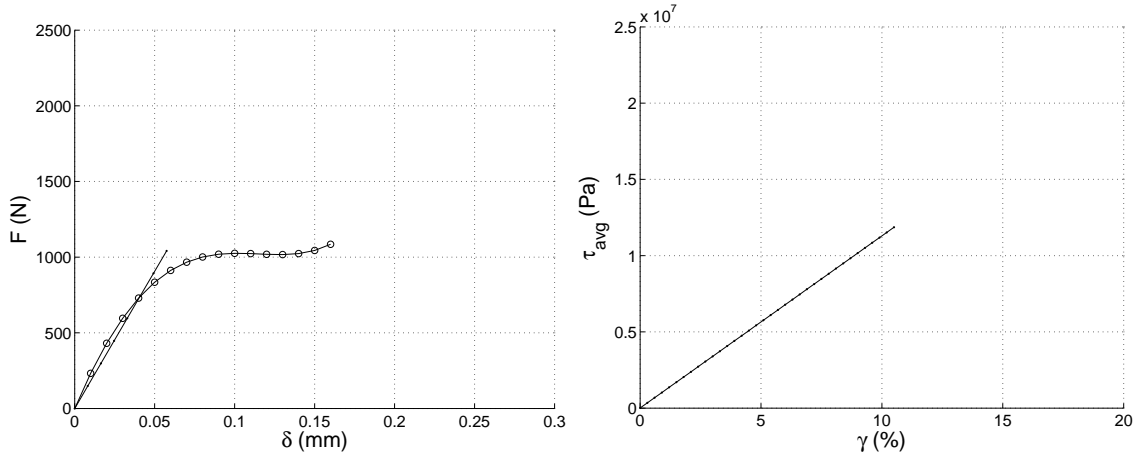
Figure 4.48: *Results from the FE-evaluation of Casco UV-hardening Glass-Glue 2987. The diagram to the left is showing the fitted curve from the tests (circles) compared to the calculated results from the FE-evaluation (line). The diagram to the right shows the average shear-stress (τ_{avg}) plotted versus the shear-strain extracted from the FE-model.*

Fracture Characteristics

The fractures occured as adhesive failure in the interface between glass and adhesive. In two of the specimens the fracture was entirely on one side with the adhesive still attached to the other glass-part. In the other two specimens the adhesive suffered failure to both glass surfaces, in these cases the adhesive kept together as a rather soft interlayer and did not break as observed with the X60. Typical fracture surfaces are shown in figure 4.49.
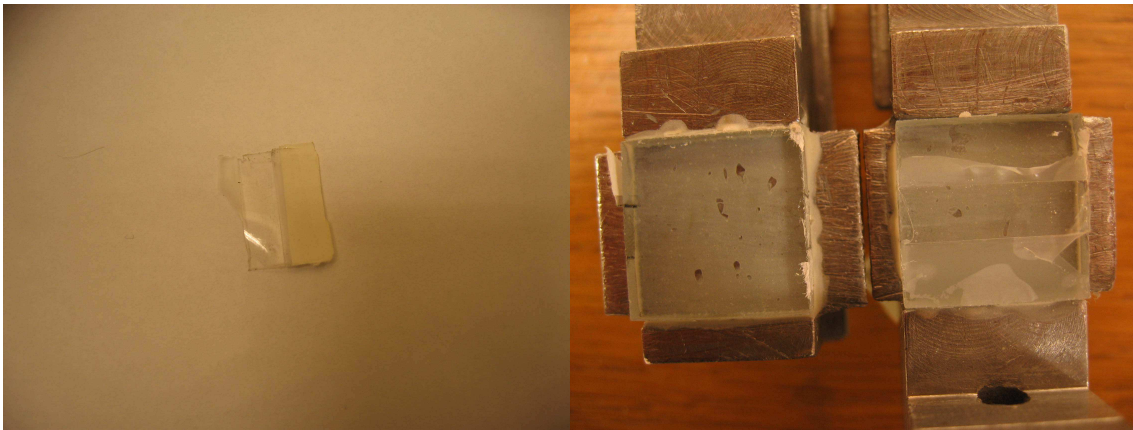
Figure 4.49: *Typical characteristics of the fracture in the specimens of Casco UV-hardening Glass-Glue 2987 glue. On the left photograph can bee observed the soft, entirely peeled of adhesive ribbon.*

Chapter 5

Large-Scale Testing

5.1 Test Set-Up

The large-scale tests were arranged in order to test a joint of larger dimensions. This was done with the purpose of testing whether it was possible to predict the mechanical behaviour of this joint from the material models that resulted from the evaluation of the small specimens.

The test arrangement was choosen to create a situation where an adhesive joint could be used in a real situation when constructing with glass. In the studied litterature many examples have been given of beams joined with bolts. In this perspective a large-scale test in the form of a beam seemed as a good construction element on where to test the adhesive joints.

In the large-scale tests, a joint of quite large geometry was tested. This was done in order to test wether the material models from the tests of the small specimens would prove valid in larger geometry. In this aspect the joint should be of such a size that differences in stress would occur over the geometry of the joint.

For practical reasons a 4-point bending test of a beam with a 3 meter span was chosen. The beam was constructed by three flat-glass elements measuring 250×2000 mm with a width of 10 mm. They were joined in the middle of the 3 meter span by two adhesive joints each measuring 250×250 mm. The arrangement of three glass elements was chosen to create a symmetrical beam in order to obtain pure shear stresses in the joints.

With the 4-point bending test the bending moment was kept constant over the entire geometry of the joint. A drawing of the test arrangement is shown in figure 5.1.
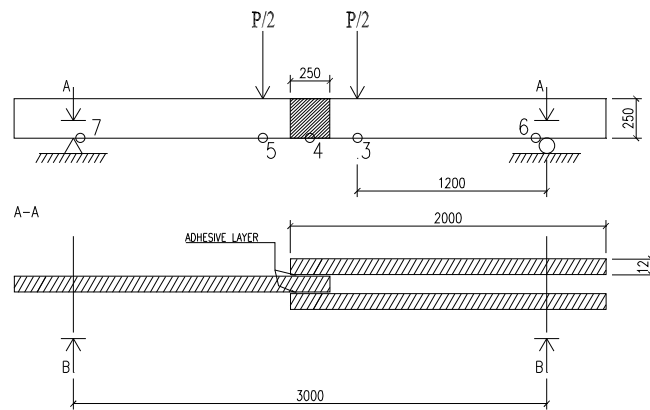
Figure 5.1: *The arrangement for the large-scale tests. Measurements of deformation were made at the points numbered 3-7.*
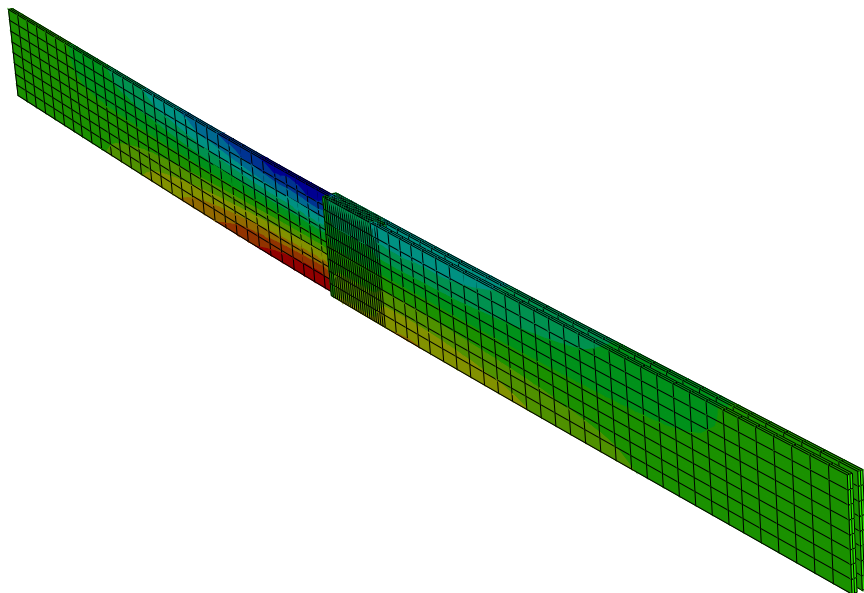
Figure 5.2: *The FE-model used to do the simulations of the large-scale tests*

5.2   FE-Simulations

In order to evaluate the tested adhesives the large-scale tests were simulated in Abaqus. The tested stiff adhesives (glues) were simulated with a thickness of 0.2 mm and the adhesives/sealants (silicones) with a thickness of 2 mm.

In Abaqus the flat glass elements were modelled with a Young's Modulus of 70 GPa and a Poissons ratio of 0.23. The joints were modelled according to the evaluated material models from the tests of the small specimens (see chapter 4 section 4.4).

To determine the ultimate load for the beams the critical shear stress (τ_{cr}) was used. When the part of the joint with the highest concentration of stresses reached the critical shear stress it was regarded having reached its ultimate load.

In the stiffer adhesives stress-concentrations occured at the corners of the joint and consequently the critical shear stress was first reached there. In the silicones the stresses were more evenly distributed, the concentrations were observed at the edges of the joint and of less magnitude than in the stiffer adhesives. The principal pattern of the stress distribution is shown in figure 5.3.

The results from the FE-simulations are shown in table 5.1 and in the figures 5.4 and 5.5. From the results can be seen that the concentration of stresses plays a decisive role in the ultimate load of the joints. The apparently stronger glues turn out to have less ultimate load than the silicones due to the high magnitude of the stress-concentrations in the corners. The only glue to compete with the silicones is
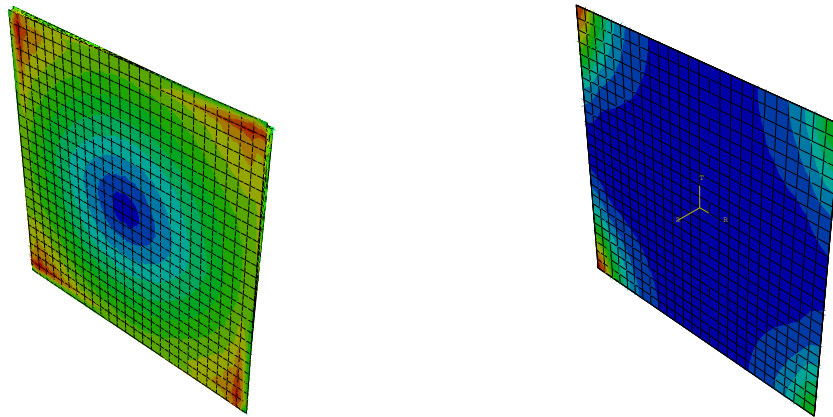
Figure 5.3: *Principal pattern of the shear-stresses in the joints of the large-scale tests (τ_{23} in a circular coordinate system with its centre in the midpoint of the joint). The left picture shows the general distribution in the silicone joints, here can be seen concentrations of stress at the corners of the adhesive. The right picture shows the distribution in the joints with stiffer adhesives (glues), here large concentrations of stress also can be observed at the corners. In the stiffer adhesives the variation in stress is significant whereas in the softer silicones the stress is more evenly distributed over the geometry of the joint. Note that the colour scales of the two pictures are not equivalent.*

the Strong Epoxy Professional, which due to its high ultimate shear stress supports the stress-concentrations better.

The FE-simulations revealed that the tensile stresses in the lower edge of the single flat-glass element would exceed the tensile capacity of the glass. This meant that the failure would occur in the glass and not, as was intended, in the joint. However the flat-glass was already ordered and delivered so the tests were done in either case with the consequence that the ultimate load of the joints in the large-scale tests could not be tested and evaluated.
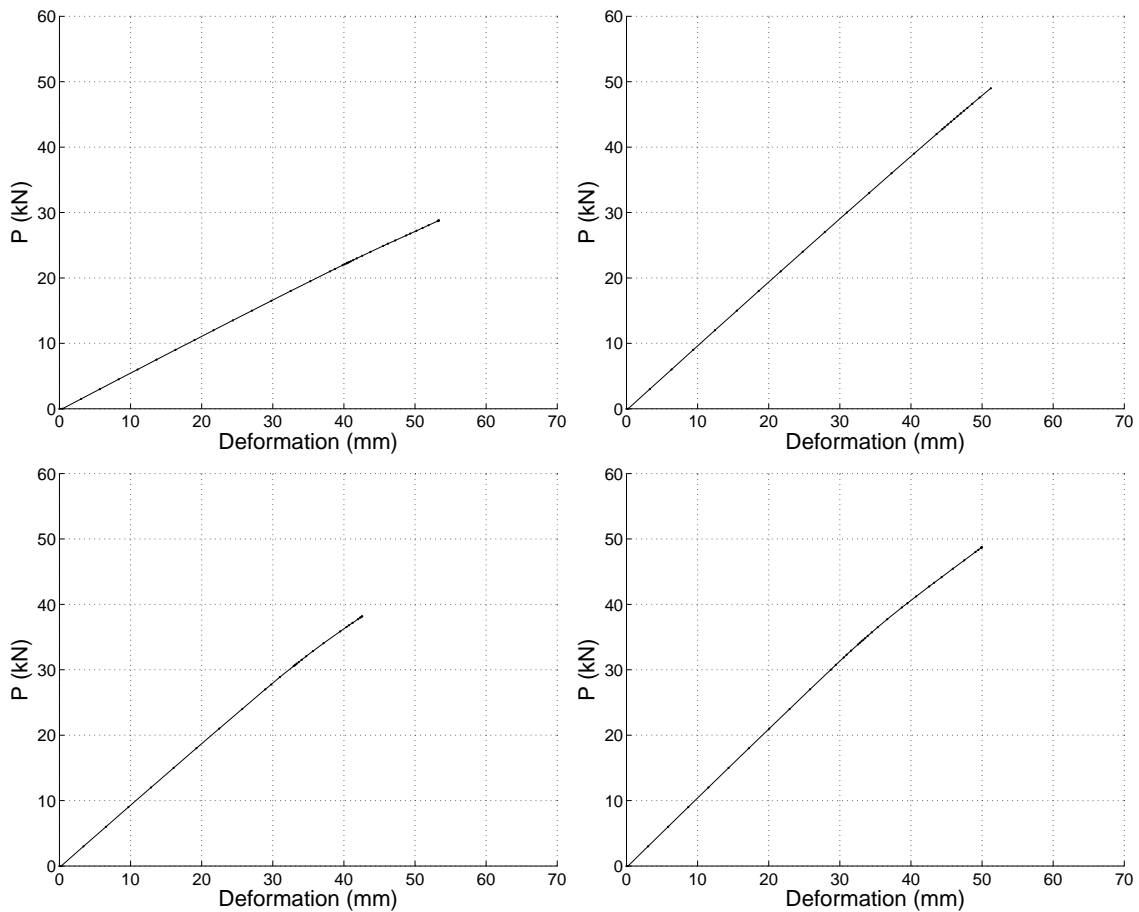
Figure 5.4: *Results from the FE-simulations of the large-scale tests of the softer adhesives (silicones). The diagrams show the applied load P (P = P/2 + P/2) versus the midpoint deformations (Point 4). The diagrams show from top left and clockwise: Multifog 2640, Simson ISR 70-03, Simson ISR 70-12, Simson ISR 70-04.*
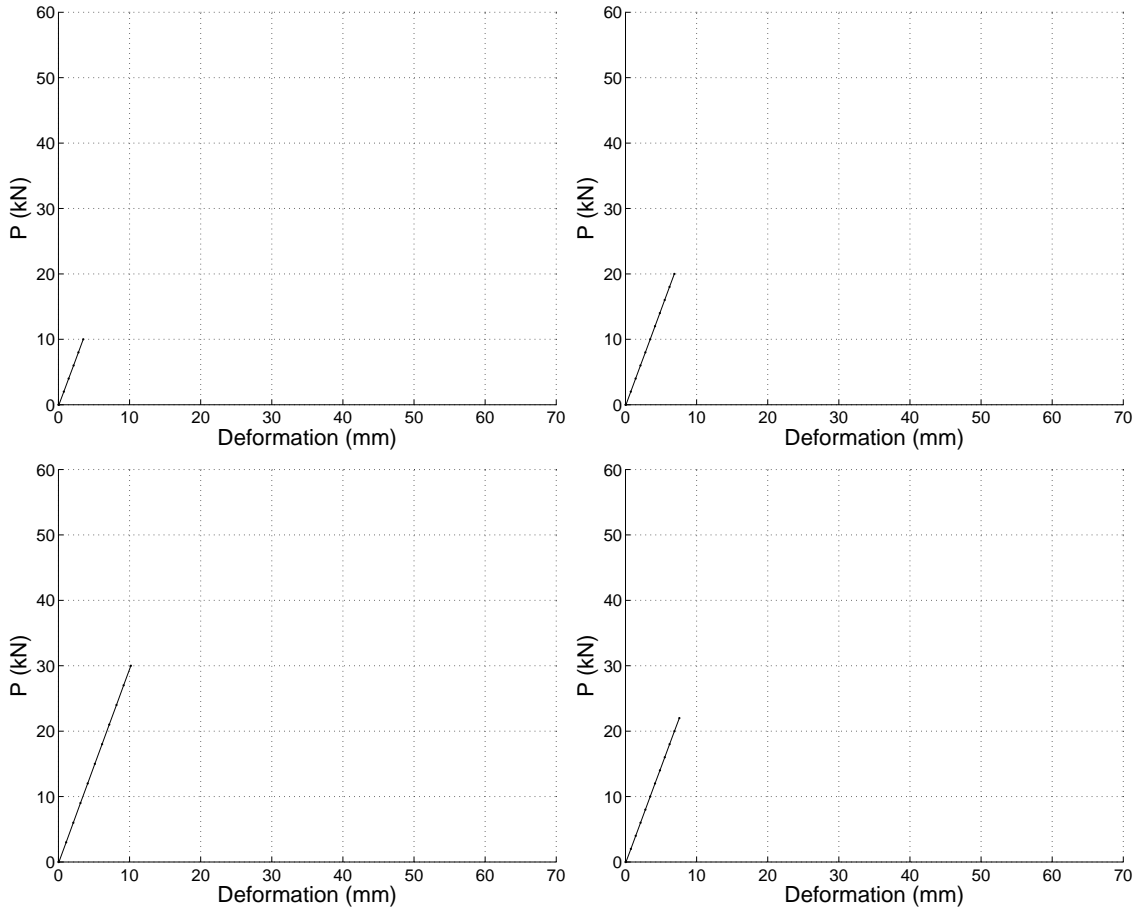
Figure 5.5: *Results from the FE-simulations of the large-scale tests of the stiff adhesives (glues). The diagrams show the applied load P (P = P/2 + P/2) versus the midpoint deformations (Point 4). The diagrams show from top left and clockwise: Casco Polyurethan 1809, HBM Rapid Adhesive X 60, Casco UV-hardening Glass-Glue, Casco Strong Epoxy Professional.*

Table 5.1: *Ultimate loads (P = P/2 + P/2) and deformations at the mid-point of the beam (Point 4) from the FE-simulations of the large-scale tests.*

	P_u (kN)	$U_{4,u}$ (mm)
Bostik Multifog 2640	28.8	53
Bostik Simson ISR 70-03	49.3	51
Bostik Simson ISR 70-04	38.2	43
Bostik Simson ISR 70-12	48.8	50
Casco Strong Epoxy Professional	30.3	10.0
Casco Polyurethan 1809	10.3	3.5
Casco UV-hardening Glass-Glue	22.3	7.5
HBM Rapid Adhesive X 60	20.3	7.0

5.3   Results

From the simulations five adhesives were chosen to be tested in the large-scale tests. The two strongest silicones, Bostik Simson ISR 70-03 and 70-12 and the stiffer adhesives Casco Polyurethan 1809, Casco UV-hardening Glass-Glue and Casco Strong Epoxy Professional were chosen for the tests. The Rapid Adhesive X 60 was regarded impossible to apply at such a large geometry due to its fast-hardening characteristics.

As revealed in the FE-simulations all the beams of the large-scale tests suffered failure in the single flat-glass of the beam. Thus no ultimate load of the joints could be measured. The results from the tests will therefore merely be a comparison of the initial deformations of the simulations and the deformations measured in the tests. Photos of each joint will be shown to show the aesthetic characteristics of each adhesive.

The results are presented with a table showing the deformation speed, ultimate load and ultimate mid-point deformation. A diagram showing a comparison of the measured data and the FE-simulations is also presented. In the diagrams the curves ending abruptly in the diagrams are from the measured data and the curves continuing through the diagrams from the FE-simulations. In the diagram the deformations are plotted versus the value of one of the applied point-loads.

5.3.1 Bostik Simson ISR 70-03

Table 5.2: *Input values and results from the large-scale test of Simson ISR 70-03 adhesive joint.*

Joint thickness	(mm)	2
Deformation speed	(mm/min)	10
Ultimate load, P_u	(kN)	9.06
Ultimate deformation, $U_{4,u}$	(mm)	12.2

The large-scale test of the Bostik 7003 suffered failure due to tensile overstressing in the lower edge of the single flat-glass element. The failure occured at a load of $P_u = 9.06$ kN. The collected data form the tests is compared with the results from the FE-simulations in figure 5.6.

The measured data from the test of Bostik Multifog 7003 seem to correspond well to the results from the FE-simulations. However the measured data shows slightly larger deformations than the FE-simulations and seems to deviate from the calculated curves at the point of the failure.
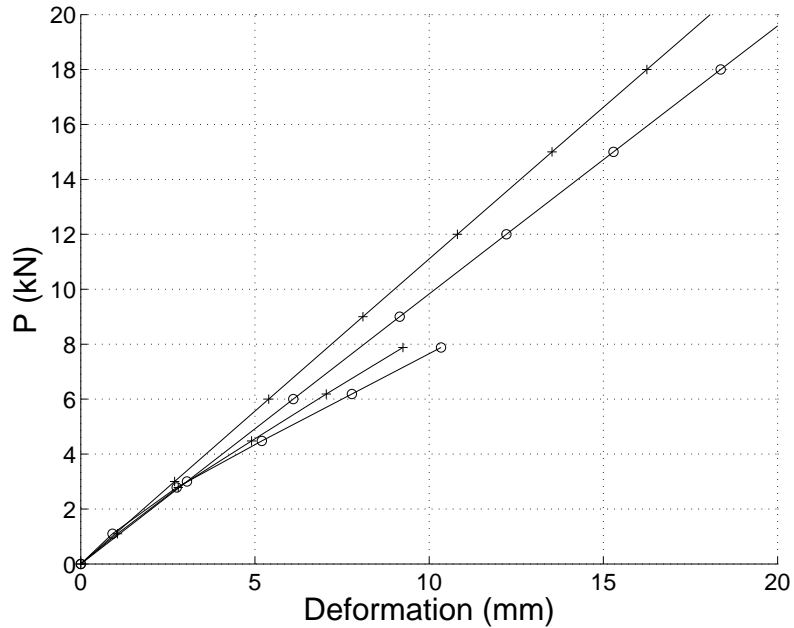
Figure 5.6: *Comparison of the deformations of the FE-simulation and the measured deformations from the test with the Bostik Simson ISR 70-03 adhesive joint. The curves continuing through the diagram are from the FE-simulations and the curves ending abruptly are the results from the tests. The different points of measurement are marked: 4 (o), 5 (+).*

5.3.2   Bostik Simson ISR 70-12

Table 5.3: *Input values and results from the large-scale test of Bostik Simson ISR 70-12 adhesive joint.*

Joint thickness	(mm)	2
Deformation speed	(mm/min)	10
Ultimate load, P_u	(kN)	9.70
Ultimate deformation, $U_{4,u}$	(mm)	20.1

The large-scale test of the Bostik 7012 suffered failure due to tensile overstressing in the lower edge of the single flat-glass element. The failure occured at a load of $P_u = 9.70$ kN. The collected data from the tests is compared with the results from the FE-simulations in figure 5.7.

The measured data shows a significantly less stiff behaviour than the FE-simulations. For the deformation of 15 mm the calculations show a load of around 16 kN while the the test shows merely 8 kN.
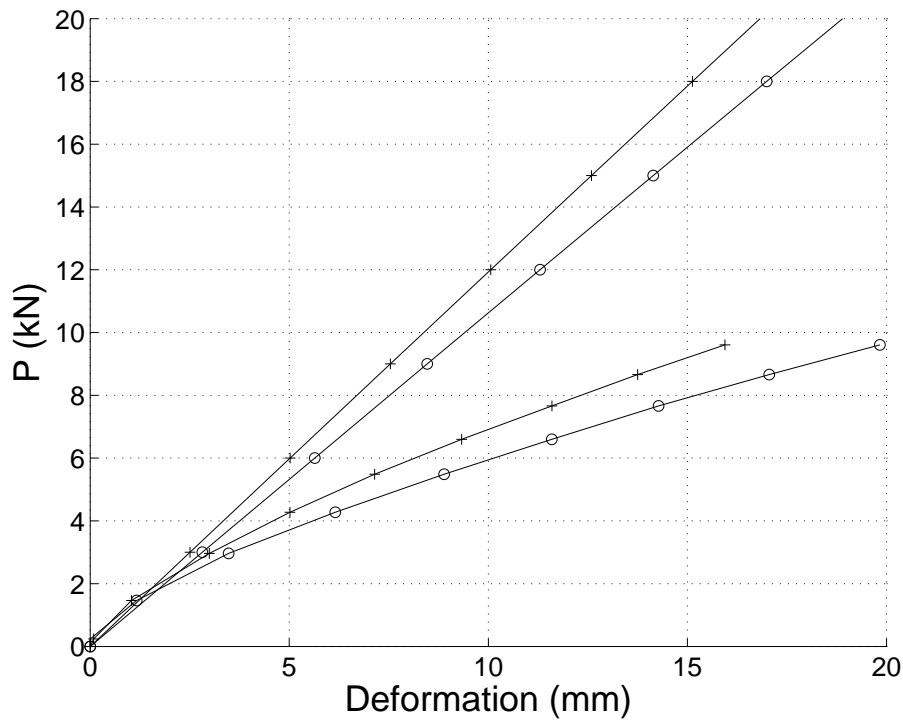
Figure 5.7: *Comparison of the deformations of the FE-simulation and the measured deformations from the test with the Bostik Simson ISR 70-12 adhesive joint. The curves continuing through the diagram are from the FE-simulations and the curves ending abruptly are the results from the tests. The different points of measurement are marked: 4 (o), 5 (+).*

5.3.3 Casco Strong Epoxy Professional 2801, 2803

Table 5.4: *Input values and results from the large-scale test of Casco Strong Epoxy adhesive joint.*

Joint thickness	(mm)	0.2
Deformation speed	(mm/min)	2
Ultimate load, P_u	(kN)	9.98
Ultimate deformation, $U_{4,u}$	(mm)	2.5

The large-scale test of the Epoxy Strong suffered failure due to tensile overstressing in the lower edge of the single flat-glass element. The failure occured at a point-load magnitude of $P_u = 9.98$ kN. The collected data from the tests is compared with the results from the FE-simulations in figure 5.8.
The measured data from the large scale test corresponded very well with the results from the FE-simulation.
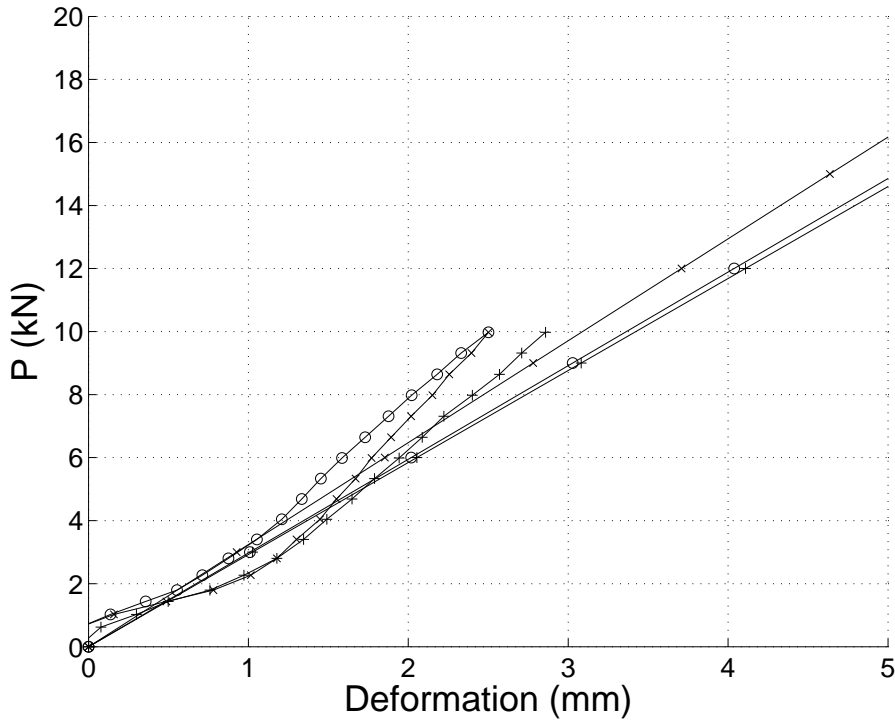
Figure 5.8: *Comparison of the deformations of the FE-simulation and the measured deformations from the test of the Casco Strong Epoxy Professional adhesive joint. The curves continuing through the diagram are from the FE-simulations and the curves ending abruptly are the results from the tests. The different points of measurement are marked: 3 (x), 4 (o), 5 (+).*

5.3.4   Casco Polyurethan Glue 1809

Table 5.5: *Input values and results from the large-scale test of Polyurethan adhesive joint.*

Joint thickness	(mm)	0.2
Deformation speed	(mm/min)	2
Ultimate load, P_u	(kN)	9.96
Ultimate deformation, $U_{4,u}$	(mm)	2.2

The large-scale test of the Casco Polyurethan glue suffered failure due to tensile overstressing in the lower edge of the single flat-glass element. The failure occured at a point-load magnitude of $P_u = 9.96$ kN. The collected data from the tests is compared with the results from the FE-simulations in figure 5.9.

The measured data shows initially a very strange behaviour with negative deformations. After this initial deviation the measured data follows the stiffness of the results from the FE-simulations, however parallelly displaced.
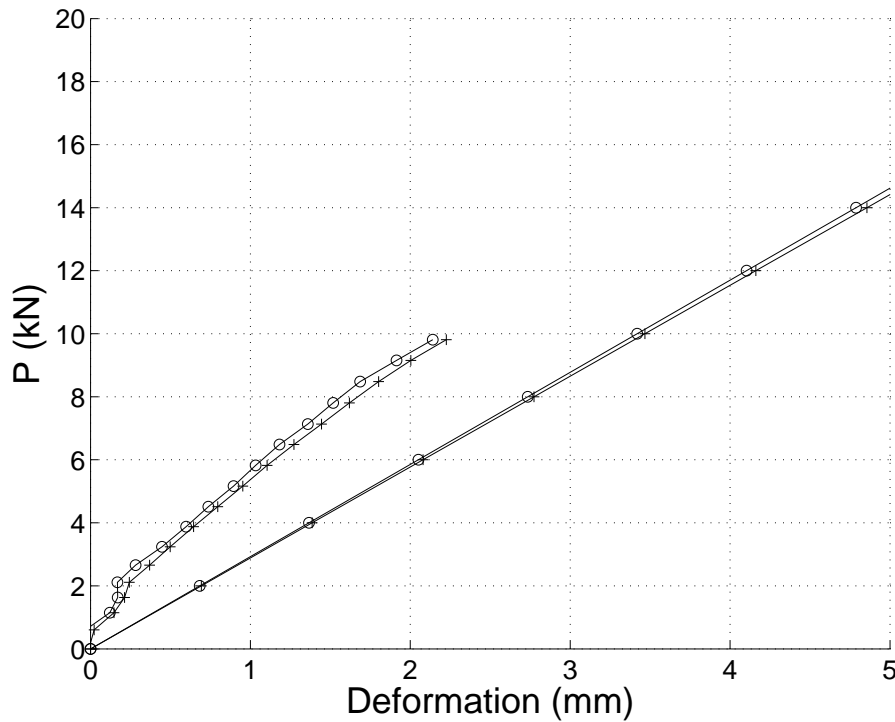
Figure 5.9: *Comparison of the deformations of the FE-simulation and the measured deformations from the test with the Casco Polyurethan adhesive joint. The curves continuing through the diagram are from the FE-simulations and the curves ending abruptly are the results from the tests. The different points of measurement are marked: 4 (o), 5 (+).*

5.3.5   Casco UV-hardening Glass-Glue 2987

Table 5.6: *Input values and results from the large-scale test of Casco UV-hardening Glass-Glue 2987 adhesive joint.*

Joint thickness	(mm)	0.2
Deformation speed	(mm/min)	2
Ultimate load, P_u	(kN)	6.20
Ultimate deformation, $U_{4,u}$	(mm)	1.1

The large-scale test of the Casco UV-hardening glass-glue suffered failure due to tensile overstressing in the lower edge of the single flat-glass element. The failure occured at a load of $P_u = 6.20$ kN. The collected data from the tests is compared with the results from the FE-simulations in figure 5.10.

The measured data shows initially a very strange behaviour with negative deformations. After this initial deviation the measured data follows the stiffness of the results from the FE-simulations, however paralelly displaced.

Figure 5.10: *Comparison of the deformations of the FE-simulation and the measured deformations from the test with the UV-hardening adhesive joint.*

5.4   Summary and Analysis of Large-Scale Tests

The results from the tests of Bostik silicones show deviation from the theoretical model. Especially strong is the deviation in the Bostik 7012. An explanation of this deviation can be that the silicones were not fully hardened at the moment of the tests. The speed of hardening in the Bostik Silicones given by the manufacturer is 3 mm the first 24 hours and 1 mm per 24 hours the following time. Following these instruction the 30-day hardening of the joints gives an approximately 35 mm thick hardened layer of adhesive. The state of the hardening was unfortunately not checked before diposing of the specimens.

It is therefore not clarified if the material models from the small specimens are valid for the joints of larger geometry. Further research must be conducted to clarify whether the material models of the silicone adhesives can be used for an arbitrary geometry.

The strange initial behaviour of the Casco Polyurethan and the Casco UV-hardening adhesives is most likely explained by a rotation of the entire beam. The beam was supported by wooden planks to stabilize it and prevent buckling. These planks were on purpose placed with a small gap to the beam to avoid friction between the beam and the planks. Thus a minor rotation was possible along the length-axis of the beam and this most probably occured when testing the Polyurethan and UV-hardening adhesive. The displacement gauges was placed on 30 mm angles on the sides of the beams which made them extra sensitive for this type of rotation.

Consequently, the initial data of the measurements in these two adhesives was disregarded in evaluation and only the following part of the measured curve was compared with the results from the FE-simulations.

The test-data of the stiffer adhesives corresponds well with the calculated data from the FE-simulations. The comparison of the measured data and the results from the FE-simulations show that the stiffness of the adhesives corresponds with the material models evaluated from the tests of the small specimens. However it can not be stated whether the fracture of the joint will occur when the stress concentrations reach the critical shear stress. For evaluation of the ultimate load of the joint further research is required.

Figure 5.11: *Test set-up of the large-scale test of the adhesive joint Bostik Simson ISR 70-03.*

Figure 5.12: *Test set-up of the large-scale test of the adhesive joint Bostik Simson ISR 70-12 after failure in the single flat-glass element.*

Figure 5.13: *The adhesive joint Casco Strong Epoxy Professional after failure in the single flat-glass element.*
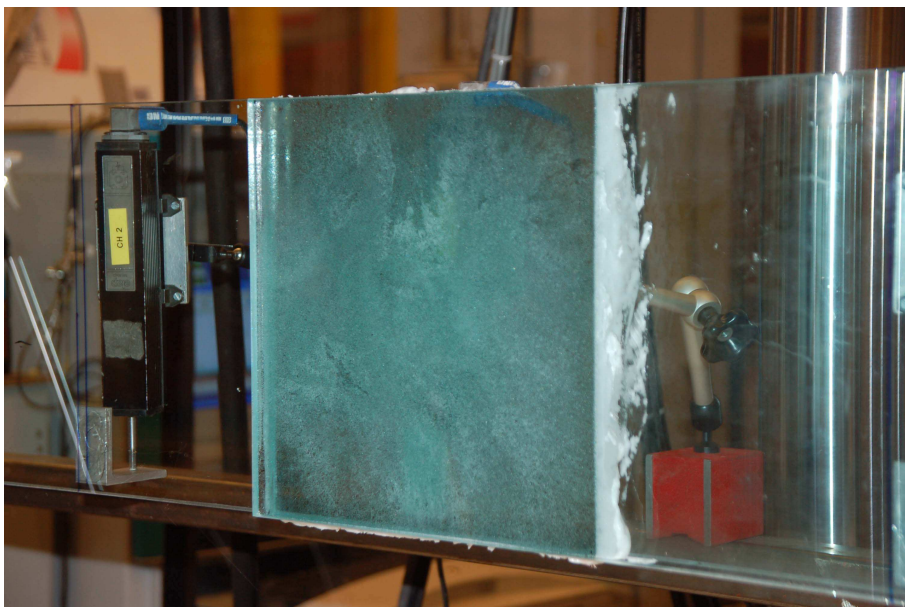
Figure 5.14: *Test set-up of the Casco Polyurethan adhesive joint. The pattern of gas-bubbles and the foam created by the emerging gas are clearly visible.*

Figure 5.15: *Test set-up of the Casco UV-hardening adhesive joint.*

Chapter 6

Conclusion

6.1 Test Method

6.1.1 Test of Small Specimens

The test method for testing the small specimens is a functioning method for evaluating the shear-capacity of the adhesives. The method is creating a state very close to pure shear.

Practical problems occured during the tests with keeping the specimens in place in the test arrangement. Especially this was a problem when the applied forces increased in magnitude as the adhesives increased in stiffness. This problem was solved by decreasing the area of contact between the glass parts and the adhesives. In this manner the applied forces were reduced and the specimens could be kept in place in the testing equipment. This design has the additonal advantage of reducing the variations of stresses in the tested adhesive which create a more homogenous state of stress in the adhesive. Therefore this design could be used for the softer adhesives (silicones) as well to minimize the stress-concentrations at the edges.

The method of using paper to protect the glass when reducing the joint works but has the disadvantage to increase the thickness of the adhesive joint. Therefore a specimen should be designed to avoid having to use the protecting paper. This specimen could preferably be designed as shown in the drawing in figure 6.1. This design means that the glass parts have to be polished which means more expensive specimens.

6.1.2 Material Models

In the large-scale tests the measured data revealed that the linear-elastic models of the adhesive glues proved valid in a larger scale of geometry. All of the tested linear-
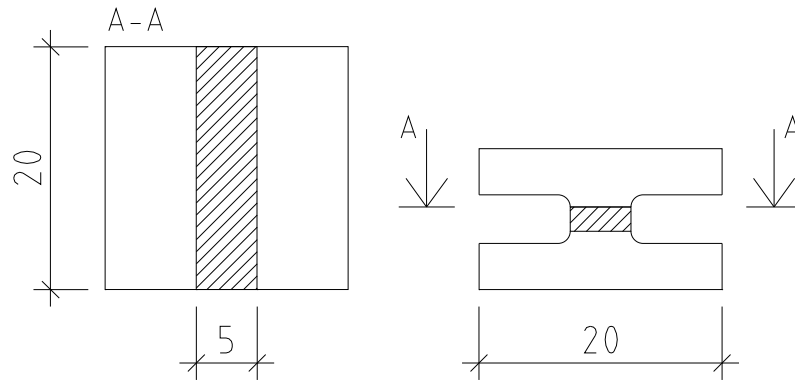
Figure 6.1: *Drawing of the suggested design of the specimens.*

elastic models showed a very good correlation between the tests and FE-simulations. Unfortunately the large-scale joints could not be followed to the ultimate load of the joint due to the failure in the glass-element. The effect of the stress-concentrations on the ultimate load can therefore not be seen in the tests.

The measured data of the silicone joints do not show the same consistency with the FE-simulations. This might be explained by that the silicones were not fully hardened and thus had a lower stiffness. The silicones need to be examined further to be able to tell whether the material models evaluated from the tests of the small specimens are valid in a larger geometry.

The testing of the Bostik silicones in the thin joints (0.3 mm) showed that the material models corresponding with the 2 mm joints were not valid for the thinner joints. The conclusion of this must be that the material models are not valid for different thicknesses. The silicones obviously have different characteristics in different joint thicknesses.

Eventually can be said that the test method proves to be valid for the stiffer glues but further research has to be made to be able to validate the silicones. The test method is a simple way of testing the shear capacity of adhesives and the testing equipment is capable of handling the forces needed to test the adhesives.

6.2   Silicone Adhesives

The silicones show generally a very high adhesive capacity in the connection with the glass. Only in two of the silicones was adhesive failure observed in the interface between glass and silicones. An entire interface failure between glass and silicone was never observed, the fractures propagated internally in the silicones even though the fracture was initiated as an adhesive failure.

The simulations of the large-scale tests revealed that the silicones were generally

stronger than the stiffer adhesives when applied to a joint of larger geometry. This is explained by the fact that the softer silicones has a higher capacity of strain that evens out the stresses and thus avoid the stress-concentrations that build up in the stiffer adhesives.

The FE-calculations show a higher ultimate load in the silicone joints but also reveals larger deformations (see table 5.1 on page 85). These deformations are not always welcome and may lead to constraining forces in other parts of the construction depending on the design. Large deformations without a significant increase in stress may be positive when joining a constructional element to a structure were constraining deformation may occur. An example of this is when attaching a window pane to a structural frame where the silicones may support the own weight and loads from the window pane and also be able to absorb constraining forces caused by possible deformations in the supporting structure.

6.3 Stiff Adhesives

The stiff adhesive joints (glues) show a higher ultimate shear-stress than the silicone joints in the tests with the small specimens. The fractures in the stiffer adhesives showed totally different characteristics than the fractures in the silicone joints. In all of the tested adhesives, except the polyurethan glue, the fractures were observed as massive adhesive interface failures where the fractures propagated entirely in the adhesive interface between glass and adhesive.

The stiff adhesives (glues) showed different mechanical characteristics with a Young's modulus between 200 and 1500 MPa and shear-stress capacities between 4 to 20 MPa.

The FE-simulations of the large-scale tests revealed stress concentrations at the corners of the adhesive joints joined with the stiffer adhesives. Due to these stress concentrations the majority of the stiff adhesive joints have a lower ultimate load than the silicone adhesive joints. This shows clearly that the ultimate load of a larger joint is not only depending on the ultimate shear-stress of the joint but more the stiffness and ability to deform and even out the stresses.

6.4 Future Research

In this report the shear-capacity of different adhesive glass-joints have been evaluated in a short-term load case. Many more investigations need to be conducted to fully determine the characteristics of adhesive joints when constructing with the material glass. During the life-time of a building an adhesive joint will not only be applied to different stresses but also exposed to the sometime hostile environment of the

out-door and in-door climate. Below follows a list of different areas of research that could follow this investigation.

- *Tensile capacity of adhesives* In larger joints it is not always possible to avoid tensile side-effects in the adhesive. Especially is this the case if tightening bolts can not be used.

- *Long-term loads* In a construction the adhesives will be applied to long-term static loads. The effects of these types of loads are an important area of research.

- *Thermal expansion of adhesives* The thermal expansion of the adhesive might lead to constraining stress in the adhesive joint and in the glass. This may lead to a significant decrease in the capacity of the joint. This especially important because the glass is often situated at facades where it is exposed to high variations in temperature.

- *Durability* The durability of the adhesives to temperature variations and ultra-violet light has to be investigated.

Bibliography

[1] Amstock, Joseph S. *Handbook of Glass in Construction.* McGraw-Hill, USA. ISBN: 0-07-001619-4, 1997

[2] Austrell, P.E. *Modelling of Elasticity and Damping for Filled Elastomers* Report TVSM-1009, Lund University, Division of Structural Mechanics 1998.

[3] Behling, Sophia and Stefan *Glass: Konstruktion und Technologi in der Architektur.* Prestel Verlag, München, Germany. ISBN: 3-7913-2155-2, 1999

[4] Button, D., Pye, B. *Glass in building. A Guide to Modern Architectural Glass Performance* Butterworth Architecture, Oxford, England. ISBN: 0-7506-0590-1, 1993

[5] Carlsson, Per-Olof *Bygga med glas* Ljungbergs Tryckeri, Klippan, Sweden. ISBN: 91-631-7680-7, 2005

[6] Gustafsson, P.J., Wernersson, H. *The Complete Stress-Slip Curve of Wood-Adhesives in Pure Shear.* Mechanical Behaviour of Adhesive Joints, pp 139-150, Pluralis, 1987

[7] Hess, R. *Material Glass* Journal of the International Association for Bridge and Structural Engineering (IABSE), Vol. 14, No. 2. ISSN: 1016-8664, 2004

[8] Lawrence, D.C. *A Review of the Durability and of Performance in Silicone Structural Glazing Systems* Glass Performance Days, Conference Proceedings. Tamglass Ltd. Oy, Finland, ISBN: 952-91-8674-6, 2007

[9] Nijsse, R. *Glass in Structures.* Birkhäuser, Basel, Germany. ISBN: 3-7643-6439-4, 2003

[10] Nijsse, R. *Special Steel and Adhesively Bonded Connections for Glass Structures.* Journal of the International Association for Bridge and Structural Engineering (IABSE), Vol. 14, No. 2. ISSN: 1016-8664, 2004

[11] Ottosen, N., Petersson, H. *Introduction to the Finite Element Method* Prentice Hall Europe, Great Britain. ISBN: 0-13-473877-2, 1992

[12] Schober, H., Schneider, J. *Developments in Structural Glass and Glass Structures* Journal of the International Association for Bridge and Structural Engineering (IABSE), Vol. 14, No. 2. ISSN: 1016-8664, 2004

[13] Weller, B., Schadow, T. *Designing of Bonded Joints in Glass Structures* Glass Performance Days, Conference Proceedings. Tamglass Ltd. Oy, Finland, ISBN: 952-91-8674-6, 2007

[14] Glafo, Glasforskningsinstitutet *Boken om glas* Allkopia, Växjö, Sweden, ISBN: 91-631-6257-1, 2005

[15] *Abaqus Version 6.4, Analysis User's manual, Volume III: Materials* Abaqus, Inc., Pawtucket, United States, 2003.

[16] *Product sheets of different Casco adhesives* Akzo Nobel Bygglim AB, Casco, Stockholm, Sweden, www.casco.se

[17] *Product sheets of X 60 adhesive* Hottinger Baldwin Messtechnik, Darmstadt, Germany, www.hbm.com

[18] *Product sheets of different Bostik adhesives* Bostik AB, Helsingborg, Sweden, www.bostik.se

Appendices

A-1 Guide to Further Reading

A-1.1 Glass

Adamsson, B., Backman, H. *Glas i hus.* Esselte Stadium, Lund, Sweden. ISBN: 91-24-17448-3, 1975

Bernard, F., Daudeville, L., Gy, R. *On the design of mechanical joints in tempered glass structures* Glass Processing Days, 2003

Carlson, P.O. *Glas möjligheternas byggmaterial.* Statens råd för byggnadsforskning, Stockholm, Sweden. ISBN: 91-540-5442-7, 1992

Kohrasani, N. *Design Pinciples for Glass used Structurally.* Department of Building Science, Lund University. ISSN: 1103-4467, 2004

O'Callaghan, J. *Apple Computer Inc Retail Store-All glass staircase and bridge. A technical review of innovative design and fabrication techniques utilized* Glass Processing Days, 2003

Sobek, W., Kutterer, M. et al. *Glass Construction Manual.* Birkhäuser, Basel, Germany. ISBN: 3-7643-6077-1, 1997

Wigginton, M. *Glass in Architecture* Phaidon Press, London, England. ISBN: 0-7148-2922-6, 1996

A-1.2 Rubber Materials

Austrell P.E., Bellander M., Stenberg B., Carlsson U., Kari L., and PerssonS., *Survey of design methods and material characteristics in rubber engineering.* Report TVSM-3036, Lund University, Division of Structural Mechanics 1998.

Charlton D.J. , Yang , The K.K. *A Review of Methods to Characterize Rubber Elastic Behaviour for use in Finite Element Analysis* Rubber Chemistry and Technology Vol. 67 pp 481-503 1993

Harris J., Stevensson A. *On the Role of Nonlinearity in the Dynamic Behaviour of Rubber Components.* Rubber Chemistry and Technology, Vol. 63, pp 792-805, 1990

Malvern L.E., *Introduction to the Mechanics of a Continous Medium.* Prentice-Hall, 1969.

Yeoh O.H *Characterization of Elastic Properties of Carbon-Blackfilled Rubber Vulcanizates.* Rubber chemistry and technology Vol. 63 pp 792-805 1990

A-2   Material Characteristics for Tested Adhesives

In this appendix a brief review of the test results from the tests of the small specimens is given. The results in the following tables in the following tables are the mean values from the series of tested specimens. The full results are presented in chapter 4 starting on page 19.

Table 1: *Comparison of the results of the tested adhesive products. The presented values are the mean values from the measured data.*

	H (mm)	$G_{20\%}$ (MPa)	$\tau_{avg,u}$ (MPa)	τ_{cr} (MPa)	γ_u (%)
Bostik Silikon Bygg 2685	6	0.24	0.534	1.2	347
Bostik Marmorsilikon	6	0.18	0.606	1.1	333
Sika Elastosil SG 20	6	0.46	0.978	2.5	213
Sika Elastosil 605 S	6	0.37	0.515	0.9	249
Bostik Multifog 2640	2	0.49	1.28	2.1	317
Bostik Simson ISR 70-03	2	1.04	2.28	4.4	263
Bostik Simson ISR 70-04	2	0.98	1.86	3.5	230
Bostik Simson ISR 70-12	2	1.17	2.29	4.0	266
Casco Polyurethan	0.2	82.5	3.8	3.8	4.5-10
HBM Rapid Adhesive X 60	0.2	139	10.9	10.9	7.8
Casco Strong Epoxy Professional	0.3	514	20.5	20.5	3.9
Casco UV-hardening Glass-Glue	0.3	113	11.9	11.9	10-15

Table 2: *Corresponding hyper-elastic material models used in the FE-simulations for the soft adhesives.*

	H (mm)	Material Model	C_{10}	C_{01}	D_1
Bostik Silikon Bygg 2685	6	Mooney-Rivlin	$51 \cdot 10^3$	$77 \cdot 10^3$	-
Bostik Marmorsilikon	6	Neo-Hooke	$93 \cdot 10^3$	-	-
Sika Elastosil SG 20	6	Neo-Hooke	$247 \cdot 10^3$	-	-
Sika Elastosil 605 S	6	Mooney-Rivlin	$10 \cdot 10^3$	$190 \cdot 10^3$	-
Bostik Multifog 2640	2	Mooney-Rivlin	$100 \cdot 10^3$	$150 \cdot 10^3$	-
Bostik Simson ISR 70-03	2	Mooney-Rivlin	$200 \cdot 10^3$	$330 \cdot 10^3$	-
Bostik Simson ISR 70-04	2	Mooney-Rivlin	$100 \cdot 10^3$	$400 \cdot 10^3$	-
Bostik Simson ISR 70-12	2	Mooney-Rivlin	$100 \cdot 10^3$	$500 \cdot 10^3$	-

Table 3: *Corresponding material models for the four tested stiff adhesives (glues).*

	Material Model	E	ν
		(MPa)	(-)
Casco Polyurethan 1809	Linear-elastic	200	0.25
HBM Rapid Adhesive X 60	Linear-elastic	320	0.25
Casco Strong Epoxy Professional	Linear-elastic	1500	0.25
Casco UV-hardening Glass-Glue	Linear-elastic	300	0.25
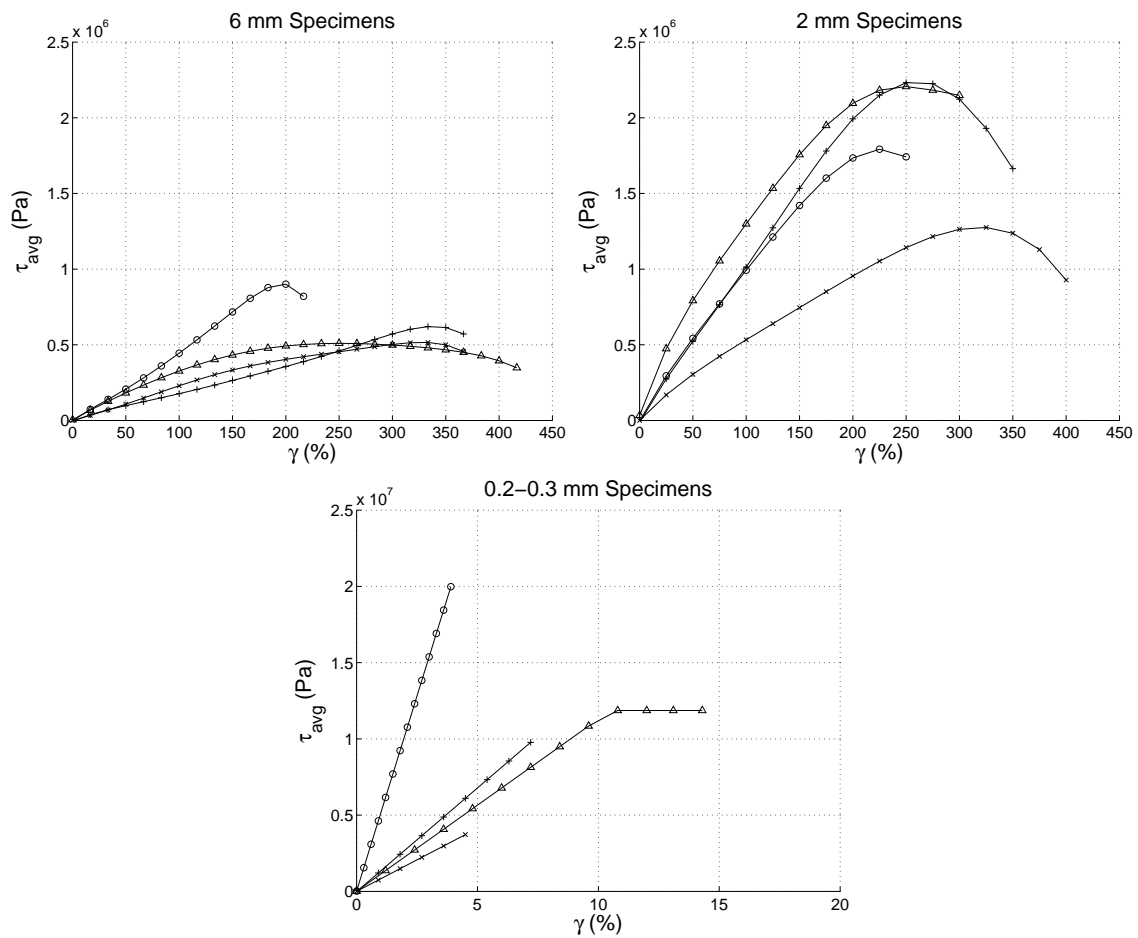
Figure 2: *Shear-stress versus shear-strain in the tested specimens. Note that the bottom diagram has a different scale.* **Top left:** *Silikon Bygg 2685 (x), Marmorsilikon (+), Elastosil SG 20 (o), Elastosil 605 S (triangle).* **Top right:** *Multifog 2640 (x), Simson ISR 70-03 (+), Simson ISR 70-04 (o), Simson ISR 70-12 (triangle).* **Bottom:** *Casco Polyurethan (x), X 60 (+), Casco Strong Epoxy (o), Casco UV-hardening glass-glue (triangle).*